On the Migration of Quantum Butterflies

Supervisors: Umut Gürsoy, Stefan Vandoren & Anna Karlsson
Student: Oscar Eastman, 5517893

July 2022

Acknowledgements

And when I am formulated, sprawling on a pin,
When I am pinned and wriggling on the wall,
Then how should I begin
To spit out all the butt-ends of my days and ways?
And how should I presume?

First and foremost, I would like to thank my extraordinary and patient partner, Charlotte. More than anyone, you have inspired me and supported me as I gradually came to embody my area of study: chaos. I would also like to thank Umut Gürsoy as well as Anna Karlsson, Juan Pedraza and Andrew Rolph for your assistance, guidance and titillating discussion throughout this past year. I would further like to thank my dear friends, Arno, Björn, Robert, Konstantinos, Roy and Margot who went beyond the reasonable expectations of any friend and were kind enough to field silly questions and help me refine my work. Finally, I want to extend my gratitude to my parents Janet and David, my old friend and former supervisor, Jared, and my dear friend Andrew for all of their encouragement in the past years. I couldn't have done it without you.

Abstract

Since its inception, AdS/CFT duality has become an indispensable tool with which to analyse quantum systems with holographic duals. Whilst the assumptions which render this theory analytically tractable do not hold for general systems of interest, the duality can provide especially powerful bounds on physical observables. This duality allows us to draw explicit connections between entanglement and geometry. This deep connection simplifies the study of entanglement spreading and place limits on physical observables for holographic systems. One such example is given by the upper bound on the so-called butterfly velocity which tells us how chaos spreads in a quantum system. In this thesis we explore a quantum corrected BTZ black hole, dubbed the QuBTZ by Emparan et al. as a model for a BTZ black hole with quantum corrections. The QuBTZ model employs a holographic braneworld construction of a BTZ black hole localised on a three-dimensional brane which receives corrections from a CFT_3 living outside its horizon. This model exactly incorporates both quantum corrections from the low-energy CFT modes and backreactions on the geometry which emerge from integrating out energy modes above a cutoff scale. New features of this model are illuminated and existing features demystified. The butterfly velocity is calculated for the QuBTZ to linear order in the backreaction using the subregion duality method of Mezei and Stanford. Using these methods, the butterfly velocity for the QuBTZ is naively found to be $v_B^{(QuBTZ)} \geq 1$. Subsequent numerical and analytic calculations of the entanglement wedge confirm this result at linear order in CFT effects. These corrections were found to be smaller than anticipated, forcing us to reconsider the assumptions of the original prescription. This realisation motivated a more general proposal for calculating the butterfly velocity for global geometries away from the planar limit. A more general approach to calculating v_B for small black holes with non-uniform energy densities and holographic duals is conjectured.

Contents

Introduction

In the decades since holography was conjectured, its application has left virtually no area of theoretical physics untouched. At the heart of its analytic power is the duality between a gravitational system in $(d+1)$-dimensions and non-gravitational system in d-dimensions. This duality suggests a profound connection between quantum information and gravity, entanglement and geometry and weakly coupled and strongly coupled systems.

The first hint of this duality emerged as a result of Bekenstein and Hawking's formula for the entropy of a Schwarzschild Black hole (1)(2),

$$S_{BH} = \frac{\mathrm{A_h}}{4G_N}$$

where A_h is the area of the horizon of the black hole and G_N is Newton's constant[1]. Unlike thermodynamic entropy, this result implied that the leading order gravitational entropy of black holes is not an extensive quantity. This observation inspired a picture of how information is distributed in black holes: to an external observer, the information about the black hole lives on its horizon with a density of $\log_2$ bits of information per four Planck areas[2].

A generalisation of the connection between area and information in quantum gravity, known as the Holographic Principle, was first put forth by t'Hooft (4) and given a precise string theoretic interpretation by Susskind (5). Soon afterwards, Maldacena's AdS/CFT conjecture provided the first and, to date, best studied realisation of the holographic principle(6).

Inspired by the AdS/CFT correspondence, Ryu and Takayanagi (RT) conjectured that, for static holographic systems, the leading order entropy contribution is proportional to the minimal surface of the bulk region homologous to the boundary CFT region(7). This conjecture was soon extended to encompass time-dependent theories in the covariant Hubeny-Ranganami-Takayanagi (HRT) formula (8) and to higher-derivative gravitational theories in (9),(10). Engelhardt and Wall then extended these theories to include corrections from bulk matter outside the horizon in the Quantum Extremal Surface (QES) prescription (11). In Part I, we provide some

[1] Throughout this paper we work in natural units, $c = h = 1$.

[2] This conclusion follows naturally from the no-hair theorem (3), ie. that black holes are highly symmetric and can be described by a very small number of parameters. A stronger claim is the so-called Central Dogma, which states that black holes essentially behave like very large quantum states.

background on quantum information theory and standard techniques in AdS/CFT and key results from the AdS/CFT dictionary. This part of the thesis is intended for those without extensive knowledge of holographic techniques and hence those well-versed in these techniques may opt to skip it.

Holographic techniques can also be applied to braneworld constructions (12)(13), allowing for exact solutions for geometries with quantum corrections and backreactions sourced by matter fields. We explore the model of (14) which exploits the AdS_4/CFT_3 duality to model a BTZ black hole with exact quantum corrections and backreactions from a CFT_3 field outside the horizon of the black hole. The second part of this thesis provides a detailed discussion of this model, dubbed the QuBTZ model by its authors. We explore the behaviour of geodesics in the QuBTZ and its holographic dual and investigate subregion dualities, neither of which were explored in the original paper. Our key results are (i) temperatures, horizons and renormalized masses of the QuBTZ solutions on the Casimir branch have dominated by high energy CFTs whilst those on the thermal branch are dominated by the classical mass parameter, (ii) the Casimir branch of QuBTZ solutions are energetically less favourable than the thermal solutions which lay perturbatively close to the classical result, (iii) infalling lightlike trajectories approach the horizon faster for the QuBTZ than for its classical BTZ equivalent, (iv) for thermal solutions with small backreaction we find that minimal surfaces are smaller than those of the classical BTZ and (v) the finite mass range of the QuBTZ solution limits the QuBTZ horizon to $0 < r_h \leq \frac{2}{\sqrt{3}}\ell_3$ such that we are unable to make the standard 'large black hole' or planar approximations. We provide analytic calculations of the minimal surface for the class of solutions where $f(r)$ has two equal negative roots and numerical results for the more general case when these roots are not equal.

The topic of holography and quantum chaos is then broached in the third part of this thesis. Following on from the work of (15) and (16), we calculate the butterfly velocity for the QuBTZ solution using the entanglement wedge duality. This naive calculation yields a superluminal value for the butterfly velocity is conjectured to result from limitations of this technique as applied to small black holes. The peculiar features of the QuBTZ solution prevent us from using the standard assumptions about large black holes, motivating a new technique. We propose that for small black holes, one ought to consider calculate the butterfly velocity near the critical point where the minimal surfaces exchange dominance rather than the near-horizon region. For the classical BTZ result we obtain a value of $v_B = 1$ consistent with the methods of (15) and (16). Using this technique we show that for small backreaction the butterfly velocity of the QuBTZ solution gives the superluminal result $v_B \geq 1$. Analytical and numerical results support this finding to first order in the backreaction parameter. Several explanations for this are proposed but remain open topics for future research. We identify a gap in the Mezei-Stanford approach for smaller black holes far away from the planar limit with non-constant energy density. We propose that in such systems, the transition point of the minimal surface from its connected to disconnected phase provides a more sensible point at which to calculate the butterfly velocity.

The final part of this thesis consists of a summary of these results and motivates future work in this direction. Due to time constraints, we were unable to explore all branches of the QuBTZ solution in detail and propose extensions of our analysis to the branch of dressed singularities, rotating solutions and solutions with large backreaction where we must account for higher-derivative gravity corrections. We argue that the QuBTZ model provides an interesting case study for the investigation of entanglement islands. This model would serve as an ideal candidate for the study of the quantum bit thread proposal of (17) and propose a concrete methodology by which to study it. Our proposed methodology for calculating the butterfly velocity for black holes with radii $r_h < \ell_{d+1}$ is only checked for the trivial case of the BTZ solution, however, an extension to higher dimensional theories would provide a non-trivial test of this proposal. This technique would be especially valuable in the study of classical black holes below the planar limit and models with horizons with significant backreaction effects as in the QuBTZ.

Part I

‘It from Qubit’
An Introduction to Holography

Entropy is an ubiquitous concept in physics. From the classical to the quantum and across all energy scales a quantifiable measure of disorder or knowledge of the system of interest allows us to make powerful physical inferences. We must, however, be cautious with what we mean by 'entropy'. In this part, we define several incarnations of entropy encountered throughout this thesis. Chapter 1 will assume that we are working in the low-energy limit in which our quantum mechanical systems are well-defined. Chapter 3 extends these notions to the continuum limit to obtain a manifestly Lorentz invariant QFT description. This chapter will closely follow (18) and (19) and references therein.

In holographic systems the link between quantum gravity and information is made explicit, allowing us to constrain holographic theories using QIT. In Chapter 3, we apply information theoretic notions to the AdS/CFT duality. In 2.2 we see that to preserve a unitary theory of quantum gravity, we require that fine grained (von Neumann) entropy be conserved under unitary time evolution. In Chapter 3.3, we introduce the Ryu-Takayanagi (RT) prescription and its extensions. These techniques provide a mathematically precise duality between geometry and entanglement which we apply to the QuBTZ solution in Parts II and III.

Chapter 1

Foray into Quantum Information

The notion of entropy was first introduced by Clausius in the context of equilibrium thermodynamics to assign a quantitative degree of order to a system(20). An infinitesimal change thermodynamic entropy, dS_{th} of an equilibrium system is given by the familiar equation

$$dS_{th} = \frac{dQ_{rev}}{T} \tag{1.1}$$

where dQ_{rev} is the (reversible) heat exchanged between the system and its bath at a fixed temperature T[3].

Soon after, Boltzmann developed his famous statistical mechanical formulation of entropy in terms of the systems constituent microstates, Ω, for the microcanonical ensemble

$$S = k_B \ln(\Omega) \tag{1.2}$$

where k_B is Boltzmann's constant. For a more general statistical ensemble, in which each microstate has probability p_i, this becomes

$$S = -k_B \sum_i p_i \ln(p_i) \tag{1.3}$$

This insight was gleaned before the development of quantum mechanics and hence firmly rooted in the classical mindset. Quantum mechanics can be straightforwardly incorporated into systems in the thermodynamic limit to produce non-trivial distinctions from the classical case. To make such generalisations, we must still define ensemble quantities and take large-N[4] such that the partition function becomes sharply peaked about a typical energy. Therefore, such definitions

[3]This of course applies to a canonical ensemble with a fixed number of particles and volume. This relationship can be extended to other forms of energy transfer, other thermodynamic systems such the grand canonical ensemble and even to non-equilibrium dynamics.

[4]We use large N to mean the thermodynamic limit, in which the number of particles is large whilst in later chapters this terminology will refer to the rank of the gauge group in the AdS/CFT correspondence

still require us to 'coarse grain' the system such that we give up some knowledge of the system. This approximation means we no longer keep track of its precise microscopic details.

Useful as coarse grained entropy is, we would like a paradigm with which to discuss information in quantum systems. Let us then suppose we have a source from which we receive some output signal and we wish to identify what data was originally generated by the source on the basis of the information we receive. The Shannon Entropy represents the limit of how successfully one can compress the output information into a noiseless channel without information loss. Though the precise mathematical definition of the Shannon Entropy is equivalent to (1.2), it is more general and can be interpreted as the average amount of uncertainty or information which is inherent to the possible outcomes of the variable.

To describe correlations in a quantum mechanical system we introduce the density matrix, ρ. If the density matrix of the state in the Hilbert space $\mathcal{H}$, $|\psi\rangle \in \mathcal{H}$ can be written in as a linear combination of a finite number of basis states then it is called pure, otherwise it is referred to as a mixed state and can be represented by an ensemble of basis states $|\psi_i\rangle$ with corresponding probabilities p_i,

$$\rho_{\text{pure}} = |\psi\rangle\langle\psi| \tag{1.4}$$

and

$$\rho_{\text{mixed}} = \sum_i^{\infty} p_i |\psi_i\rangle\langle\psi_i| \tag{1.5}$$

with

$$\sum_i^{\infty} p_i = 1 = \text{Tr}[\rho_{\text{mixed}}] \tag{1.6}$$

for which we define the expectation value of an operator $\mathcal{O}$ as[5],

$$\langle\mathcal{O}\rangle = \text{Tr}(\mathcal{O}\rho) = \sum_{i=0}^{\infty} p_i \langle\psi_i|\mathcal{O}|\psi_i\rangle \tag{1.7}$$

The Shannon Entropy was then extended to include quantum correlations by von Neumann,

$$S_{vN} = -\text{Tr}[\rho \log \rho] \geq 0 \tag{1.8}$$

The von Neumann Entropy is a fine-grained entropy which quantifies our ignorance about the precise state of the quantum system. The von Neumann entropy obeys four important properties,

1. $S_{vN} = 0$ for pure states

[5]The density matrix of a pure state can be thought of as a special case of the mixed density matrix for which $p_i = 1, \forall i$ and so we assume that $\rho = \rho_{\text{mixed}}$ unless specified.

2. The entropy of a maximally mixed state (where $p_i = p_0, \forall i$) with density matrix ρ_{mm} is

$$S_{vN} = \ln \Omega \tag{1.9}$$

where Ω is the dimension of the Hilbert space $\mathcal{H}$. In units of $k_B = 1$ we recover the answer for the microcanonical ensemble (1.2)

3. It is manifestly invariant under unitary time evolution,

$$S_{vN}(\rho) = S_{vN}(U(t)\rho U^{-1}(t)); \quad UU^{-1} = U^{-1}U = \tag{1.10}$$

ie. a pure state cannot evolve into a mixed state and vice-versa.

4. Course graining always discards information about the system such that we always know less about a course grained system than we do about our fine grained system. The fine grained entropy then acts as a lower bound to the coarse grained entropy,

$$S_{vN} \leq S_{th} \tag{1.11}$$

The thermodynamic entropy of a quantum system is that which maximizes S_{vN} with respect to all possible density matrices of the system yielding the same expectation value of some set of coarse grained observables,

$$S_{th}(\rho) = \max_{\rho'}[S_{vN}(\rho')] = S_{vN}(\rho_{th}) \tag{1.12}$$

where the thermal density matrix for a fixed temperature is given by

$$\rho_{th} = \frac{e^{-\beta H}}{Z}; \quad Z = \mathrm{Tr}\left[e^{-\beta H}\right] \tag{1.13}$$

where $\beta = \frac{1}{T}$, H is the Hamiltonian of the system and Z is the thermodynamic partition function. We note that this definition holds only for states which are at thermal equilibrium with some temperature bath.

1.1 Entanglement Entropy and Purification

We can also consider a bipartite system with Hilbert space $|\psi\rangle \in \otimes_\alpha \mathcal{H}_\alpha$. Suppose it can be separated into two spatial regions A and its complement $\bar{A}$ such that their Hilbert spaces are $\otimes_\alpha \mathcal{H}_\alpha \cong \mathcal{H}_A \otimes \mathcal{H}_{\bar{A}}$. Supposing we are only privy to the information in A and we wish to find its density matrix from the full density matrix of the system, we must then trace over the degrees of freedom in the complement $\bar{A}$,

$$\rho_A = \langle \psi_{\bar{A}} | \psi \rangle \langle \psi | \psi_{\bar{A}} \rangle = \mathrm{Tr}_{\bar{A}}(|\psi\rangle\langle\psi|) \tag{1.14}$$

This corresponds to determining the state of the degrees of freedom in A while remaining ignorant about the microscopic details of region $\bar{A}$. It is important to understand that this entropy is defined in terms of traces and as such is determined by the eigenvalues of the density matrices. Crucially, unitary transformations acting on ρ_A or $\rho_{\bar{A}}$ do not change the entanglement properties of the system. To change the entanglement entropy of the system a unitary transformation must be performed on the entire system, $A \cup \bar{A}$.

One can then define the entanglement entropy of the system by the von Neumann entropy of the reduced density matrix,

$$S(A) = -\mathrm{Tr}_A(\rho_A \log \rho_A) \tag{1.15}$$

For a pure system, it follows trivially that $S(A) = S(\bar{A})$. This leads us to purification which takes a mixed state given by ρ_A and expresses it as the reduced density matrix of a subregion A within some larger pure state. Physically, one can imagine that we are simply coupling our system to a heat bath at equilibrium. Purification is always possible and admits infinitely many possible purification states to which one may couple the mixed state. For an ensemble given by ρ_A or the set $\{|\psi_i\rangle_A, p_i\} \in \mathcal{H}_A$, a general purification is given by,

$$|\Psi\rangle = \sum_i \sqrt{p_i}\, |\psi_i\rangle_A \otimes |\psi_i\rangle_B \tag{1.16}$$

where n is the number of replicas and $\{|\psi_i\rangle_B\}$ is an orthogonal set of states in some Hilbert space $\mathcal{H}_B$ whose dimension is at least as large as the number of non-zero eigenvalues of ρ. A state represented in the form (1.16) is known as a Schmidt composition and allows us to represent any state of a combined system. Generally, the simplest purifications are of the form $\{|\psi_i\rangle_B\} = \{|\psi_i\rangle_A\}$. The fact that the entanglement spectrum of the system of interest and the purifying state in (1.16) follows directly from $S(A) = S(\bar{A})$. We should not take for granted the fact that the existence of a purification is always possible in quantum systems: as there is no way to take a classical probability distribution and purify it as its purification relies on the presence of quantum entanglement.

1.2 Rényi Entropies

From Equation (1.8), we see that to calculate the fine grained entropy, one must take a trace over a non-linear operator of our density matrix. In general, such a computation is difficult to perform and so we must look for alternative methods. To circumvent the challenges of calculating the von

Neumann entropy, we introduce the Rényi entropy for a reduced density matrix ρ_A[6],

$$S^{(n)}(A) = \frac{1}{1-n}\log \mathrm{Tr}_A(\rho_A^n) = \frac{1}{1-n}\log\left(\sum_i \lambda_i^n\right) \tag{1.17}$$

where T is temperature and λ^i are the eigenvalues of the reduced density matrix under the assumption that the system is finite. These values further comprise the entanglement spectrum of the density matrix.

There are several things to note:

1. The Rényi Entropy is not an entropy in the physical sense but is simply defined in terms of moments of the reduced density matrix

2. The canonical definition of n should require that $n \in \mathbb{Z}_+$ however it will be convenient for us to analytically continue it such that $n \in \mathbb{R}_+$

3. If a pure system is properly normalised then, $\mathrm{Tr}\,\rho^2 = 1$ whilst if it is in a mixed state then $\mathrm{Tr}\,\rho^2 < 1$. The Rényi Entropy then gives a measure for quantum purity despite its non-linearity.

4. Taking limit as $n \longrightarrow 1$ we see that using (1.17), the the sum $\lim_{n\to 1}\log\left(\sum_i \lambda_i^n\right) = \log(\sum_i \lambda_i) = \log(1) = 0$. The denominator clearly diverges and so we must use l'Hopital's rule,

$$\lim_{n\to 1} S_A^{(n)} = \lim_{n\to 1}\frac{\partial_n(\log(\sum_i \lambda_i^n))}{\partial_n(1-n)} = \lim_{n\to 1} -\partial_n \log\left(\sum_i \lambda_i^n\right)$$

$$= \lim_{n\to 1} -\frac{\partial \log(\sum_i \lambda_i^n)}{\partial(\sum_i \lambda_i^n)}\frac{\partial(\sum_i \lambda_i^n)}{\partial n} = -\lim_{n\to 1}\frac{\sum_i \lambda_i^n \log(\lambda_i)}{\sum_i \lambda_i^n}$$

$$= -\sum_i \lambda_i \log(\lambda_i) = S_A$$

recovering the von Neumann Entropy in this limit.

5. The Rényi Entropy is analagous to the thermodynamic free energy at a temperature $\frac{1}{n}$. If we define the modular Hamiltonian as $\mathcal{K}_A = -\log \rho_A$ Then we can view the Rényi entropy as the free energy modulo the normalizing factor as we have

$$S_A^{(n)} = \frac{1}{1-n}\log Tr\left(e^{-q\mathcal{K}_A}\right)$$

[6]This could of course be substituted for some more general density matrix ρ, however, we will be primarily concerned with entanglement entropies of subregions hence we have chosen to write it in this form.

which compares (schematically) to the standard thermodynamic form of the free energy,

$$F = -T\log(Z) = -\frac{1}{\beta}Tr(e^{-\beta H})$$

Assuming we can analytically continue n, it is clear why calculating the Rényi entropy is preferable to calculating the von Neumann entropy directly: one need only calculate $Tr(\rho^n)$, take the logarithm of this quantity (which is a now just a function of n) and then take the limit that $n \longrightarrow 1$.

We may further consider another entropy-like quantity known as the modular entropy:

$$\tilde{S}_A^{(n)} = \frac{1}{n^2}\partial_n\left(\frac{n-1}{n}S_A^{(n)}\right) \tag{1.18}$$

We can see that one may also define the modular entropy as:

$$\tilde{S}_A^{(n)} = -\frac{1}{n^2}\partial_n\left(\frac{1}{n}\log Tr_A\left(e^{-q\mathcal{K}_A}\right)\right) = -\frac{1}{n^2}\partial_n\left(\frac{1-n}{n}S_A^{(n)}\right) \tag{1.19}$$

We can likewise make the analogy with the thermodynamic entropy by the relation:

$$S = -\frac{\partial F}{\partial T} = -\beta^2\partial_\beta\left(\frac{1}{\beta}\log Tr\left(e^{-\beta H}\right)\right) \tag{1.20}$$

Therefore, if we neglect rescaling of the this result with respect to the inverse temperature we see that the modular entropy has a direct interpretation as an entropic quantity.

1.3 Entropy Constraints

Having defined some useful notions of entropy in quantum mechanics, it is worth exploring some of the inequalities one can derive purely from the information theoretic definitions. These inequalities allow us to prove various equivalences between holographic descriptions as well as various bounds and limitations which enables the classification of holographic systems as a subset of general quantum theories. Unfortunately, this thesis does not give scope for a thorough calculation of the relevant inequalities here, however, for those interested readers we recommend the resources (19)(20)(21)(22). Whilst classical information theoretic quantities generally have clearly defined physical interpretations, the presence of entanglement muddies the water when extended to QIT. Regardless, we shall endeavor to provide some intuition motivated by classical notions.

1.3.1 Subadditivity, Strong Subadditivity and the Araki-Lieb Inequality

Thankfully, there exist some universal features which hold for both classical and quantum notions of entropy. These inequalities are extremely useful when determining bounds on other information theoretic notions defined below.

For subregions A and B the subadditivity property is

$$S(A \cup B) \leq S(A) + S(B) \tag{1.21}$$

which along with the Araki-Lieb Inequality,

$$|S(A) - S(B)| \leq S(A \cup B) \tag{1.22}$$

define the triangle inequality for entropy. The Araki-Lieb Inequality is an upper bound on the difference of entanglement entropies of a system and its complement in terms of the entropy of the total density matrix of their union. The subadditivity constraint implies that we can never know more about a system from observing its individual constituents than we can from the complete system. Subadditivity also has a stronger cousin, Strong Subadditivity (23),

$$S(A \cup B) + S(B \cup C) \geq S(A \cup B \cup C) + S(B) \tag{1.23}$$

which is difficult to prove for continuum systems. In holographic theories, however, we can take advantage of the geometrisation of entropy to produce significantly simpler proofs (24).

1.3.2 Mutual Information

A related quantity is the mutual information, defined in both the classical and quantum cases as,

$$I(A;B) = S(A) + S(B) - S(A \cup B) \tag{1.24}$$

The classical mutual information quantifies how much information we can obtain about A just from observing B. For both its classical and quantum incarnations, $I(A;B) \geq 0$. In the quantum case, the non-negativity of mutual information follows directly from the Araki-Lieb Inequality (25) and one sees that $I(A;B) = 0$ only for the case in which the density matrix of the full space factorizes such that $\rho_{AB} = \rho_A \otimes \rho_B$. In holographic systems, we also have the property of monotonicity of mutual information,

$$I(A; B \cup C) \geq I(A;B) \tag{1.25}$$

which states that mutual information is non-decreasing under the addition of additional regions. Another important feature of mutual information particular to holographic systems is that

it is monogamous,

$$I(A; B \cup C) \geq I(A; B) + I(A; C) \tag{1.26}$$

For holographic systems, the Monogomy of Mutual Information (MMI) or $I_3(A; B; C)$ is always negative, suggesting that correlations in holographic theories arise primarily through entanglement rather than classical correlations.

1.3.3 Conditional and Relative Entropy

Both classical and quantum conditional entropy are given by,

$$H(A|B) = S(A \cup B) - S(B) \tag{1.27}$$

Classically, one interprets this quantity as the entropy remaining in the probability distribution A conditioned on knowing B. The classical conditional entropy is positive semi-definite, $S(A|B) \geq 0$, whilst the quantum conditional entropy can be negative. Take for example, a pure state $A \cup B$ for which $A = B$ and in which A, B are mixed such that $S(B) = S(A) > 0$ ergo $H(A|B) = -S(B) < 0$.

The classical relative entropy requires demands qualitative discussion. Suppose we have some random variable X and some theory which predicts the probability distribution, $Q_{(X)}$ for the final state. Suppose our theory states that the probability to observe the final state $X = x_i$, where i runs over all possible outcomes, is $q_i = Q_{(X)}(x_i)$. Furthermore, we entertain the possibility that our theory is in fact incorrect and the distribution follows some other probability distribution $p_i = P_{(X)}(x_i)$. Once we have observed N such events, we wish to be able to form a notion for how correct our model is. This can be measured by the relative entropy,

$$S(P_{(X)}||Q_{(X)}) = \sum_i p_i(\ln p_i - \ln q_i) \tag{1.28}$$

which can also be used to prove the positivity of mutual information (18). Its quantum extension is then given in terms of two density matrices, ρ and σ which are quantum analogs to $P_{(X)}$ and $Q_{(X)}$,

$$S(\rho||\sigma) = \mathrm{Tr}\, \rho(\ln \rho - \ln \sigma) \tag{1.29}$$

which, unlike some of the previous definitions, is identical in classical and quantum descriptions along with the property,

$$S(\rho||\sigma) \geq 0 \tag{1.30}$$

Suppose we have some density matrix $\sigma_{A\cup B} = \rho_A \rho_B$ such that:

$$\ln \sigma_{A\cup B} = \ln(\rho_A \otimes {}_B) + \ln({}_A \otimes \rho_B) \tag{1.31}$$

Such that,

$$\begin{aligned} S(\rho_{A\cup B}||\sigma_{A\cup B}) &= \mathrm{Tr}_{A\cup B}\,\rho_{A\cup B}(\ln\rho_{A\cup B} - \ln\sigma_{A\cup B}) \\ &= \mathrm{Tr}_{A\cup B}\,\rho_{A\cup B}(\ln\rho_{A\cup B} - \ln(\rho_A \otimes {}_B) + \ln({}_A \otimes \rho_B) \\ &= S(A) + S(B) - S(A\cup B) = I(A;B) \geq 0 \end{aligned} \tag{1.32}$$

hence proving the positivity of mutual information.

Chapter 2

Holography and AdS/CFT Correspondence

Black holes are a resplendent source of intrigue for theoretical physicists, offering a limit within which we are able to simultaneously explore significant gravitational and quantum mechanical effects. Not only do black holes display high degrees of symmetry, but the broadly accepted central dogma of black hole information asserts that to a distant observer, a black hole can be described by a unitary quantum mechanical system with a large but finite number of degrees of freedom set by the area of the event horizon. What's more, the quantum numbers we require to describe the black hole are simple quantum numbers such as angular momentum, mass and charge. The central dogma then tells us that black holes can be treated as simple thermodynamic objects, an observation which lead Bekenstein and Hawking to define the laws of black hole thermodynamics and later allowed Hawking to show that black holes can evaporate[7]. This work on black hole thermodynamics resulted in the the Black Hole Information Paradox (BHIP), a central conundrum to be resolved by any consistent theory of quantum gravity. The non extensive property of black hole entropy can be interepreted as though the information is projected onto its surface like a hologram. It was this observation which first spawned the notion that quantum gravity is holographic.

This chapter is devoted to a formal definition and the best known example of holography, the AdS/CFT correspondence. For context, Chapter 2.1 will introduce the basics of black hole thermodynamics and briefly sketch how the BHIP comes about. In Chapter 2.2 we formally introduce the concept of holography. Chapter 2.3 delves into the AdS/CFT correspondence, including some elementary background on Anti-de Sitter space (AdS) and Conformal Field Theory (CFT). In preparation for the central topic of this paper, Chapter 2.4.1 provides an in-depth treatment of black holes in AdS space.

[7]The use of 'small' here will be made more precise in Chapter 2.4.1

2.1 Black Hole Thermodynamics

While long assumed that black holes obeyed standard conservation laws, the similarities between between black hole horizons and classical thermodynamic systems were first studied by Bekenstein (1) (26). The laws of black hole thermodynamics can be summarised as in the table below(27).

	Thermodynamics	Black hole
Zeroth law	Temperature T is constant at equilibrium	Surface gravity κ is constant for a stationary solution
First law	$dE = TdS$	$dM = \frac{\kappa}{8\pi G_N} dA$
Second law	$dS \geq 0$	$dA \geq 0$
Third law	$S \longrightarrow 0$ as $T \longrightarrow 0$	$S \longrightarrow 0$ as $T \longrightarrow 0$

where G_N is Newton's constant. But how exactly can one ascribe temperature to a black hole? Suppose we throw some infinitesimal mass dM into a Schwarzschild black hole[8], the horizon of the black hole responds dynamically,

$$\frac{\kappa}{8\pi G_N} dA = dM - \Omega dJ \tag{2.1}$$

where κ is the surface gravity of the black hole, A is the area of its horizon, Ω is its rotational velocity and and J is its angular momentum. Using energy-mass equivalence, Bekenstein argued that the total difference in the energy of the black hole must be, $dE = dM - \Omega dJ$ such that

$$dM - \Omega dJ = dE = TdS \tag{2.2}$$

Hence, one can deduce that the entropy of the black hole is proportional to the area of its event horizon,

$$S_{BH} = \frac{A_h}{4G_N} \tag{2.3}$$

and its characteristic temperature is therefore given by the famous Hawking Temperature(28)(29),

$$T_H = \frac{\kappa}{2\pi} \tag{2.4}$$

Whilst we have presented this result in a rather ad hoc manner, Hawking derived this by noting that directly outside of a large black hole the tidal forces are negligible and the space near its horizon is approximately flat with a constant acceleration given by its surface gravity κ. In this regime, we are free to use semi-classical gravity.

[8] Or any black hole in which we keep angular momentum and charge constant

The metric for a Schwarzschild black hole in asymptotically Minkowski space in $(d+1)$-dimensions is given by:

$$ds^2 = -F(r)dt^2 + \frac{dr^2}{F(r)} + r^2 d\Omega_{d-1}^2 \tag{2.5}$$

where

$$F(r) = \left(1 - \frac{2G_N M}{r}\right) = \left(1 - \frac{r_h}{r}\right) \tag{2.6}$$

where $d\Omega_{d-1}^2$ is the metric of a $(d-1)$-sphere, r_h is the horizon of the black hole, r is the distance from the centre of the black hole and t is the time experienced by an observer at $r = \infty$.

Near the horizon, we can perform a similar procedure by Taylor expanding the metric about $r = r_h$ such that,

$$F(r) \approx \frac{4\pi}{\beta}(r - r_h) \quad \text{where } \beta = \frac{4\pi}{\partial_r F(r)|_{r=r_h}} \tag{2.7}$$

For a geometry with a timelike Killing vector we can Wick rotate, $t = it_E$, where t_E is Euclidean time. In the near horizon limit,

$$ds^2 \approx \frac{4\pi}{\beta}(r - r_h)dt_E^2 + \frac{\beta}{4\pi}\frac{dr^2}{r - r_h} \tag{2.8}$$

We can then make the substitutions

$$\rho = \sqrt{\frac{\beta}{\pi}(r - r_h)}; \quad \theta = \frac{2\pi}{\beta}t_E \tag{2.9}$$

which yields,

$$ds^2 \approx d\rho^2 + \rho^2 d\theta^2 \tag{2.10}$$

This looks like Euclidean space in polar coordinates provided that there are no conical singularities. To remove this possibility, we require that $\theta \sim \theta + 2\pi$ and therefore the Euclidean time t_E has period β as in Figure 2.1. Recalling that Euclidean time at equilibrium can be related to the inverse temperature of the system, we find

$$T = \frac{1}{\beta} = \frac{\partial_r F(r)|_{r_h}}{4\pi} \tag{2.11}$$

2.1.1 The Black Hole Information Paradox

According to (2.1), as black holes evaporate, they radiate energy to the environment and hence their horizons shrink. At first glance the second law of thermodynamics appears to have been

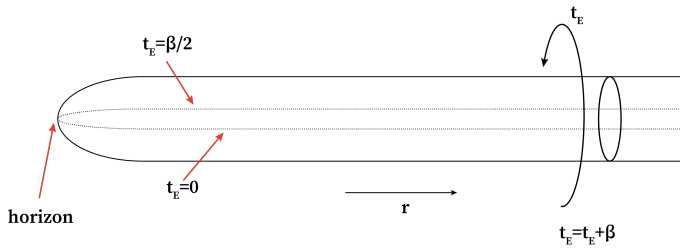

Figure 2.1: The Euclidean cigar representing the geometry of a Schwarzschild black hole.

violated however we note that what really obeys the second law is the generalised entropy,

$$S_{gen} = \frac{A}{4G_N} + S_{out}; \quad \Delta S_{gen} \geq 0 \tag{2.12}$$

where S_{out} is the contribution from any fields outside the horizon. But this is not the end of our troubles. For classical black holes, black holes can only grow or stay static and therefore we can simply apply the No Hair Theorem(30) claiming that the information about the state of anything which fell in is encoded on its horizon, but microscopic details of what happens inside the black hole are fundamentally inaccessible to an external observer. Unsettling as this may be, the details are not lost, simply inaccessible due to the presence of a physical horizon. This is not so when quantum mechanics is included and we must eventually explain what is left when everything has evaporated. In fact, the trouble starts well before this at the so called Page Time(31).

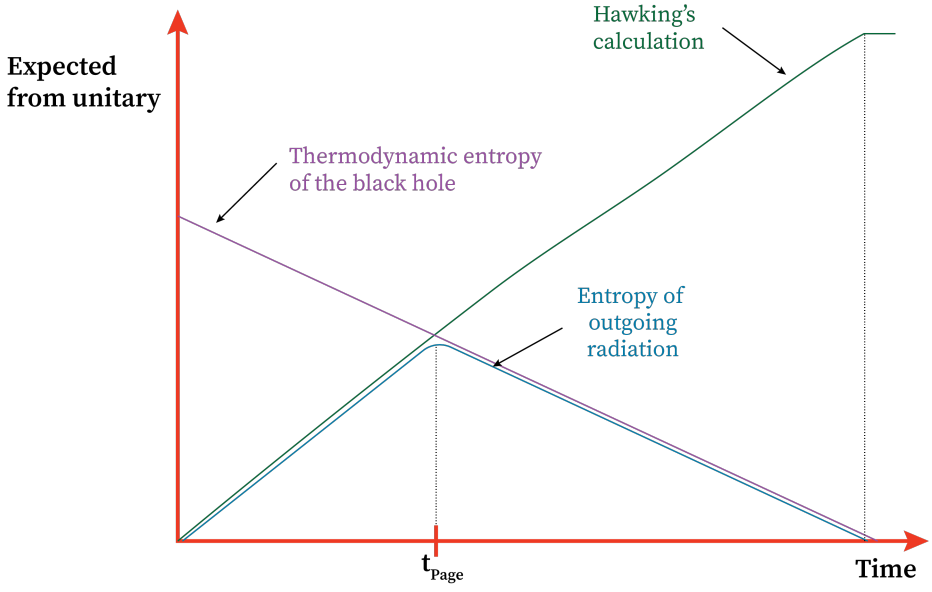

Figure 2.2: A diagram illustrating the Page Curve. The Page Time is the time at which the fine and course grained entropies are equal(32).

In Chapter 1, we pointed out that the thermodynamic entropy places an upper bound on the fine-grained entropy. In the semi-classical picture, the entropy of the radiation increases monotonically implying that information about our pure state is lost. Each ingoing mode is entangled with at most one outgoing mode. When the number of outgoing modes exceeds the number of ingoing modes, the Black Hole Information Paradox (BHIP) already emerges(33)(34)(32). Eventually, the energy of the outgoing radiation modes will be larger than the energy of the remaining energy in the black hole system. The time at which this occurs is referred to as the Page Time. Beyond this time, the entropy bound (1.11) is violated as there is not enough mass remaining in the black hole to accommodate all outgoing radiation. For the black hole system to remain unitary, the fine grained entropy of the Hawking radiation cannot continue unbounded. There must exist some turning point near the Page Time at which it is now monotonically decreasing and the curve follows the Page Curve shown in Figure 2.2. Page pointed out that this turning point should coincide with the time at which approximately half the mass of the black hole has evaporated such that if we started with a black hole made from a pure state, our Hawking radiation should also eventually have a von Neumann entropy, $S_{vN}^{(rad)}(t \longrightarrow \infty) = 0$(31).

The Bekenstein-Hawking radiation in tandem with the Central Dogma imply some fundamental link between the information which forms the black hole and its horizon, however its details are obfuscated. So, what happens to the information which was hidden behind the horizon and can we recover the details? As explained in Chapter 1, the conservation of information is equivalent to unitary evolution of quantum mechanical systems and hence any loss of information strikes to the heart of fundamental quantum mechanics or, at least, any quantum theory of gravity.

To labour the point, consider that we take some very large system of particles whose collective state is pure and we collapse this into a black hole. The black hole then evaporates through the emission of Hawking quanta (each of which together form a pure state). Let us suppose that the entire black hole evaporates and we are left with nothing but the Hawking radiation as our final state. Though we started with pure states, the emission of the Hawking quanta is thermal and so we have evolved from a pure state into a mixed state, a clear violation of unitarity. Another way of seeing the issue is to imagine that we have an evaporating black hole, but for every Hawking quantum which is emitted, we compensate by throwing an identical quantum in. In this manner, we can continue to fill the black hole up with information indefinitely whilst keeping its horizon fixed. By the Bekenstein-Hawking entropy this should not be allowed as we are directly violating our statement linking the black hole horizon to the information stored within. This enigma has two obvious solutions: either the information is permanently lost and we must discard unitarity or the information is somehow encoded in the remnants of the evaporation[9].

Whilst the black hole information paradox is a consequence of semi-classical approximations,

[9]This is an extremely rich topic which we unfortunately do not have time to explore. For a general review of the topic, see (32)

it was shown in (33) that small corrections do not resolve the problem. Under the assumption that a unitary quantum theory of gravity exists, it is broadly believed that a resolution to this paradox will provide significant support for this mechanism as a suitable model for quantum gravity. We can categorise some interpretations and their suggested solutions to the paradox as:

1. **Information is left as a remnant**. In this interpretation, the black hole does not completely evaporate and what is left behind is some remnant acting as a black box storing the information which formed the black hole. Both Planckian sized (35)(36) and large remnant cases have been considered (37)(38). In the Planckian case, an object this small containing so much information is a violation of the Bekenstein bound(39). For non-Planckian remnants, there must be some mechanism to prevent the black hole from radiating well before the Planckian limit which cannot be accounted for in semi-classical gravity and the Bekenstein bound is similarly violated. Another offshoot is that black holes could form a Euclidean time wormhole to another universe or causally disconnected region of spacetime(40)(41). Unfortunately, this also seems to violate unitary evolution without an explicit way in which to recover the information from these causally disconnected regions.

2. **Information escapes during evaporation** One possibility is in non-Markovian dynamics where there is some correlation between the past and future evolution(42). This formulation is consistent with semi-classical gravity but contradicts our normal notions of causality. In (43) (44) (45) the information is encoded in the outgoing Hawking radiation or some disconnected island region. These theories preserve unitarity and reversibility criteria but require a significant deviation from semi-classical predictions.

The latter theories in which the information is recoverable and eventually escapes the black hole will be of most interest to us. In Chapter 3.4 we will discuss entanglement islands which are believed to resolve the BHIP in AdS/CFT.

2.2 Holography

What other features of quantum gravity could be deduced from semi-classical black hole thermodynamics? The Bekenstein Hawking entropy of a black hole seems to imply that to leading order, information is encoded in a co-dimension two subregion of the full Lorentzian spacetime[10], inspiring the holographic principle.

The holographic principle was first conjectured by t'Hooft and later formalised more explicitly by Susskind (46) (47)(5)(47). According to this principle, one can describe a theory of quantum gravity in $(d + 1)$ dimensions using a dual non-gravitational theory in d dimensions.

[10]For non-static cases, this subregion generically becomes codimension one

Returning to (2.3) we may consider the microscopic degrees of freedom of the black hole are encoded entirely on the macroscopic boundary surface of the black hole[11]. Because black holes represent the most entropic configuration that can be constructed within a region of spacetime, we may consider the Bekenstein-Hawking radiation to be some upper entropy bound for regions, Σ, in a theory of quantum gravity[12],

$$S(\Sigma) \leq \frac{A(\partial\Sigma)}{4G_N} \tag{2.13}$$

Whilst this expression holds for static spacetimes, covariant generalisations such as Bousso's covariant entropy bound preserves the general claim of the holographic principle(48). In the following Section 2.3 we devote significant time to the best understood manifestation of holography in quantum gravity, the AdS/CFT correspondence. We then briefly discuss the famous ER=EPR conjecture as another manifestation of the holographic principle.

2.3 AdS/CFT

Maldacena first proposed a holographic duality in the low energy limit of type IIB string theory living on $AdS_5 \times S^5$ and the $\mathcal{N} = 4$ supersymmetric Yang-Mills theory in four spatial dimensions(6). While this initial observation came from a top-down approach, a more general correspondence between AdS_{d+1} and CFT_d can be described from the bottom-up approach and need not make a direct connection to strings [13](49)(50)(51)(52)(53) (54). This AdS/CFT correspondence is the best understood and most studied example of holographic duality and can be generalised to any d-dimensional CFT and any theory of quantum gravity on an asymptotically $AdS_{d+1} \times \mathcal{M}$ spacetime in which $\mathcal{M}$ is a compact manifold. Though the AdS/CFT conjecture has not been rigorously proven, it has been shown to work in many important cases. Furthermore, precise maps which allow us to reconstruct the bulk from states on the conformal boundary are non-trivial, however, some progress has been made using tensor networks for example. Cosmological studies suggest that our universe is asymptotically de Sitter rather than Anti-de Sitter, however, as it is widely believed that quantum gravity is generically holographic, one hopes that the study of holography in the AdS/CFT correspondence will yield insights and tools into how to describe holography in more general non-compact spacetimes(27).

[11] Though we have so far limited the discussion to black holes, there is no reason to believe that the black hole case is simply a limit of a more general feature of quantum gravity

[12] For now we shall assume that the spacetime is static and Σ is just a constant time hypersurface.

[13] Top-down meaning that one starts from a string theory and takes the low energy limit and the bottom-up approach is to ground the result in the low energy-limit directly

2.3.1 Anti de Sitter Space

Einstein's field equations are given by,

$$G_{\mu\nu} = R_{\mu\nu} - \frac{1}{2}Rg_{\mu\nu} + \Lambda g_{\mu\nu} = \kappa T_{\mu\nu} \tag{2.14}$$

where $R_{\mu\nu}$ is the Ricci curvature tensor, R is the Ricci scalar, Λ is the cosmological constant, κ is the Einstein gravity constant and $T_{\mu\nu}$ is the energy momentum tensor. In the vacuum case $T_{\mu\nu} = 0$ and the sign of the intrinsic curvature of solutions is determined entirely by the sign of Λ. In the case that $\Lambda < 0$, one obtains the maximally symmetric Anti-de Sitter solution which can be embedded in $(d+2)$- dimensional Minkowski space with $(2, d)$ signature as:

$$ds^2 = -dX_0^2 - dX_{d+2}^2 + \sum_{i=1}^{d+1} dX_i^2 \tag{2.15}$$

We can further define the AdS_{d+1} space as the hypersurface

$$\ell_{d+1}^2 = X_0^2 + X_{d+2}^2 - \sum_{i=1}^{d+1} X_i^2 \tag{2.16}$$

where for pure AdS, the radius of curvature ℓ_{d+1} is related to Λ by $\Lambda = \frac{-(n-1)(n-2)}{2\ell_{d+1}^2}$. For non-vacuum cases, we can also relate the vacuum energy density ρ_0 to ℓ_{d+1} in the case that $T_{\mu\nu} = -\rho_0 g_{\mu\nu}$ by,

$$\rho_0 = -\frac{d(d-1)}{16\pi G_N \ell_{d+1}^2} \tag{2.17}$$

From the embedding coordinates, it is clear that the AdS space inherits the symmetries of the Lorentz group $SO(2, d)$ as well as the property of homogeneity from the ambient space $\mathbb{R}^{2,d}$. Being homogenous, all points in the vacuum AdS solution are equivalent and are related by a symmetry transformation from the $SO(2, d)$ group. There exist two standard coordinates of AdS in the literature, the global and Poincaré patch coordinates.

In global coordinates we map,

$$X_0 = \ell_{d+1} \cosh\rho \cos\tau \tag{2.18}$$

$$X_{d+2} = \ell_{d+1} \cosh\rho \sin\tau \tag{2.19}$$

$$X_i = \ell_{d+1} \sinh\rho \hat{x}_i \tag{2.20}$$

where $i \in [1, d+1]$, $\sum_i \hat{x}_i^2 = 1$, $\tau \in [0, 2\pi]$ and $\rho \in [0, \infty)$. The corresponding metric in global coordinates is then,

$$ds^2 = \ell_{d+1}^2(-\cosh^2\rho d\tau^2 + d\rho^2 + \sinh^2\rho d\Omega_{d-1}^2) \tag{2.21}$$

To see directly that on scales much smaller than l_{AdS} the metric is approximately flat, we can also consider the static coordinates,

$$r = \ell_{d+1} \sinh \rho \tag{2.22}$$

$$t = \ell_{d+1} \tau \tag{2.23}$$

such that we can write the metric as:

$$ds^2 = -\left(1 + \frac{r^2}{\ell_{d+1}^2}\right) dt^2 + \frac{dr^2}{\left(1 + \frac{r^2}{\ell_{d+1}^2}\right)} + r^2 d\Omega_{d-1}^2 \tag{2.24}$$

Here, we see that as we consider scales $r^2/\ell_{d+1}^2 \ll 1$ we recover spherical Minkowski coordinates.

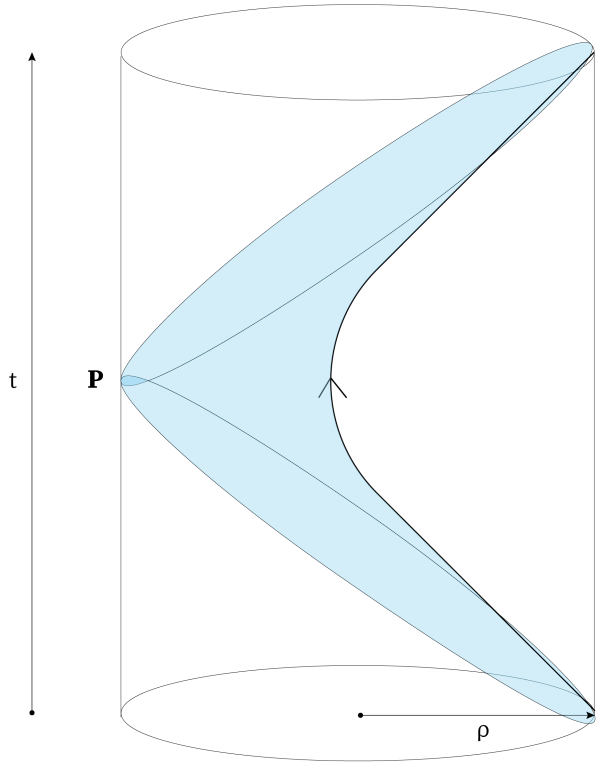

Figure 2.3: A representation of the subspace of global AdS covered by the Poincaré patch coordinates (2.30) embedded in global coordinates (2.21). The full Poincaré patch is indicated in light blue. Timeslices represent hyperbolic discs with ρ moving from 0 at the centre to $\pi/2$ at the boundary.

The Poincaré patch coordinates will often be useful to us despite only covering a finite patch of the global AdS space where $z \in [0, \infty)$. In these coordinates, we have:

$$X_0 = \frac{\ell_{d+1}^2}{2r}\left(1 + \frac{r^2}{\ell_{d+1}^4}(\ell_{d+1}^2 + \vec{x}^2 - t^2)\right) \tag{2.25}$$

$$X_{d-1} = \frac{\ell_{d+1}^2}{2r}\left(1 - \frac{r^2}{\ell_{d+1}^4}(\ell_{d+1}^2 - \vec{x}^2 + t^2)\right) \tag{2.26}$$

$$X_{d+2} = \frac{r}{\ell_{d+1}}t \tag{2.27}$$

$$X_{i<d-1} = \frac{r}{\ell_{d+1}}x_i \tag{2.28}$$

$$z = \frac{\ell_{d+1}^2}{r} \tag{2.29}$$

In these coordinates, the timelike conformal boundary is located at $z = 0$ and the metric is given by,

$$ds^2 = \frac{\ell_{d+1}^2}{z^2}\left(-dt^2 + dz^2 + dx_\mu dx^\mu\right) \tag{2.30}$$

where $\mu \in [1, d-1] \in \mathbb{Z}$. The region of the full AdS space covered by the Poincare coordinates can be seen in Figure 2.3. In general, we will be interested in non-vacuum solutions which are asymptotically $\mathrm{AdS}_{d+1} \times \mathcal{M}$ (where $\mathcal{M}$ is compact) such that near the boundary $z = 0$ the space is locally identical to the vacuum solution.

2.3.2 Conformal Field Theory

Conformal field theories (CFTs) are a subset of QFTs which exhibit conformal symmetry. Conformal transformations are given by changes of coordinate $x^\mu \longrightarrow y^\mu$ such that,

$$g'_{\rho\sigma}(y) = \frac{\partial x^\mu}{\partial y^\rho}\frac{\partial x^\nu}{\partial y^\sigma}g_{\mu\nu}(x) = \Omega(x)g_{\rho\sigma}(x) \tag{2.31}$$

where $\Omega(x)$ is referred to as the Weyl factor. A conformal transformation can therefore be considered as a particular type of diffeomorphism which changes the metric up to some Weyl factor. Physically, conformal transformations locally preserve angles and shapes but change scale and curvature.

The conformal group is isomorphic to $SO(2, d)$ which we note is the same group structure of the embedding space $\mathbb{R}^{(2,d)}$ inherited by AdS_{d+1}. As the two spaces share the same group structure, the bottom-up duality can be easily shown by making the appropriate transformations from the generators of the embedding space(53)(27). The group $SO(2, d)$ has four generators:

1. P^μ which generates spacetime translations

$$x^\mu \longrightarrow x^\mu + \alpha^\mu \tag{2.32}$$

where α is some constant vector.

2. $J_{\mu\nu}$ which generates boosts and rotations:

$$x^\mu \longrightarrow \Lambda^\mu_\nu x^\nu \tag{2.33}$$

where Λ^μ_ν is a Lorentz transform.

3. D which generates dilations that rescale the system,

$$x^\mu \longrightarrow \lambda x^\mu \tag{2.34}$$

where λ is some scalar.

4. $K_{\mu\nu}$ which generate the special conformal transformations (SCTs):

$$x^\mu \longrightarrow \frac{x^\mu + \alpha^\mu x^2}{1 + 2\alpha^\mu x_\mu + \alpha^2 x^2} \tag{2.35}$$

The first two generators form the familiar Poincaré group, dilations simply rescale the system and the SCTs can be understood as an inversion of x^μ such that $x^\mu \longrightarrow x^\mu/x^2$ followed by a translation α^μ and a second inversion(55)(56). SCTs are not globally defined as the denominator in (2.35) can go to zero and therefore additional points must be added. In the case of two dimensions we can use the identification that on the Euclidean plane $\mathbb{R} \simeq \mathbb{C}$. In order to make the SCTs globally defined, we can include a point at infinity such that we conformally compactify $\mathbb{R}^2$ to get $S^2 \simeq \mathbb{C} \cup \{\infty\}$. The case of two dimensional Euclidean space is a special one in which the algebra of conformal transformations is infinite dimensional. The two dimensional case then has an additional set of constraints allowing for exact solutions.

Returning to the arbitrary dimensional case, we can represent the conformal group by the explicit generators,

$$P_\mu = -i\partial_\mu \tag{2.36}$$

$$J_{\mu\nu} = i(x_\mu \partial_\nu - x_\nu \partial_\mu) \tag{2.37}$$

$$D = -ix_\mu \partial^\mu \tag{2.38}$$

$$K_\mu = i(x^2 \partial_\mu - 2x_\mu x\nu \partial^\nu) \tag{2.39}$$

The non-vanishing commutators of the generators are given by:

$$\begin{gathered}\left[D, P_\mu\right] = iP_\mu, \quad \left[D, K_\mu\right] = -iK_\mu, \quad \left[K_\mu, P_\nu\right] = 2i\left(\eta_{\mu\nu}D - J_{\mu\nu}\right) \\ \left[K_\mu, J_{\nu\rho}\right] = i\left(\eta_{\mu\nu}K_\rho - \eta_{\mu\rho}K_\nu\right), \quad \left[P_\rho, J_{\mu\nu}\right] = i\left(\eta_{\rho\mu}P_\nu - \eta_{\rho\nu}P_\mu\right) \\ \left[J_{\mu\nu}, J_{\rho\sigma}\right] = i\left(\eta_{\nu\rho}J_{\mu\sigma} + \eta_{\mu\sigma}J_{\nu\rho} - \eta_{\mu\rho}J_{\nu\sigma} - \eta_{\nu\sigma}J_{\mu\rho}\right)\end{gathered} \tag{2.40}$$

where $\eta_{\mu\nu}$ is the Minkowski metric.

The most interesting class of operators in CFTs are those which transform under dilations, $x^\mu \longrightarrow \lambda x^\mu$ as

$$\mathcal{O}_\Delta(\lambda x) = \lambda^{-\Delta}\mathcal{O}_\Delta(x) \tag{2.41}$$

where we refer to Δ as the conformal scaling dimension of the operator $\mathcal{O}_\Delta$. These operators are referred to as primary operators. From each primary operator, we can take n derivatives to obtain another primary operator, $\partial^n\mathcal{O}_\Delta$, which we refer to as a descendent. Each derivative can be thought of as a introducing an additional energy dimension to the original primary field such that the scaling dimension of the n-th descendent is $\Delta + n$ and under dilatations they scale as $\lambda^{\Delta-n}$.

Another useful feature of CFTs is that we can deduce correlation functions quite easily from their symmetry properties alone. For example, it can be shown that the time ordered two-point function of primary operators is constrained by

$$\langle\Psi|\,\mathcal{T}\left[\mathcal{O}_{\Delta_2}(x_2, t_2)\mathcal{O}_{\Delta_1}(x_1, t_1)\right]|\Psi\rangle = \frac{C_{12}\delta_{\Delta_1,\Delta_2}}{\left(|x_2 - x_1|^2 - (t_2 - t_1)^2 + i\epsilon\right)^{\Delta_1}} \tag{2.42}$$

where C_{12} is some constant. This property does not rely on the existence of a Lagrangian for the theory and can be used to obtain non-perturbative results. This process is referred to as the 'Conformal Bootstrap'.

A crucial feature of CFTs is that the complete set of their primary operators (including descendants) form a basis for the CFT living on S^{d-1}. If, for example, we centre a Euclidean ball about the operator and perform a path integral on it we can obtain a state such that there exists a bijective map between operators in the CFT and states. This relationship is the so called state-operator correspondence and forms a crucial role in the AdS/CFT correspondence. For every such primary operator in the CFT, there must exist a primary state $\mathcal{O}_\Delta(x)$ obeying,

$$[D, \mathcal{O}_\Delta(x)] = i\Delta\mathcal{O}_\Delta(x); \quad [K_\mu, \mathcal{O}_\Delta(x)] = 0 \tag{2.43}$$

In the following, we shall see that we can draw mathematically precise relationships between

states in the bulk of AdS spaces and primary operators which reside on the light-like conformal boundary in one lower dimension.

2.3.3 The AdS/CFT Dictionary

Armed with a familiarity with both AdS and CFTs we can formally state the AdS/CFT correspondence (57)(27):

A relativistic conformal theory on $\mathbb{R} \times S^{d-1}$ *is equivalent to a theory of quantum gravity existing in a bulk* $AdS_{d+1} \times \mathcal{M}$ *spacetime, where* $\mathcal{M}$ *is a compact manifold.*

We may make this conceptually and mathematically precise through the so-called AdS/CFT Dictionary. It must be noted, however, that whilst we have a 'dictionary' it is often difficult to form full sentences as we do not yet have a rigorous way to reconstruct systems calculated in one description from its dual.

A direct mathematical statement follows from this correspondence, namely, that the Hilbert space of the CFT and that of the quantum gravitational theory in the bulk are equivalent,

$$\mathcal{H}_{QG} = \mathcal{H}_{CFT} \tag{2.44}$$

Therefore, states in the bulk are in one-to-one correspondence with local operators (including descendants) in the CFT. A corollary of this is the GKP-Witten relation(58)(49), which states that thermodynamic quantities such as partition functions Z at inverse temperature $\beta = \frac{1}{T}$ must also agree,

$$Z_{QG}(\beta) = Z_{CFT}(\beta) = \mathrm{Tr}\, e^{-\beta H_{CFT}} = \mathrm{Tr}\, e^{-\beta H_{QG}} \implies H_{CFT} = H_{QG} \tag{2.45}$$

A direct consequence is that unitary boundary CFTs are dual to unitary bulk descriptions. This fact is encouraging in the context of the BHIP and we shall return to it in due course.

As argued in Chapter 2.3.1, the light-like conformal boundary of AdS_{d+1} has the topology $\mathbb{R} \times S^{d-1}$ which can be seen by taking (2.30) in the limit $z \longrightarrow 0$. To describe the spectrum of the CFT defined on this boundary, we consider the dilaton operator in Euclidean space. We can perform a conformal transformation of this d-dimensional cylinder by taking $\rho \longrightarrow e^{\tau}$,

$$ds^2 = d\rho^2 + \rho^2 d\Omega_{d-1}^2 = e^{2\tau}(d\tau^2 + d\Omega_{d-1}^2) \tag{2.46}$$

From this, we see that the dilations $\rho \longrightarrow e^{\alpha}\rho$ are equivalent to time translations on $\mathbb{R} \times S^{d-1}$ and therefore the dilaton acts as the Hamiltonian for the CFT on S^{d-1}. To obtain the eigenspectrum of the CFT, we must need only diagonalise the dilaton operator. We note that the UV singularities in the CFT correspond to IR divergences in the bulk due to the infinite volume of the AdS space.

Strongly coupled systems in the CFT then correspond to weakly coupled systems in the bulk[14]. Furthermore, taking this particular transformation ensures that the boundary is flat and therefore non-gravitational[15].

Another tool in this dictionary is the field/operator correspondence. Whilst the general details depend upon which string theory one is working with in the top-down approach, there are some common results which are informative(52)(27). One such example is that the bulk metric $g_{\mu\nu}$ is dual to the stress-energy tensor $T_{\mu\nu}$ of the boundary CFT. The stress-energy tensor is a quasi-primary field with conformal dimension $\Delta_{T_{\mu\nu}} = d$ and is a conserved quantity, $\partial_\mu T^{\mu\nu} = 0$. Likewise, continuous global symmetries of the boundary CFT generate a Noether current J_μ with conformal dimension $\Delta_{J_\mu} = d - 1$ which is dual to a $U(1)$ symmetry in the bulk. Therefore, J_μ in the CFT generates spin-1 gauge fields A_μ in the bulk. Because mass breaks conformal symmetry, the current A_μ is only conserved for massless excitations. We can then consider a scalar field, ϕ in the bulk which is dual to a scalar primary operator $\mathcal{O}$ in the CFT for which we have the relation

$$\lim_{r\to\infty} r^{\Delta_\phi}\phi(t, r, \Omega) \equiv \mathcal{O}(t, \Omega) \tag{2.47}$$

where the conformal dimension, Δ_ϕ is related to the mass of the scalar field, m, by

$$\Delta_\phi = \frac{1}{2}\left(d + \sqrt{d^2 + 4m^2}\right) \tag{2.48}$$

Therefore, the boundary value of the scalar field (ϕ), the metric ($g_{\mu\nu}$) and the spin-one gauge field (A_μ) source the primary field ($\mathcal{O}$), the stress-energy tensor ($T_{\mu\nu}$) and the current (J_μ) respectively.

To calculate correlation functions for the CFT using the bulk gravitational theory we can simply evaluate correlation functions of the scalar field at the boundary[16],

$$\langle\Omega|\,\mathcal{O}_1(x_1)\ldots\mathcal{O}_n(x_n)\,|\Omega\rangle_{CFT} = \lim_{\rho\to\pi/2}\langle\Omega|\,\phi_1(\rho, x_1)\ldots\phi_n(\rho, x_n)\,|\Omega\rangle_{QG} \tag{2.49}$$

The expectation value in this case is computed for the ground state of the CFT on S^{d-1}. Similarly, for equilibrium configurations we can make use of the thermal partition function by taking the usual variational derivatives with respect to bulk sources at the boundary,

$$\langle\Omega|\,\mathcal{O}_1(x_1)\ldots\mathcal{O}_n(x_n)\,|\Omega\rangle_{CFT} = \frac{\delta^n}{\delta\phi(x_1)\ldots\delta\phi(x_n)} Z_{CFT}[\phi]|_{\phi=0} \tag{2.50}$$

[14]This property is one of the main reasons AdS/CFT is so useful. For strongly coupled systems such as those involving strong force interactions, we can treat the system perturbatively in the gravitational dual whilst in the CFT theory the quarks are confined and perturbation theory breaks down.

[15]It is worth noting that we have once again assumed that we can go to Euclidean space by Wick rotating and, mentioned previously, this is not always possible outside of static cases. This need not worry us for the vacuum case and furthermore the logic follows analogously in the Lorentzian signature.

[16]Up to some divergent quantity. These divergences will be revisited in more detail in Chapter 3

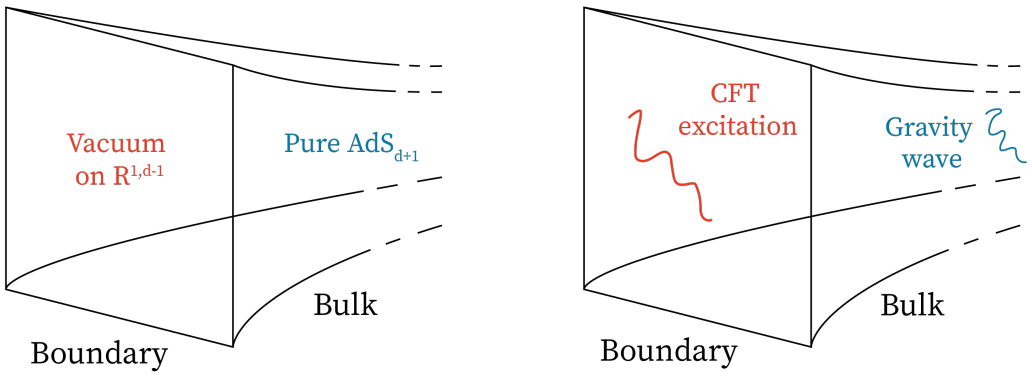

Figure 2.4: (Left) The vacuum state of the CFT on $\mathbb{R}^{1,d-1}$ is dual to a pure AdS_{d+1} bulk spacetime (Right) CFT excitations correspond to bulk excitations such as gravitons or gauge fields. Figure inspired by (59)

.

where ϕ is evaluated at $\rho = \pi/2$.

Earlier, we noted that in general UV and IR divergences emerge without inserting appropriate cut-offs. Suppose we have a finite set of primary CFT operators $\mathcal{O}_i$[17] and a local bulk effective action, $S_{eff}[\phi_i, \epsilon]$, with a UV cutoff such that $\frac{1}{l_{AdS}} \ll \epsilon < \frac{1}{l_{plank}}$. We can then state that the CFT has a semi-classical dual provided,

$$\langle \Omega | \mathcal{O}_1(x_1) \dots \mathcal{O}_n(x_n) | \Omega \rangle_{CFT} = \int \mathcal{D}\phi_i e^{iS_{eff}[\phi_i,\epsilon]} \mathcal{O}_1(x_1) \dots \mathcal{O}_n(x_n) \tag{2.51}$$

The bulk fields in this case must obey asymptotic AdS boundary conditions. We further note that not all CFTs admit a well-defined semi-classical description which can be approximated by Einstein's equations when we go to the deep IR. For example, in Chapter II we encounter a model in which the the holographic CFT is coupled to a defect (dCFT), inducing a higher-derivative gravity theory rather than Einstein gravity.

So far we have provided several useful tools which allow us to make use of the AdS/CFT correspondence. In the following chapter, we will elaborate on precisely how we can connect this correspondence to more interesting states in the bulk and how this effects the geometry of the boundary CFT.

2.4 Thermal States in AdS

In the previous chapter we outlined some key definitions in the AdS/CFT dictionary. We now discuss how thermal states in the AdS bulk manifest in the AdS/CFT correspondence. From the

[17] These need not be scalar and could include gauge fields such as gravitons.

GKP-Witten relation (2.45), thermal states in the bulk correspond to thermal states in the CFT. Most importantly, this duality will also allow us to describe black holes in AdS as well as their formation and evaporation allowing us to gain valuable insight into the BHIP in the context of asymptotically AdS spaces. Entanglement plays a crucial role in the following discussion. By purifying a thermal CFT state we can construct a pure CFT state dual to a double-sided AdS black hole. This purified state is referred to as the Thermofield Double State (TFD) and allows us to simplify calculations in the pure state and retrieve our initial values by tracing out the purifying state at the end(52). To cap off this chapter, we shall see how the tools developed offer an heuristic solution to the BHIP.

2.4.1 Black Holes in AdS

From the perspective of the dual CFT, the excited states on the boundary correspond to non-trivial AdS geometries in the bulk which can be found using the Einstein equations. In the simplest example of such an excitation is the thermal state of the CFT_d which is dual to a black hole in the AdS_{d+1} bulk. The simplest AdS black hole is described by the familiar Schwarzschild black hole (SAdS) embedded in an asymptotically AdS space. There exist two such black hole solutions, the planar black hole and the spherically symmetric solution both of which have simple interpretations on the CFT dual.

In the Einstein static universe where our CFT resides on $\mathbb{R}^{d-1}$, the ground state bulk spacetime is given by the global AdS metric (2.24). The excited states in this case correspond to the spherically symmetric global solutions in the bulk with metric

$$ds^2 = -f(r)dt^2 + \frac{dr^2}{f(r)} + r^2 d\Omega_{d-1}^2; \quad f(r) = 1 + \frac{r^2}{l_{d+1}^2} - \frac{r_h^{d-2}}{r^{d-2}}\left(1 + \frac{r_h^2}{l_{d+1}^2}\right) \tag{2.52}$$

where r_h is the position of the black hole horizon and is determined by the mass of the black hole. Using the previously detailed techniques, the temperature of the black hole can be related to the horizon radius by

$$T = \frac{1}{4\pi\ell_{d+1}}\left(d\frac{r_+}{\ell_{d+1}} + (d-2)\frac{\ell_{d+1}}{r_+}\right) \tag{2.53}$$

It is worth noting that such black holes only exist above a minimum temperature, $T > T_{min} = \frac{\sqrt{d(d-2)}}{2\pi\ell_{d+1}}$. This critical temperature is referred to as the Hawking-Page Transition(60), below which small black holes are thermodynamically unstable and will quickly evaporate. Correspondingly, only large (or eternal) black holes with $r_h > \sqrt{\frac{d-2}{d}}\ell_{d+1}$ dominate the globally[18].

[18]Physically, we recall that lightlike paths are reflected by the AdS boundary in finite proper time such that the lightlike Hawking radiation coming from a large enough black hole will simply bounce back into the black hole and it reaches equilibrium.

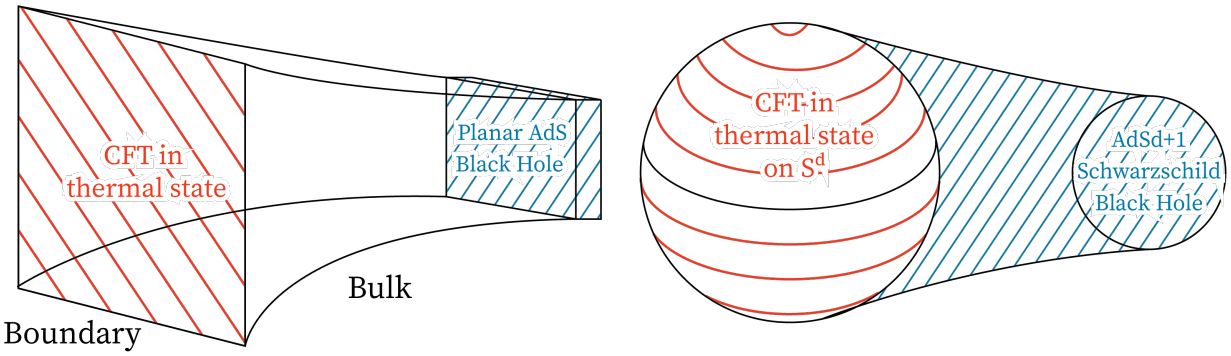

Figure 2.5: Constant time Cauchy slices corresponding to (a) The thermal excitation of the Minkowski CFT_d state corresponds to a planar black hole defined in the Poincaré patch (b) Thermal excitation of the CFT_d state on a the cylinder corresponds to a spherical black hole in the global AdS bulk. Figure inspired by (59).

We may also be interested in limiting to excitations of the Poincaré patch of the AdS_{d+1} whose CFT_d dual exists on a Minkowski spacetime $\mathbb{R}^{d-1,1}$. These excitations correspond to the planar SAdS_{d+1} given by:

$$ds^2 = \frac{\ell_{d+1}^2}{z^2}\left(-f(z)dt^2 + d\vec{x}_{d-1}^2 + \frac{dz^2}{f(z)}\right); \quad f(z) = 1 - \frac{z^d}{z_+^d} \tag{2.54}$$

where z_+ is the location of the horizon and its temperature is

$$T = \frac{d}{4\pi z_+} \tag{2.55}$$

In the limit that $r_h \gg \ell_{d+1}$ the curvature of the spacelike sphere in global coordinates becomes negligible at the black hole horizon and (2.50) reduces to (2.52).

Of particular interest to us is the SAdS_3 or BTZ (61) solution,

$$ds^2 = -\frac{r^2 - r_h^2}{\ell_3^2}dt^2 + \frac{\ell_3^2 dr^2}{r^2 - r_h^2} + r^2 d\phi^2 \tag{2.56}$$

where $\phi \in [0, 2\pi]$. The boundary of the global BTZ black hole is then $S^1 \times \mathbb{R}$. We can, consider several interesting cases of the BTZ black hole:

1. For $r_h \gg l_3$ can decompactify the BTZ solution by taking $\phi \longrightarrow \frac{x}{l_3}$ to find the planar BTZ black hole.

2. We can analytically continue such that $r_h = i\ell_3$ to find the global AdS solution. Since we obtain the black hole solution by making identifications (ie. quotienting the space by an isometry), this makes sense.

3. Solutions with $r_h = i\ell_{AdS}\sqrt{1-\mu}$ where $\mu \in [0,1)$ describe conical defects (horizon free singularities). Conical singularities, also referred to as cosmic strings, can be thought of as the geometry backreacting against the presence of some energy $\propto \mu$.

In the remainder of this thesis, we shall further elaborate on the BTZ black hole and a specific model of a quantum corrected BTZ solution.

2.4.2 Purification and the Thermofield Double State

We may further detail QIT-gravity connection through the thermofield double (TFD). The TFD allows us to purify a thermal state of the boundary CFT dual to a double sided black hole.

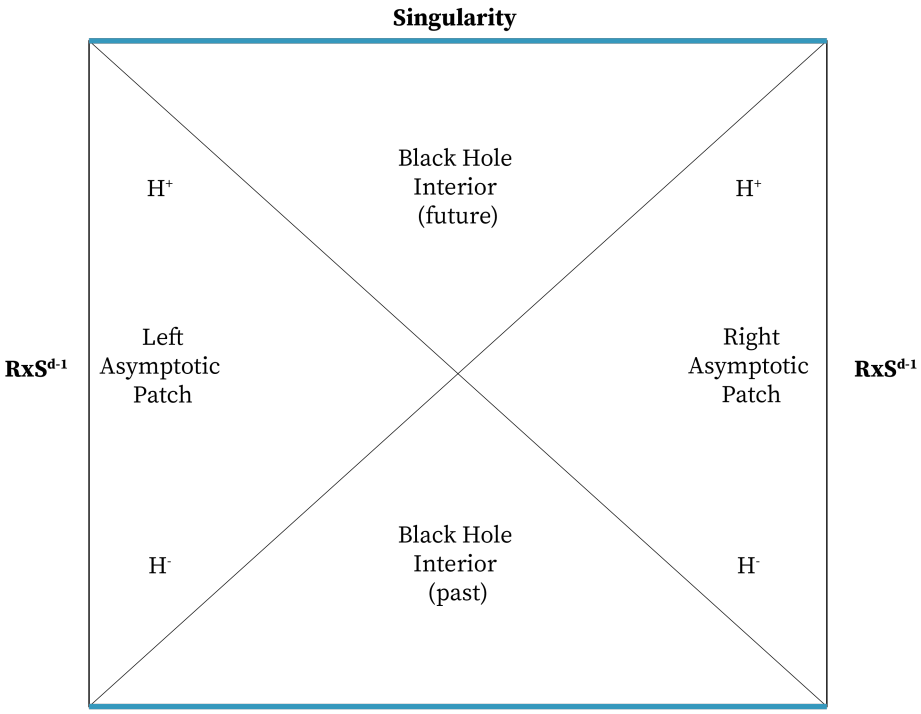

Figure 2.6: The Penrose diagram of the global SAdS solution with the future/past horizons given by $\mathcal{H}^{\pm}$. The topology of the boundary in these coordinates is $\mathbb{R} \times s^{d-1}$ as we would expect.

One can find the Penrose diagrams in the usual manner described in standard books on general relativity (62)(63). The Penrose diagram for a large maximally extended black hole is divided by the presence of the black hole horizon into four patches:

1. **Right Asymptotic Region (Region 1):** Future oriented lightcones can either asymptotically reach the vacuum AdS solution on the right boundary or fall into the black hole.

2. **Black Hole Interior (Region 2):** All future oriented lightcones hit the black hole singularity.

3. **Left Asymptotic Region (Region 3):** Future oriented lightcones can either asymptotically reach the vacuum AdS solution on the left boundary or fall into the black hole.

4. **White Hole Interior (Region 4):** Future oriented lightcones can reach Regions 1 and 2. This region also contains the past spacetime singularity of the black hole.

In the previous chapter, we showed that AdS black holes are dual to thermal states of the boundary CFT. As it is generally easier to work with pure states, we would like some way to purify these thermal states. In section 1 we discussed that any mixed state can be purified by introducing an auxiliary system such the original state can be found by tracing out the purification state.

Maldacena was the first to apply this observation in the context of black holes by showing that the maximally extended black hole solution is dual to the TFD(64). The TFD consists of an entangled state of two non-interacting, identical copies of the boundary CFT living on the asymptotic boundary regions (Regions 1 and 2 in Figure 2.6). The TFD state, $|\psi\rangle_{TFD}$ is

$$|\psi\rangle_{TFD} = \sum_i \frac{e^{-\beta E_i/2}}{\sqrt{Z(\beta)}} |E_i\rangle_L \otimes |E_i\rangle_R \tag{2.57}$$

where $Z(\beta) = \sum_i e^{-\beta E_i}$ and $|E_i\rangle_{R/L} \in \mathcal{H}_{R/L}$ is an energy eigenstate with eigenvalue E_i corresponding to the CFT on the right (left) boundary. Applying the GKP-Witten conjecture, the thermal partition function of the bulk quantum gravity theory corresponds to that of the boundary CFT, $Z_{QG}[\mathcal{M}; \partial\mathcal{M} = \Sigma] = Z_{CFT}[\Sigma]$. Since the spacetime is static, we can go to Euclidean signature without issue and compactify along the τ direction $\tau = \tau + \beta$ such that the topology of its boundary is $S_\beta \times S^{d-1}$.

As a sanity check, let us consider the density matrix of the TFD, ρ_{TFD},

$$\rho_{TFD} = \sum_{i,j} \frac{e^{-\beta(E_i+E_j)/2}}{Z(\beta)} |E_i\rangle_L \otimes |E_i\rangle_R \left\langle E_j\right|_L \otimes \left\langle E_j\right|_R \tag{2.58}$$

Tracing out the left system to returns the original thermal state,

$$\rho_{TFD} = \sum_n \langle n|_L \left(\sum_{i,j} \frac{e^{-\beta(E_i+E_j)/2}}{Z(\beta)} |E_i\rangle_L |E_i\rangle_R \left\langle E_j\right|_L \left\langle E_j\right|_R \right) |n\rangle_L \tag{2.59}$$

$$= \sum_i e^{-\beta E_i} |E_i\rangle_R \langle E_i|_R = e^{-\beta H_R} \tag{2.60}$$

where n is some index of orthogonal basis states and H_R is the Hamiltonian of the right CFT. We have therefore illustrated that the original state is indeed thermal. Using the cyclicity of the

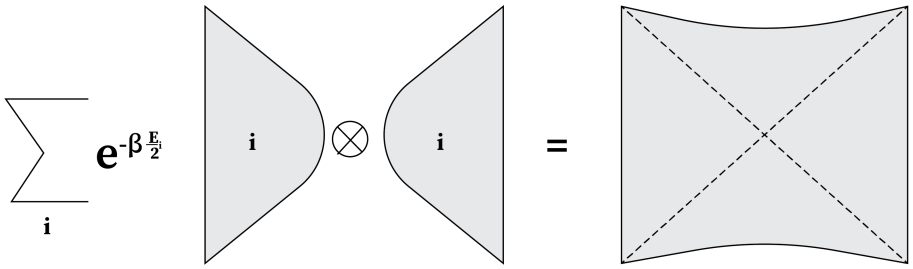

Figure 2.7: A schematic representation of the TFD. Entangling two non-interacting copies of the boundary CFT in the a thermal state is holographically dual to a maximally extended double sided SAdS geometry.

trace can therefore compute thermal expectation values of operators $\mathcal{O}_R$ defined on the right CFT as an expectation value of an operator in the TFD,

$$\langle \mathcal{O}_R \rangle = \mathrm{Tr}[\rho_R \mathcal{O}_R] = \langle \psi_{TFD} | \mathcal{O}_R | \psi_{TFD} \rangle \tag{2.61}$$

If the TFD Hamiltonian is time independent then

$$H_{TFD} = H_R - H_L \tag{2.62}$$

where H_L has an opposite sign due to the fact that the timelike killing vector on the left asymptotic patch runs with opposite orientation to that of the right.

It is worth reiterating some subtle points on the surprising nature of the gravitation TFD. We have managed to create a pure gravitational state made of two non-interacting CFTs which must correspond to completely distinct asymptotically AdS spacetimes. The individual terms in the TFD (2.57) are entirely independent, however, the quantum superposition of these states correspond to the two-sided black hole where both sides are smoothly connected by a classical wormhole. What is remarkable about this is that we can create a connected spacetime by entangling degrees of freedom from two non-interacting gravitational systems together to create a new smooth geometry. This set-up is especially useful for the analysis of entanglement and entanglement spreading in holographic settings. Notably, this set-up has a very specific entanglement structure which is can be destroyed by an infalling perturbation as we discuss in Part III.

2.4.3 Shockwaves

Due to the special entanglement structure of the TFD, the time-evolved thermofield double depends only on the combination $t_L + t_R$, where L and R indicate time evolution on the left side and the right side respectively. Let us suppose that the L side is the original system in which

time runs forwards and the R side is a copy in which time runs backwards. For the unperturbed TFD in the infinite temperature limit, the TFD simply corresponds to many entangled pairs and therefore there exists a large mutual information between regions L and R. If we allow time to evolve on the left hand side, the initially localised entanglement spreads in space and the $L-R$ mutual information decreases. Suppose we evolve the L system back to time $t_L = -t_W$ and apply a simple operator W_x and then evolve the system back to time $t_L = 0$ such that the system is the same but with some small perturbation in the past. If we suppose that this perturbation happens in the distant past such that $t_W \gg \beta$, one may wonder what impact this has on the entanglement structure of the system. Neither the L or R system will note any significant differences. In other words, we suppose that in the distant past, we throw some localised probe into the black hole from the left and leave the right unperturbed. Assuming that the perturbation on the left hand side has a rest frame energy, E, that is small compared to the mass of the black black hole, M, this probe will only have a small local effect on the system. The memory of this effect, such as which operator W_x we applied will be lost at large t_W and hence its effect will not be visible to simple probes at $t_L = 0$. In fact, the boost ambiguity allows us to go to a frame in which the energy is small and hence we have no reason to expect any large local invariants.

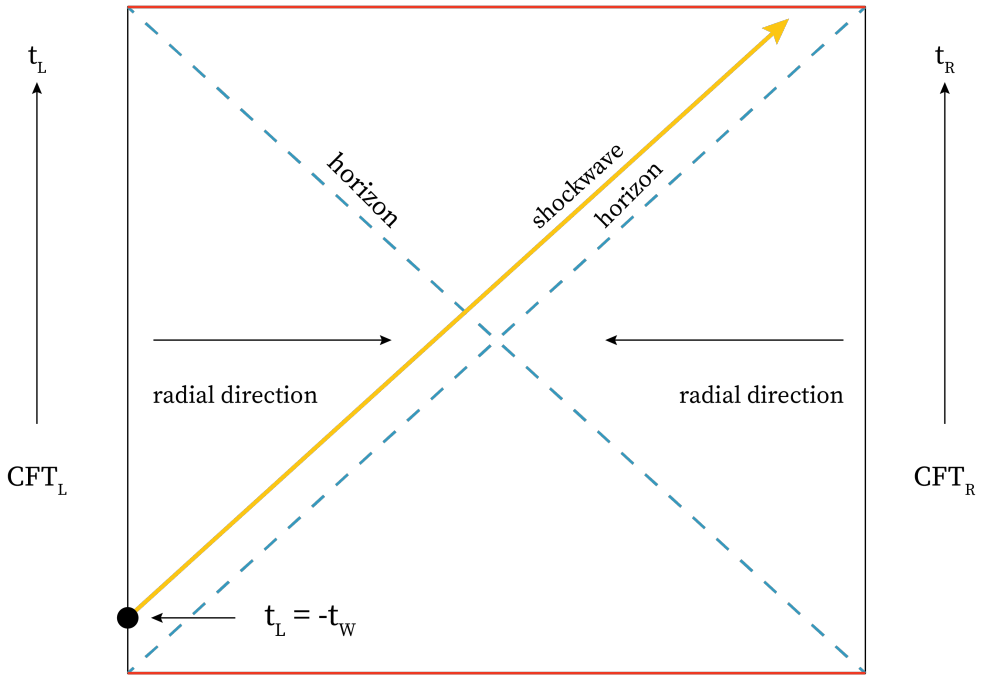

Figure 2.8: A Penrose diagram of the shockwave setup. We have emphasized the distance of the infalling perturbation (yellow) from the horizon for the sake of clarity, but as t_W is increased then it will hug the horizon, causing a shockwave at $t = 0$.

There must, however, be some significant clue as to its presence. If we take $t_W \longrightarrow \infty$, then the probe will fall close to the black hole horizon at the $t_L = 0$. According to the local frame at $t_L = 0$, this probe has been accelerating towards the black hole for such a long time that it will appear to be travelling close to the speed of light and hence its energy is blue shifted according to a stationary observer outside the horizon.

We can explicitly write the metric in the Kruskal coordinates. We start with a generic metric of the form,

$$ds^2 = -f(r)dt^2 + f^{-1}(r)dr^2 + r^2 d\phi^2 \tag{2.63}$$

We assume that there exists some horizon radius r_h defined by the positive root of $f(r)$. We can then pass to Kruskal coordinates

$$ds^2 = -\frac{f(r)}{f'(r_h)^2} e^{-f'(r_h)r_*(r)} du dv + r^2 d\phi^2 \tag{2.64}$$

which in three dimensions gives

$$ds^2 = \frac{-4\ell_3^2 du dv + r_h^2(1-uv)^2 d\phi^2}{(1+uv)^2} \tag{2.65}$$

such that the right exterior has $u < 0, v > 0$, the boundaries are at $uv = -1$ and the singularities are at $uv = 1$. We define the tortoise coordinate as $r_* = \int dr f^{-1}(r)$ and $uv = e^{f'(r_h)r_*(r)}$ and $u/v = -e^{-f'(r_h)t}$. In these coordinates, a translation in t corresponds to a boost in the Kruskal coordinates and so the energy of the probe as it hits the horizon at $t_L = 0$ is given by:

$$E_p \approx \frac{E\ell_3}{r_h} e^{r_h t_W/\ell_3^2} \tag{2.66}$$

According to the frame at $t_L = 0$, the probe appears as a high energy shockwave following an effective null trajectory and hence its backreaction must be taken into account. To do so, we construct a perturbed metric by gluing the unperturbed metric with mass M and the perturbed metric with mass $M + E$ along the null surface defined by $u = u_W = e^{-r_h t_W/\ell_3}$. We define the coordinates to the right of the shell to be u, v and those to the left of the shell to be $\tilde{u}, \tilde{v}$. The change in mass induces a change in the radius,

$$\tilde{r}_h = \sqrt{\frac{M+E}{M}} R \tag{2.67}$$

The relative boost ambiguity between tilded and non-tilded coordinates can be fixed by demanding that the time coordinate flows continuously at their boundary. The location of the shell is then determined by $\tilde{u}_W = e^{-\tilde{r}_h t_W/\ell_3^2}$. We further demand the radius of the S^1 generated by rotations

about ϕ to have a constant radius across the shell,

$$\tilde{r}_h \frac{1 - \tilde{u}_W \tilde{v}}{1 + \tilde{u}_W \tilde{v}} = r_h \frac{1 - u_W v}{1 + u_W v} \tag{2.68}$$

For small E/M we make the ansatz,

$$\tilde{v} = v + \alpha; \quad \alpha = \frac{E}{4M} e^{r_h t_W / \ell_3^2} \tag{2.69}$$

where for fixed α, $E/M \longrightarrow 0$ and $t_W \longrightarrow \infty$ this relationship becomes exact. Assuming the perturbation happens for $T_W \gg \beta$ we can shift the coordinates, $U = u$ and $V = v + \alpha\theta(u)$, where $\theta(u)$ is the Heaviside theta function. The metric then takes the standard shockwave form

$$ds^2 = \frac{-4\ell_3^2 dU dV + 4\ell_3 \alpha \delta(U) dU^2 + r_h^2 (1 - UV)^2 d\phi^2}{(1 + UV)^2} \tag{2.70}$$

This geometry is continuous, however the presence of the impulsive curvature at $U = 0$ means that its first derivative is not. The Einstein equations imply a stress tensor,

$$T_{uu} = \frac{\alpha}{4\pi G_N} \delta(u) \tag{2.71}$$

the interpretation of which is a shell of null particles distributed across the horizon. By examining the mutual information between the boundary subregions, (15) illustrated that the mutual information between equally sized regions on the L and R CFT, A and B respectively, is destroyed by the propagation of the shockwave. For small regions where $\sinh(r_h \phi / 2\ell_{d+1}) < 1$, the mutual information is zero for all values of α. For larger regions and small α, the mutual information becomes positive and is given by

$$I(A; B) = \frac{\ell}{G_N} \left[\log \left(\sinh \frac{\pi \ell_3}{\beta} \right) - \log \left(1 + \frac{E\beta}{4 S_{BH} e^{2\pi t_W / \beta}} \right) \right] \tag{2.72}$$

where S_{BH} is the Bekenstein-Hawking entropy of the black hole. The mutual information is then a monotonically decreasing function of t_W. In the high-temperature limit, $I(A; B) \longrightarrow 0$ when t_W approaches

$$t_*(\phi) = \frac{\phi \ell_3}{2} + \frac{\beta}{2\pi} \log \frac{2 S_{BH}}{\beta E} \tag{2.73}$$

Assuming large N on the boundary CFT, we have a large entropy $S_{BH} \approx N^2$ and we can take the smallest reasonable energy value, $E \approx T = 1/\beta$ such that correlations between L and R are destroyed when

$$t_* \approx \frac{\beta}{2\pi} \log S_{BH} \tag{2.74}$$

where t_* is defined as the fast scrambling time. Physically, the scrambling time is the time that

it takes for the effect of the perturbation to become of order one and gives us a notion of how long it takes a system to effectively forget the perturbation. This result suggests that black holes are the fastest scramblers in nature (65). We return to this set-up later when investigating how chaos spreads in holographic systems.

Chapter 3

Quantum Extremal Surfaces

Through our discussion of the BHIP we were able to discern that the semi-classical approximation was a poor candidate theory of quantum gravity. To resolve the paradox, it would therefore appear that we must be precise in how we define quantum information and its relation to gravity.

The holographic principle implies that bulk geometries can be encoded in a higher dimensional non-gravitational space. More explicitly, the AdS/CFT dictionary provides us with a precise sense in which this is true. Making use of this toolbox we can directly relate information on the boundary theory to bulk structures living in the asymptotically AdS spacetimes. One can then view particular configurations of the CFT state as corresponding to the emergence of gravity in the bulk. A key ingredient in how this emergent theory of gravity is realised was related to the entanglement entropy between a region and its complement(s) (52)(66).

In Chapter 1, we worked under the assumption that we were working with a low-energy quantum mechanical description which allows us to conserve particle number and sidestep divergences. To resolve the BHIP, we then wish to extend these notions of information in quantum mechanical systems to a more general QFT description in such a way that the low energy limit returns the quantum mechanical notions of QIT. In general, however, the task of calculating entanglement entropy requires new techniques. In this section we shall elaborate upon methods in which we may calculate the entropy and, more specifically, the entanglement entropy of systems. Using such a definition leads us to the notion of entanglement islands which act as disconnected regions of space encoding the information escaping an evaporating black hole. Within asymptotically AdS space, it has been shown that for toy models the islands appear to resolve the BHIP and follow curves very close to that predicted by Page (67)(68)(69)(32). Remarkably, these islands appear to be features of several independent prescriptions by which we can calculate entanglement entropy. Using a path integral formulation, we can construct replica Euclidean wormholes which appear to encode gravitational information(69)(67). We shall also see that an equivalent description can be found using the holographic principle directly which leads to the Quantum Extremal Surfaces (QES).

Chapter 3.2 will introduce the so-called replica trick which simplifies the calculation of entanglement entropy in quantum field theories by taking n-copies of the field theory. In Chapter 3.3 we introduce the Ryu-Takayanagi (RT) conjecture directly linking entanglement entropy in the boundary to minimal surfaces in the bulk. Finally, in Chapter 3.4 we make use of these constructions to define how entanglement islands emerge and briefly discuss how they resolve the BHIP in holographic systems.

3.1 Entanglement Entropy in Quantum Field Theories

Of all techniques for calculating entanglement entropy for continuum systems, the path integral formulation is the most general approach we have. The path integral applies to general quantum mechanical systems and is by construction covariant and valid to all orders in perturbation theory for renormalizable QFTs.

In Chapter 1 we introduced some notions from QIT which allowed us to define various notions of information in quantum systems. Naturally, when we consider Lorentz invariant QFTs or semi-classical gravity, we lose some of the more intuitive interpretations of what this information is in the material sense[19]. Following Chapter 3, we saw that notions of entanglement present a fungible resource with which we may probe potential theories of quantum gravity. We wish to formally show how quantum gravity emerges from the dynamics of a CFT. In the specific context of AdS/CFT, field theories in the bulk and must correspond to local field theories on the boundary and so we are primarily interested in defining these notions of information on the boundary CFT can be mapped to its gravitational dual. The inclusion of arbitrarily high energy states in the CFT[20] means that entanglement entropies are divergent and must therefore be regulated. Intuitively, the entanglement entropy can be thought of as the number of EPR pairs which are separated across the entangling surface. In this subsection, we will discuss both general behaviour of entanglement entropy in QFTs as well as a convenient way to measure entanglement entropies in QFTs known as the Replica Trick.

3.2 The Path Integral and Replicas

To extend the QIT notions to a QFT, we need to take the continuum limit of our quantum lattice theory and specify some key constraints placed on density matrices and entanglement measures

[19] In the quantum mechanical case we retain notions which allow us to imagine that two electrons are in a Bell-state, for example. In the QFT case we must consider quantum fluctuations which contribute to the correlation functions as well as a frame dependence which, as we encountered in the discussion of the Unruh effect, prevents such neat interpretations.

[20] In the dual description this divergence is in fact a consequence of IR divergences owing to integrating over infinite distances.

for our QFTs. A discussion of these constraints can be found in Appendix A. Henceforth, we discard the operator formalism in favour of the functional integral formalism. From introductory QFT courses, we are accustomed to calculating observables by calculating Euclidean path integrals leading to Wightman Functions. In this paradigm, the temporal and spatial components are on equal footing. In the Lorentzian context, we impose temporal ordering which gives a number of possible interaction pathways which must be reflected in the final path integral. When we include non-static spacetimes in our path integral, the Euclidean prescription becomes ill-defined and more work must be done to identify appropriate saddle points. The Euclidean framework, however, is best suited to non-dynamic cases where we do not have to worry about some time-dependent interaction Hamiltonian. We can also extend the Euclidean proscription to the special cases where we calculate the observable at a moment of time reflection symmetry. For general cases, we assume that the Hamiltonian is time dependent which requires us to adopt a non-equilibrium path integral method known as the Keldysh-Schwinger (SK) formalism (70).

We define a reduced density matrix ρ_A on a Cauchy slice $\Sigma_{t=0}$ where there exists some time dependent Hamiltonian acting on the system. We can split the fields on this Cauchy slice into two sets based on their domains of dependence $\Phi(x) = \{\Phi_A(x \in A), \Phi_{A_c}(x \in \bar{A})\}$. The reduced density matrix is an operation acting on the Hilbert space $\boldsymbol{\mathcal{H}}_{\mathcal{A}}$ and its matrix elements depending on the support of $x \in A$ alone. Let us now imagine that we regulate the path integral by applying the boundary conditions for fields defined in A,

$$\Phi_A|_{t=0^-} = \Phi_-, \quad \Phi_A|_{t=0^+} = \Phi_+ \tag{3.1}$$

where $t^{\pm} = 0^{\pm}$ represents an infinitesimal approach from above (below). This is equivalent to cutting open the path integral about $t^{\pm} = 0^{\pm}$ and then projecting this result onto well defined field values. To enact this, we include a delta functional in our path integral which acts as a projection operator,

$$\rho_A^{(\pm)} = \int \left[\mathcal{D}\Phi\right] e^{-S_{QFT}[\Phi]} \delta_E\left(\Phi_{\mp,A}\right) \tag{3.2}$$

where $\delta_E\left(\Phi_{\mp,A}\right) = \delta(\Phi_A(t = 0^-) - \Phi_-)\delta(\Phi_A(t = 0^+) - \Phi_+)$.

To find the elements of our reduced density matrix, we slice open the functional integral about the region of interest A and then impose the boundary conditions just above and below this region ($A \in \Sigma_{t=0}$) and impose the boundary conditions above and below as we would in the case of trivial time evolution. We can then write out our real time dependent reduced density matrices,

$$\rho_A^{(\pm)} = \int_{J^-[\Sigma_t]} \left[\mathcal{D}\Phi_R\right]\left[\mathcal{D}\Phi_L\right] e^{iS_{QFT}[\Phi_R] - iS_{QFT}[\Phi_L]} \delta_L\left(\Phi^{\mp}_{RL,A}\right) \tag{3.3}$$

where $\delta_L\left(\Phi^{\mp}_{RL,A} = \delta(\Phi_{R,A}(t = 0^-) - \Phi_-)\delta(\Phi_{L,A}(t = 0^+) - \Phi_+)\right.$. Heuristically one can consider that

we have our right fields evolving forwards in time from the infinite past and the left handed fields evolve from $t = 0$ to the initial state.

Having successfully constructed a method by which to calculate the density matrix, we are interested in finding higher moments $(\rho_A)^n$. Using this, we may calculate the Rényi entropy which we may analytically continue to find the von Neumann entropy. This method is referred to as the replica method.

To apply the replica method, we take n-copies of our path integral for ρ_A and make some identifications. This is required as the density matrices so to apply matrix multiplication we must apply the boundary conditions $\Phi_+^{(k)} = \Phi_-^{(k+1)}$. For the static case in Euclidean time, we have:

$$\begin{aligned}(\rho_A)^n_{-+} = \int \prod_{j=1}^{n-1} d\Phi_+^{(j)} \delta(\Phi_+^{(j)} - \Phi_-^{(j+1)}) \times \\ \left[\int \prod_{k=1}^{n} \left[\mathcal{D}\Phi^{(k)}\right] \left\{ e^{-\sum_{k=1}^{n} S_{QFT}[\Phi^{(k)}]} \delta_E(\Phi^{(k)}_{\mp A}) \right\} \right]\end{aligned} \tag{3.4}$$

We see that the first integral identifies the $(n-1)$ boundary conditions we wish to impose and the second functional integral acts to replicate the path integral for the individual matrix elements.

To picture this, we should view the situation as one in which each copy of the density matrix is computed on a copy of the background spacetime. In the Euclidean case, this background spacetime would be $\mathcal{M}_{Euc}$ or in the Lorentzian case would be two copies of the causal past $J^-[\Sigma_t] \subset \mathcal{M}$ joined together along the Cauchy slice that we wish to compute our state on. One can also imagine that we are merely identifying the spacetimes together along the boundary ∂A. We can equivalently consider this to be a new manifold $\mathcal{M}_n$. Following the canonical construction from topology, we will refer to this manifold $\mathcal{M}_n$ as the n-fold branched cover of $\mathcal{M}$.

We can now compute the path integral of the theory by integrating over all the fields living on this background $\mathcal{M}_n$. We define this as the partition function

$$Z_n[A] = \mathrm{Tr}(\rho_A^n) \tag{3.5}$$

with Rényi entropy

$$S_A^{(n)} = \frac{1}{1-n} \log \left(\mathrm{Tr} \left[\frac{\rho_A}{\mathrm{Tr}\, \rho_A} \right]^n \right) = \frac{1}{1-n} \log \left(\frac{Z_n[A]}{Z_1[A]^n} \right) \tag{3.6}$$

where we have renormalised our partition function on $\mathcal{M}_n$ by dividing by the n-copies of the single sheet partition function.

As on the discrete lattice, we now wish to take the appropriate limit as $n \longrightarrow 1$. Using the

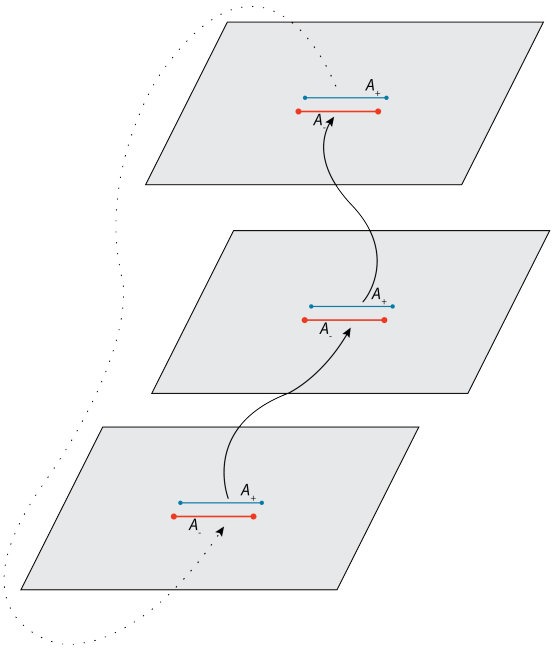

Figure 3.1: A visualization of (3.4) for $n = 3$. Identifications are indicated by arrows(19).

functional integrals we have just defined, we can take the trace by identifying $\Phi_{-}^{(1)}$ with $\Phi_{+}^{(q)}$ in the Euclidean computation to get the Rényi entropy.

The trace is a central operation to this calculation, generating a $\mathbb{Z}_n$ cyclic permutation symmetry between copies of the path integral. On the other hand, the Lorentzian case can be considered to contain $2n$-copies of the background manifold. These copies, however, are also sewn together in a way which also respects the cyclic $\mathbb{Z}_n$ replica symmetry so that we do not find any contradiction.

Finally, one can calculate the entanglement entropy itself by taking the limit that $n \longrightarrow 1$. This throws up more issues as formally, our definition is restricted to integer values of n which does not *a priori* allow us to analytically continue the argument to real values. However, if the function is defined on integers which are also well-behaved as $z \longrightarrow \pm\infty$ then we can define a unique analytic continuation away from the integers[21]. A simple example of the replica trick is provided in Appendix B.

[21]This can be shown by Carlson's theorem, which can be derived from the Phragmén-Lindelhöf principle. Carlson's theorem simply requires that functions do not grow rapidly (sub exponential) at imaginary infinity. By bounding these numbers in certain directions, these results assert that the function itself is bounded in the complex plane.

3.3 Holographic Entanglement Entropy

In AdS/CFT, the crucial entanglement entropy of a bulk subregion can be calculated simply from the entropy of the CFT region dual to it. We introduce here the Ryu-Takayanagi (RT) conjecture which posits an explicit link between the boundary region and the geometry of the bulk for static spacetimes. We then discuss the Quantum Extremal Surface (QES) prescription which allows for arbitrary order quantum corrections to the RT prescription. The QES prescription appears to provide solutions to the BHIP through the formation of disconnected regions known as islands. Discussion of the covariant HRT extension are left to Appendix C.

3.3.1 The Ryu Takayanagi Conjecture

The RT conjecture stands as one of the most useful results in AdS/CFT to date. Previously, we discussed the role of entanglement as the glue which holds spacetime together in holographic theories. From the perspective of quantum gravity, the holographic entanglement entropy (HEE) is a rich source of information which offers progress on bulk reconstruction, is generally easier to compute than the complete path integral and places stronger constraints on holographic theories through direct connection to QIT identities.

In (71) and (72), Ryu and Takayanagi conjectured that the entanglement entropy of some subregion of a CFT, A, is given by a co-dimension two minimal surface $m(A)$ projected into the bulk AdS spacetime. To find this surface, one must take the area with the smallest area over the set of all possible surfaces in the bulk which are homologous to the region A. This simple theory also provides a convenient interpretation which connects directly back to holography in that the minimal surface can be interpreted as a sort of holographic screen upon which the boundary information is projected.

Consider a constant time Cauchy slice Σ of the AdS bulk and some subset of the conformal boundary $A \subset \partial\Sigma$ with reduced matrix ρ_A. The RT formula states that the von Neumann entropy of the region A in the CFT is

$$S(\rho_A) = \frac{\mathrm{A}[m(A)]}{4G_N} \tag{3.7}$$

where $\mathrm{A}[m(A)]$ is the area of the bulk subregion homologous to A. The appropriate minimal surface must obey the conditions(52)(19)(71)(72):

1. The boundary of the minimal surface must be the same as the CFT subregion, A: $\partial A = \partial m(A)$

2. The minimal surface is homologous to A such that $A \cup m(A)$ form the boundary of some d-dimensional spacelike surface in $\mathcal{M}$

3. The minimal surface minimizes the area functional with respect to all possible surfaces $m_i(A)$: $S(\rho_A) = \min_{m_i(A)} \frac{\mathrm{A}[m_i(A)]}{4G_N}$

Suppose we have a $|\Psi\rangle$ associated with the region A of the CFT. The boundary region which encodes the dual of this state, $\mathcal{M}_\Psi \subset \mathcal{M}$ is referred to as the entanglement wedge. The entanglement wedge is denoted as the $W[A]$ and can be interpreted as the bulk domain of dependence bounded by the A and $m(A)$ (73). If one considers some local boundary perturbation, the spread of the microscopic information it contained is bounded by this entanglement wedge.

Making reference only to the geometric notions, one can prove that the HEE calculated by the RT formula obeys the desired QIT identities given in Chapter 1. In Appendix C, we detail the covariant Hubeny-Rangamani-Takayanagi (HRT) generalization of the RT formula for the sake of keeping our discussion self-contained.

3.3.2 The Quantum Extremal Surface

So far we have only defined the leading order contributions to the entanglement entropy given by the classical spacetime. For a more complete description, we wish to capture the full entanglement entropy including quantum fields in the bulk and how they backreact on the geometry. The first such attempt to incorporate these corrections was published by Faulkner, Lewkowyckz and Maldacena (FLM) who were able to incorporate first order quantum corrections (74). They found that the total entanglement entropy up to first order in a bipartite state is found by simply including the next to leading order terms by hand

$$\begin{aligned} S_{vN}[\rho_A] &= S_{RT}(\rho_A) + S_{quant}(\rho_A) \\ &= \min_{m_i(A)} \left(\frac{\mathrm{A}[m_i(A)]}{4G_N} + S_{bulk}(\rho_{\Sigma_A}) \right) \end{aligned} \tag{3.8}$$

where we define S_{bulk} as the entanglement entropy between quantum fields living on the bulk region described by the boundary region A (Σ_A) and those on the bulk region described by the boundary region $\bar{A}$ ($\Sigma_{\bar{A}}$). Higher order terms mixing the quantum fields and the classical geometry are not included at this level, nor are linear order backreactions on the geometry itself.

Let's consider the generalised entropy of a black hole,

$$S_{gen}[\rho_{BH}] = \frac{\mathrm{A}_H}{4G_N} + S_{out}(\rho_{BH}) \tag{3.9}$$

where S_{out} is the fine grained entropy of anything between the black hole horizon and the cutoff. This formulation satisfies the second law of black hole thermodynamics. The density matrix ρ_{BH} encodes the state which corresponds to the degrees of freedom in the central dogma. In the black hole context, one can imagine that the region A represents the region dual to the Hawking

radiation while the region $\bar{A}$ is the region dual to the black hole degrees of freedom. In this case, the FLM estimation of the first order quantum correction reduces to the generalised entropy and the minimal surface corresponds to the black hole horizon as expected.

Not long after the FLM proposal, Engelhardt and Wall were able to take this a step further by modifying the HRT proposal to include quantum corrections(11). In Engelhardt and Wall's conjecture, the required quantum corrected and covariant entanglement between the subregion A and its complement $\bar{A}$ is given by the minimal extremal generalised entropy $S_{gen}(\rho_\chi)$ which corresponds to the quantum extremal surface (QES) in the bulk χ,

$$S_{vN}[\rho_A] = S_{gen}(\rho_\chi) = \frac{\mathrm{A}[\chi(A)]}{4G_N} + S_{bulk}(\rho_{\chi(A)}) \tag{3.10}$$

We now return to the notion of the entanglement wedge $W[A]$ whose information is encoded in the density matrix ρ_χ which in general need not describe connected subregions. The QES must satisfy the properties:

1. The boundary of the CFT subregion A is the same as the boundary of the extremal surface $\chi(A(t))$: $\partial A(t) = \partial\chi(A(t))$.

2. The QES is homologous to $A(t)$ such that $A(t) \cup \chi(A(t))$ form the boundary of some d-dimensional spacelike surface in $\mathcal{M}$.

3. The QES must extremise the generalized entropy such that for candidate surfaces $\chi_i(A(t))$ which satisfy the previous conditions, there exists some subset of surfaces $\chi(A(t))$ for which

$$S_{gen}(\rho_\chi) = \mathrm{ext}_{\chi_i}\, S_{gen}(\rho_{\chi_i}) \tag{3.11}$$

   where $\chi \in \{\chi_{ext}\}$.

4. The QES is then defined as the extremal surface which yields the minimal generalized entropy,

$$S_{gen}(\rho_\chi) = \min_{\chi_{ext}} S_{gen}(\rho_{ext}) \tag{3.12}$$

   We can now state the full QES conjecture as

$$\begin{aligned} S_{vN}(\rho_A) &= \min_{\chi_i} \mathrm{ext}_{\chi_i}\, S_{gen}(\rho_{\chi_i}) \\ &= \min_{\chi_i} \mathrm{ext}_{\chi_i} \left[\frac{\mathrm{A}[\chi_i]}{4G_N} + S_{bulk}(\rho_{\chi_i}) \right] \end{aligned} \tag{3.13}$$

   where the extremization and minimization should be read as being with respect to the variations in the location of the co-dimension two candidate extremal surface χ_i which obeys the first two conditions.

A QES maximin prescription was proposed in (75),

$$S_{vN}(\rho_A) = \max_{\Sigma_A} \min_{\chi_i} S_{gen}[\chi_i(\Sigma_A)] = \max_{\Sigma_A} S_{gen}[\chi_{min}(\Sigma_A)] \tag{3.14}$$

where the minimization is performed over all bulk surfaces χ_i. The maximin procedure is especially useful when proving that the information theoretic properties described in Chapter 1 hold. In the following subsection we shall also touch on the QES prescription in the context of the BHIP.

3.4 Entanglement Islands

It transpires that the QES appear to provide a unitary Page Curve for the evaporation of asymptotically AdS black holes(67). Before the Page Time, t_{Page}, the QES is the empty surface but for $t > t_{Page}$, a QES forms in the interior region of the black hole (76)(77)(78) near the horizon. Therefore, the QES prescription tells us that there should indeed be a phase transition near the Page Time. The maximin prescription allows us to foliate the spacetime into Cauchy slices and consider the portion of slices which extend from the QES to the cutoff surface. The cutoff surface is simply defined in this context as the region which partitions the region which collects the Hawking radiation from the black hole. From the QES formula, we know that given a minimal QES, χ, it is possible to write the generalised entropy as

$$S_{vN}(\rho_{BH}) = \frac{\mathrm{A}[\chi]}{4G_N} + S_{bulk}(\rho_\chi) \tag{3.15}$$

where $\mathrm{A}[\chi]$ is the area of the QES.

For $t < t_{Page}$ the area term vanishes as the QES is the empty surface, ie. during early times the QES simply lies very close to the horizon. The only non-vanishing contribution is then from the bulk entropy of any fields in the entanglement wedge of the black hole $W[BH]$. This entanglement wedge contains the entirety of the black hole's interior region and extends up to the cutoff surface. Due to the evaporation of the black hole, outgoing radiation escapes the entanglement wedge of the black hole. As the Hawking radiation escapes, interior modes begin to accumulate within the entanglement wedge of the black hole which results in a steady increase in the entanglement entropy. Equivalently, we can say that the second term in (3.15) dominates.

For $t > t_{Page}$, the bulk entanglement entropy contribution becomes negligible because only a minute portion of Hawking modes are contained within the QES which lies just inside the horizon and the cutoff surface. This is a consequence of the fact that interior modes have fallen deeper than the QES and most of their outgoing partners are now far from the cutoff surface. At this point, however, the gravitational area term is non-vanishing such that we have a contribution to the entanglement entropy from the QES proportional to its area. The QES remains close to

the shrinking horizon of the black hole and so this contribution to the entropy will decrease proportional to the horizon of the black hole and will eventually go to zero. Therefore, we recover the desired Page Curve behaviour required for unitarity. This can also be seen in Figure 3.2.

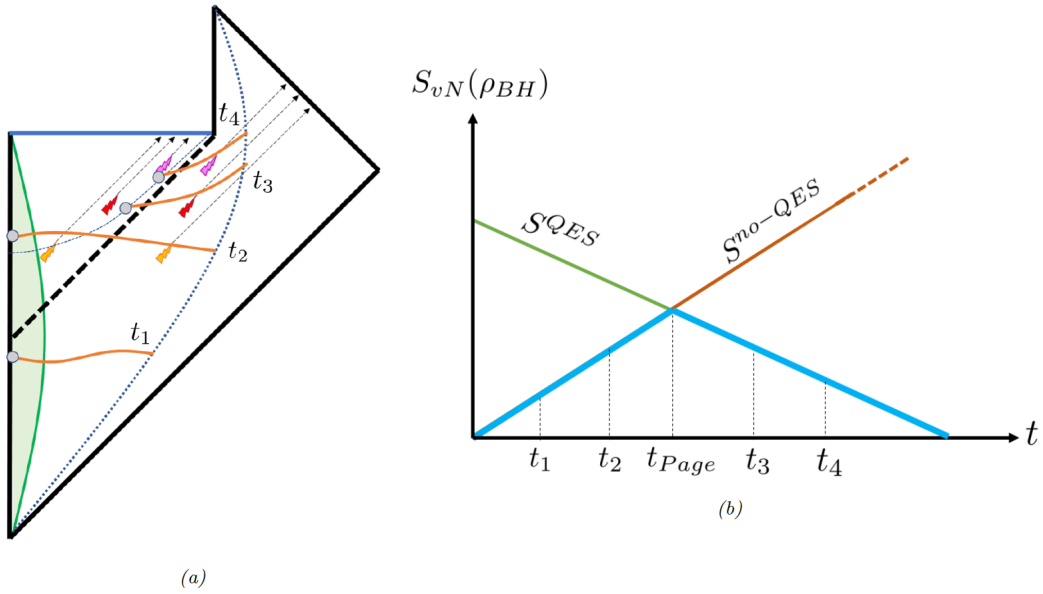

Figure 3.2: (a) A visualisation of the QES for an evaporating black hole. Hawking modes are represented by the squiggles which always appear in pairs, one inside and the other outside of the horizon. For early times, $t_1, t_2 < t_{Page}$ the QES shown by the grey dot vanishes. The only contribution at early times is from the Hawking modes in the bulk which are defined on the orange lines which extend from the QES to the cutoff surface which is represented by the dotted blue lines. For later times, $t_3, t_4 > t_{Page}$ the QES is no longer vanishing and becomes dominant. The QES then stays close to the interior of the horizon such it decreases monotonically as the black hole shrinks. (b) The unitary Page Curve for the fine grained entropy of the black hole. The vanishing-QES contribution is shown in red whilst the QES contribution is shown in green. We see that they are monotonically increasing and decreasing respectively and follow the Page Curve showed in blue due to the phase transition at t_{Page}. This figure can be found in (32).

The black hole system only gives half of the total Hilbert space as the horizon physically divides the spacetime into two complementary regions: the black hole and radiation regions. If the fine grained entropy of the black hole follows the Page Curve and the total state (interior and exterior) of the black hole is pure, then the radiation entanglement entropy must necessarily follow the same Page Curve. We therefore collect the Hawking radiation far away from the black hole but at the Page Time, there must be a phase transition. This can be illuminated by the QES prescription. At early times, all of the information which composes the black hole is contained within the horizon. Therefore, information remains encoded within the entanglement wedge of the black hole. The formation of the non-vanishing QES at the Page Time in the interior of the

black hole implies that for late times, the degrees of freedom of the black hole are only encoding information about what lies between the QES and the cutoff surface.

This warrants the question of what happened to the interior modes which have passed the QES. Where is this information encoded? As the outgoing radiation is entangled with the infalling modes, it would then make sense that this information was encoded in the entanglement wedge of the radiation instead. This implies that the information about the state of the system associated to the region deeper than the QES is encoded in an 'entanglement island' disconnected from the radiation region. This island can be defined by making the appropriate changes to the radiation region such that it also follows the Page Curve.

3.4.1 Rules on the Island

Let us take some boundary subset A dual to the radiation region in the bulk. The generalised entropy we must now consider is given by

$$S_{vN}(\rho_A) = S_{gen}(A \cup I) = \frac{\mathrm{A}[\partial I]}{4G_N} + S_{mat}(A \cup I) \tag{3.16}$$

where I is the disconnected island region with boundary ∂I. The union, $A \cup I$ is the region of the bulk spacetime extremizing the generalized entropy. The island exhibits the following features:

1. The boundary of the island's boundary coincides with the boundary of the radiation region of the CFT
$$\partial A = \partial(\partial I) \tag{3.17}$$

2. The boundary of the island ∂I is homologous to the radiation region such that their union forms a spacelike surface in the bulk.

3. The island extremizes the generalized entropy of the union of the radiation and the island. This means that it belongs to the set of extremal bulk regions $\{I_{ext}\}$ satisfying
$$\begin{aligned} S_{gen}(A \cup I_{ext}) &= \mathrm{ext}_{I_i}\, S_{gen}(A \cup I_i) \\ &= \mathrm{ext}_{I_i} \left[\frac{\mathrm{A}[\partial I_i]}{4G_N} + S_{mat}(A \cup I_i) \right] \end{aligned} \tag{3.18}$$

4. If there exist multiple candidates extremizing the generalised entropy in the last step, then the island is the candidate which yields the minimal generalised entropy:
$$S_{gen}(A \cup I) = \min_{I_{ext}} S_{gen}(A \cup I_{ext}) \tag{3.19}$$

such that we can express (3.16) as

$$S_{vN}(\rho_A) = \min_{I_{ext}} \left\{ \text{ext}_I \left[S_{gen}[A \cup I] \right] \right\} \tag{3.20}$$

There also exists a maximin prescription for islands (75). In this case, we must foliate the spacetime with a set of spacelike Cauchy slices Σ containing the boundary CFT region representing the radiation, A, such that $\partial A \subset \Sigma$. We pick a single Cauchy slice Σ_i and then find the minimal QES, $\chi_{min}(\Sigma_i)$ which minimizing the generalized entropy (defined as the quantum fields and area terms from $\Sigma_{A\cup I}$ which is the portion of the Cauchy slice enclosed by the entangling surface union region A). We then maximize the minimal surface over time or Cauchy slice within the set $\{\Sigma_i\}$,

$$S_{vN}(\rho_A) = \max_{\Sigma} \min_{\chi} \left[\frac{\text{A}[\chi(\Sigma)]}{4G_N} + S_{mat}(\Sigma_{A\cup I}) \right] \tag{3.21}$$

Islands exhibit several non-trivial features. The island can be empty, at which point it reduces to the normal entanglement entropy on the boundary region describing the radiation A which is described by the non-gravitational CFT. Due to the minimization procedure, the island only dominates when its entanglement entropy that is smaller than the one associated with the vanishing island solution. Non-vanishing islands are always spacelike separated from A. As previously mentioned, the island can be disconnected and in this case is simply the union of disjoint subregions of the bulk. For asymptotically AdS spacetimes, the island's boundary turns out to be a quantum extremal surface $\partial I = \chi$, which requires that the first two conditions hold.

Maldacena et al. illustrated that a new dominant saddle point emerges in the path integral which corresponds to the case where all replica manifolds are fully connected by replica wormholes(67). This new saddle point can be interpreted as the emergence of the islands. It is therefore believed that this island prescription should hold for more general systems where there exist CFTs living in the same bulk spacetime as the island region or in a disjoint bulk region. Whilst this result is encouraging, we recall that the Euclidean path integral formulation cannot generally be assumed valid for dynamic spacetimes and that these results were only illustrated for CFTs with central charge $c \gg 1$(67).

Part II

From Qubits to QuBTZ

Even armed with the QES prescription, exact results in quantum gravity are difficult to come by. There exists, however, another class of exact solutions to Einstein's equations exploiting the AdS/CFT duality to construct effective theories localised on branes. These 'holographic braneworld' constructions have been used to good effect to find useful results ranging from normalizable gravity theories localised on the brane (79)(12), novel models of entanglement islands (13) and branes accounting for quantum corrections to classical black holes(14)(80).

This part of the thesis will focus on the quantum corrected QuBTZ model proposed in (14). The QuBTZ employs the AdS_4/CFT_3 duality to construct a backreacted BTZ geometry with corrections sourced by CFT_3 fields outside of its horizon. We provide a brief overview of this fascinating model in Chapter 4. In Chapter 5, we turn our attention to physics on the brane. We calculate thermodynamic properties and geodesics on the brane, focussing on the small backreaction limit allowing us to use the RT prescription on the brane. Unfortunately, this limits us to linear order CFT and backreaction effects and we leave higher-derivative corrections to future research.

Chapter 4

The Quantum Corrected Black Hole

Sans a complete theory of quantum gravity, one cannot construct a reliable notion of a general quantum black hole. However, we are able to glean some insight into quantum gravity from holography and semi-classical approximations. In such limits, a sensible approach is to treat gravity as a classical field generated by the expectation value of the fully quantum fields in the theory,

$$G_{\mu\nu}(g_{\alpha\beta}) = 8\pi G \left\langle T_{\mu\nu}\left(g_{\alpha\beta}\right)\right\rangle \tag{4.1}$$

Obviously, this approach is often impractical and analytically intractable for non-symmetrical matter configurations. Furthermore, the inclusion of fields within a bulk naturally generates some backreaction to the black hole which is not well accounted for in this scheme.

In this chapter we introduce the quantum BTZ (QuBTZ) geometry which applies the braneworld construction to account for the presence and backreaction of bulk CFT_3 fields on a BTZ black hole. Branes are geometric objects embedded in a non-trivial higher dimensional geometry and localised at a fixed position. The formulation of this model involves concepts such as C-metrics and other unnecessary details well described in (81) (82). We will spare the reader a detailed review of these concepts as they are not vital to our discussion.

The AdS_4/CFT_3 duality maps CFT_3 fields to a problem of gravitational dynamics in a 4D bulk geometry. Using the tools of holography we can construct a gravity theory described by

$$\mathcal{G}_{\mu\nu}\left(g_{\alpha\beta}\right) = 8\pi G \left\langle T_{\mu\nu}\left(g_{\alpha\beta}\right)\right\rangle_{\text{planar}} \tag{4.2}$$

where the $\mathcal{G}_{\mu\nu}$ captures higher curvature corrections. Using holography the problem reduces to simply solving the classical gravitational equations of the braneworld in one more dimension(83)(84).

In the QuBTZ, an effective three-dimensional gravity theory becomes localised on the brane. This theory is dual to a CFT_3 with cutoff scale $1/\ell$. The higher-derivative curvature terms on

the left of (4.2) are then induced by the CFT above the cutoff of the theory backreacting directly on the geometry. Correspondingly, the energy momentum tensor on the right is induced by the CFT below the cutoff. Hence, the left hand side emerges as an effective theory of gravity on the brane resulting from integrating out modes above the cutoff scale in the CFT. This remarkable construction thus incorporates both high and low energy quantum effects in an exact manner.

Backreactions can be treated perturbatively in the limit of small cG_3/L_3 where G_3 and L_3 are the effective three dimensional Newton's constant and AdS_3 radius. For the low energy limit, the backreation is proportional to the central charge and hence linear in this parameter. The curvature corrections appearing on the left of (4.2), however are quadratic in this parameter due to the cutoff length of the effective theory being proportional to cG_3. For this reason, we can consider linear corrections in which we can extract the leading order CFT backreaction while ignoring higher-derivative gravity modifications.

Previously, we introduced the concept of the generalised entropy,

$$S_{gen} = S_{Wald} + S_{out} \tag{4.3}$$

where we recall that S_{out} is the entropy of all fields living outside the BH once the leading divergent term proportional to the area has been reabsorbed into the renormalisation of $G_N^{(d+1)}$. For higher-curvature theories, we must instead use the Bekenstein-Hawking-Wald entropy, S_{wald} rather than S_{BH} (85). As stressed previously, the CFT entropy $S_{out} \propto c$ and is hence distinct from the leading curvature corrections in the Wald entropy appearing on the left of (4.2).

However, the holographic approach allows us to instead calculate S_{gen} in the bulk of the higher dimensional picture in which the brane lives,

$$S_{gen} = \frac{A_{bulk}}{4G_N^{(d+1)}} \tag{4.4}$$

In this interpretation, the second picture allows us to simply calculate the entropy by finding the RT surface in the four dimensional picture (86). The entire entropy should therefore be considered as an entanglement entropy in contrast to the S_{out} on the brane. The reason for this is that both the Einstein-Hilbert and higher-derivative terms in the action are induced by integrating out the UV degrees of freedom in the CFT. Therefore, the Wald entropy can be interpreted as being induced by the entanglement of short wavelength modes across the black hole horizon. This method also allows us to calculate the QES for a system localised on a brane. In (14), it was shown explicitly that S_{gen} indeed obeys the first law of black hole thermodynamics,

$$TdS_{gen} = dM - \Omega dJ \tag{4.5}$$

where M, J, T and Ω are all measured on the brane. In contrast, the Wald Entropy of the black hole was found not to obey the first law. To reconcile this, one can interpret that generalised

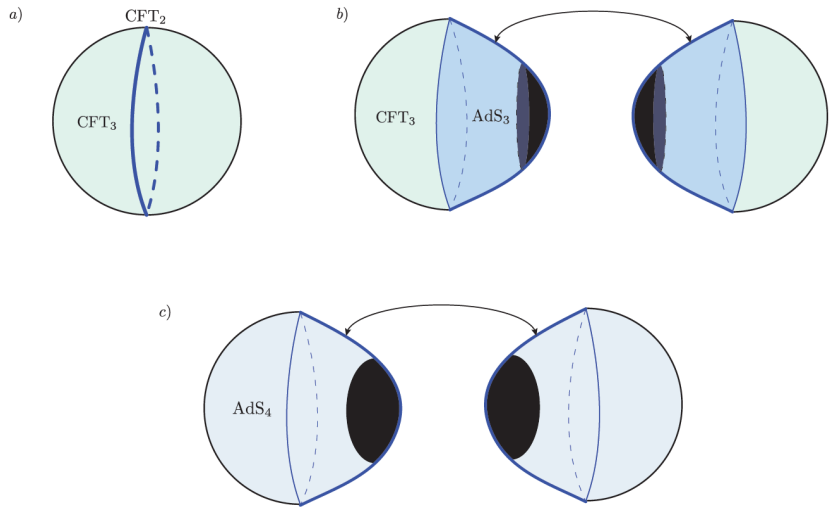

Figure 4.1: A schematic of the braneworld setup from (80). a) shows the CFT picture in which two copies of a thermal CFT_3 are coupled to a thermal CFT_2 defect. b) The thermal CFT_2 can be replaced with its dual representation. c) The two thermal CFT_3 can also be replaced with asymptotically AdS_4 bulks. The boundary conditions between the defect and the CFT_3 are transparent.

entropy in the brane picture as being composed of the Wald entropy and an entanglement entropy sourced by the CFT_3 fields outside its horizon defined by the difference between the Wald and the generalised entropy. This result is non-trivial and rather remarkable considering that S_{bulk} lives in the higher dimensional picture.

4.1 Bulk Dual to the QuBTZ

In this chapter, we follow methods developed in (87) and (88) for solving a quantum corrected black hole using a classical bulk dual with a black hole localized on the braneworld.

We start by introducing the AdS_4 C-metric (11)(89)(90),

$$ds^2 = \frac{\ell^2}{(\ell + xr)^2}\left(-H(r)dt^2 + \frac{dr^2}{H(r)} + r^2\left(\frac{dx^2}{G(x)} + G(x)d\phi^2\right)\right) \tag{4.6}$$

with

$$H(r) = \frac{r^2}{\ell_3^2} + \kappa - \frac{\mu\ell}{r}; \quad G(x) = 1 - \kappa x^2 - \mu x^3 \tag{4.7}$$

which solves the Einstein equations with

$$R_{ab} = -3\left(\frac{1}{\ell^2} + \frac{1}{\ell_3^2}\right)g_{ab} \tag{4.8}$$

such that the AdS_4 radius is given by $\ell_4 = \left(\frac{1}{\ell^2} + \frac{1}{\ell_3^2}\right)$. The parameters μ, κ, ℓ and ℓ_3 are parameters whose physical interpretations can be given as:

1. μ is the strength or state of the CFTs which determine the strength of the quantum corrections

2. $\kappa = \{-1, 0, 1\}$ depending on the curvature of the space. For $\kappa = 1$ one finds a dressed conical singularity, whilst for $\kappa = -1$ we have a dressed BTZ solution. We assume that $\kappa = -1$ throughout our work.

3. ℓ_3 is the induced AdS_3 radius on the brane such that $\ell_3 \propto L_3 +$Higher Curvature Corrections

4. ℓ can be expressed as
$$\frac{1}{\ell^2} = \frac{1}{\ell_4^2} - \frac{1}{\ell_3^2} \tag{4.9}$$
where ℓ_4 is the AdS_4 radius in the bulk. We will assume that $0 \leq \ell < \infty$ so that $\ell_3 > \ell_4$. This parameter contains a great deal of physical information, providing a notion of the brane position (and hence the cutoff scale of the 3D effective theory and the strength of the backreaction) and the inverse of the brane tension.

In the effective three-dimensional picture on the brane, we will generally be interested in keeping ℓ_3 fixed and instead looking at ℓ/ℓ_3 and μ. Though we have presented an *ad hoc* picture, it should be obvious that ℓ_4 is a derived scale such that we can interpret the four-dimensional bulk as emerging from the boundary physics.

Setting $\mu = 0$, we can recast the metric for the bulk as

$$\cosh\sigma = \frac{\ell_3}{\ell_4}\frac{\sqrt{1 + \frac{r^2x^2}{\ell_3^2}}}{\left|1 + \frac{rx}{\ell}\right|}, \qquad \hat{r} = r\sqrt{\frac{1 - \kappa x^2}{1 + \frac{r^2x^2}{\ell_3^2}}} \tag{4.10}$$

then the geometry becomes more explicitly pure AdS_4,

$$ds^2 = \ell_4^2 d\sigma^2 + \frac{\ell_4^2}{\ell_3^2}\cosh^2\sigma\left(\frac{d\hat{r}^2}{\frac{\hat{r}^2}{\ell_3^2} + \kappa} - \left(\frac{\hat{r}^2}{\ell_3^2} + \kappa\right)dt^2 + \hat{r}^2 d\phi^2\right) \tag{4.11}$$

We can now foliate this spacetime along constant σ slices with familiar asymptotically AdS_3 geometries with radius given by $\ell_4\cosh(\sigma)$. Each value of κ gives either global, Poincaré or BTZ branes at each σ for $\kappa = \{-1, 0, 1\}$ respectively.[22]

[22] if we cut a $\kappa = 1$ solution at $\sigma = \sigma_b$ and integrate out $\sigma > \sigma_b$, this gives the ground state of the Karch-Randall set-up (12)

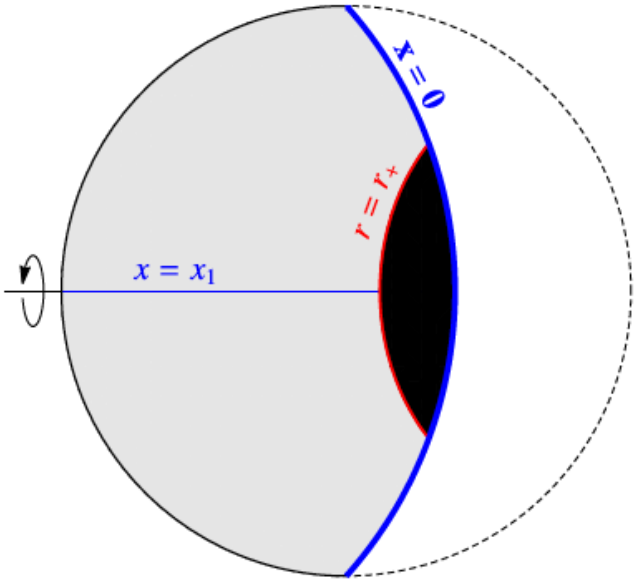

Figure 4.2: The bulk geometry at a constant t and ϕ for the braneworld construction with a black hole in it(14). The thin black border is the asymptotic AdS_4 boundary, the thick blue region is the brane and the black region represents the bulk black hole with horizon at $r = r_+$. We cut off the bulk at $x = 0$ so only the gray region $0 \leq x \leq x_1$ is retained, where x_1 is the smallest positive root of $G(x)$. This root is also now the ϕ axis. In our construction, we glue a second copy of this region along the brane to make a $\mathbb{Z}_2$-symmetric two sided braneworld. The dual three dimensional fields satisfy transparent boundary conditions at the AdS_4 boundary.

Turning on the quantum corrections, the geometry naturally becomes more complicated. Along the axis $x = 0$, however, the induced metric is totally umbilic such that the intrinsic curvature is given by,

$$K_{ab} = -\frac{1}{\ell} h_{ab} \tag{4.12}$$

so we choose the $x = 0$ surface for the position of the brane as in Figure 4.2.

To gain insight, we consider the case of $\mu = 0$. We fist glue the metric at $x = 0$ to a copy of itself, imposing the Israel junction conditions(91) across the gluing surface at $x = 0$. The metric is continuous across the brane but its derivative becomes discontinuous due to the stress tensor on the brane,

$$S_{ab} = -\frac{2}{8\pi G_4}(K_{ab} - h_{ab}) = -\frac{1}{2\pi G_4 \ell} h_{ab} \tag{4.13}$$

giving a brane tension,

$$\tau = \frac{1}{2\pi G_4 \ell} \tag{4.14}$$

which is found by relating the discontinuity of the extrinsic curvature tensor across the position of the gluing surface to the stress tensor induced by the brane. In the limit $\ell \longrightarrow \infty$ we find $\ell_3 \longrightarrow \ell_4$ such that the brain becomes tensionless and we are on an equatorial $\sigma = 0$ slice of the AdS_4 bulk. In the opposite limit $\ell \longrightarrow 0$, the brane moves closer to the asymptotic bulk boundary at $\sigma \longrightarrow \infty$. Karch and Randall showed that for $0 < \ell < \infty$, there is a massive graviton bound state localised on the brane (12). When ℓ is very small, however, the brane is close to the boundary and the graviton is almost massless.

The effective theory on the brane is obtained by solving the bulk Einstein equations for the excluded region between the brane at $x = 0$ and the AdS_4 conformal boundary (the white region in Figure 4.2) in an expansion for small ℓ. The holographic interpretation of this is that we are integrating out the ultraviolet CFT degrees of freedom down to the cutoff ℓ^{-1}(92) inducing the gravitational dynamics on the brane.

The action on the brane is[23]

$$I = \frac{1}{16\pi G_3} \int d^3x \sqrt{-h} \left[\frac{2}{L_3^2} + R + \ell^2 \left(\frac{3}{8} R^2 - R_{ab} R^{ab} \right) + \ldots \right] + I_{\text{CFT}} \tag{4.15}$$

where the effective three-dimensional Newton's constant is

$$G_3 = \frac{1}{2\ell_4} G_4, \tag{4.16}$$

and the three-dimensional cosmological constant term as

$$\frac{1}{L_3^2} = \frac{2}{\ell_4^2} \left(1 - \frac{\ell_4}{\ell} \right) = \frac{1}{\ell_3^2} \left(1 + \frac{\ell^2}{4\ell_3^2} \right). \tag{4.17}$$

where in the final step in this expression, we expanded $\ell_4 = \left(\frac{1}{\ell^2} + \frac{1}{\ell_3^2} \right)^{-1/2}$ to quadratic order in ℓ.

On the brane the number of microscopic degrees of freedom in the holographic CFT is measured by an effective central charge c normalised as

$$c = \frac{\ell_4^2}{G_4} \tag{4.18}$$

Together with our previous relationship for ℓ_4 we can relate this to terms in the dual three-dimensional theory,

[23] We note that in the limit that the graviton becomes massless, the higher curvature corrections become irrelevant and we can use the Bekenstein-Hawking entropy.

$$\frac{\ell}{1+(\ell/\ell_3)^2} = \frac{cG_4}{2\ell_4} = 2cG_3 \tag{4.19}$$

This relation is exact, but we can also consider the relevant small ℓ expansion,

$$\ell = 2cG_3\Big(1+\mathcal{O}(cG_3/L_3)\Big) \tag{4.20}$$

Importantly, as long as we keep c and L_3 finite, the brane approaches the AdS_4 boundary such that the gravitational coupling G_3 vanishes and there is backreaction of the CFT.

We note that there is no contradiction between requiring $c \gg 1$ and performing a small ℓ expansion as long as we expand in orders of

$$\frac{\ell}{\ell_3} \sim \frac{c\hbar G_3}{L_3} \ll 1 \tag{4.21}$$

which allows us to use the three dimensional description and the limit of the large central charge is

$$c \sim \frac{\ell}{\hbar G_3} \gg 1 \tag{4.22}$$

so that both limits are satisfied provided that $\ell \ll \ell_3$ and we do not include quantum corrections to the bulk. From (4.21), we see that leading order CFT contributions enter at linear order in c in I_{CFT} are also in linear order of $\frac{\ell}{\ell_3}$, distinguishing them from the higher-curvature corrections which are $\mathcal{O}\Big(\big(\frac{\ell}{\ell_3}\big)^2\Big)$.

4.2 Global Features of Bulk and Physical Parameters

The presence and variety of black holes depends on the functions $H(r)$ and $G(x)$, introduced earlier. Clearly, the positive roots of $H(r)$ correspond to Killing horizons of ∂_t. Provided there is a positive root of $H(r)$, we can identify it as the black hole horizon r_h but we also want to ensure that the horizon is compact. To ensure this, we consider the (x,ϕ) sector in which the real roots of $G(x)$ are symmetry axes of ∂_ϕ. The properties of these solutions determine the topology of the horizons. We can consider a different parameterization for $G(x)$ and $H(r)$ allowing for cleaner expressions.

To have a C-metric which contains a finite black hole in the bulk[24], we restrict our parameters to the range where there exists (at least) one positive root of $G(x)$. The smallest of these roots we refer to as x_1(89). This root will therefore be the axis of rotation for the brane. We can then

[24] As opposed to an infinite black string

restrict the range of x to $0 \leq x \leq x_1$. Using x_1, we can then paramaterize the CFT state by,

$$\mu = \frac{1 - \kappa x_1^2}{x_1^3} \tag{4.23}$$

In the cases of interest where $\kappa = -1$, $x_1 \in (0, \infty)$[25]. The strength, μ, is a monotonically decreasing function of x so that as $\mu \longrightarrow 0$, $x_1 \longrightarrow \infty$ and as $\mu \longrightarrow \infty$, $x_1 \longrightarrow 0$.

Furthermore, we want to remove the conical singularity at $x = x_1$ such that we identify,

$$\phi \sim \phi + 2\pi\Delta \tag{4.24}$$

with

$$\Delta = \frac{2}{|G'(x_1)|} = \frac{2x_1}{3 - \kappa x_1^2} \tag{4.25}$$

We can then consider that for constant t and r, variations in $0 \leq x \leq x_1$ give topological discs. Conveniently, we can think of them as caps where x corresponds roughly to the cosine of the polar angle along the cap. We note that $G'(x_1) < 0$ in this range and Δ is independent of ℓ. A trivial calculation shows that Δ reaches it maximum $\Delta = \frac{1}{\sqrt{3}}$ at $x_1 = \sqrt{3}$.

4.3 Physical Parameters

The metric induced on the brane at $x = 0$ is asymptotic to AdS_3 at $r \longrightarrow \infty$, but the coordinates are not canonically normalized since ϕ has periodicity $2\pi\Delta$. To rectify this, we rescale the variables

$$t \longrightarrow \frac{t}{\Delta}, \quad \phi \longrightarrow \frac{\phi}{\Delta}, \quad r \longrightarrow \Delta r, \tag{4.26}$$

so that now $\phi \sim \phi + 2\pi$ and the metric takes the form

$$ds^2 = -\left(\frac{r^2}{\ell_3^2} - 8\mathcal{G}_3 M - \frac{\ell F(M)}{r}\right) d\vec{t}^2 + \frac{dr^2}{\frac{r^2}{\ell_3^2} - 8\mathcal{G}_3 M - \frac{\ell F(M)}{r}} + r^2 d\phi^2 \tag{4.27}$$

where $\mathcal{G}_3$ is a 'renormalized Newton's constant' given by

$$\begin{aligned} \mathcal{G}_3 &= \left(1 - \frac{\ell^2}{2L_3^2} + \mathcal{O}\left(\frac{\ell}{L_3}\right)^4\right) G_3 \\ &= \frac{1 - \frac{\ell^2}{2\ell_3^2}}{2\ell_4} G_4 + \mathcal{O}\left(\frac{\ell}{L_3}\right)^4 = \frac{\ell_4}{\ell} G_3 = \frac{1}{2\ell} G_4 \end{aligned} \tag{4.28}$$

[25]The case where $\kappa \longrightarrow 0$ can be taken to be a limiting case

where the last line is equivalent up to order $\mathcal{O}(\ell/L_3)^4$. We can also identify the three-dimensional mass M,

$$M = -\frac{\kappa}{8G_3}\frac{\ell}{\ell_4}\Delta^2 = -\frac{1}{2G_3}\frac{\ell}{\ell_4}\frac{\kappa x_1^2}{\left(3-\kappa x_1^2\right)^2}, \tag{4.29}$$

and the mass parameter of the solution given by

$$F(M) = \mu\Delta^3 = 8\frac{1-\kappa x_1^2}{\left(3-\kappa x_1^2\right)^3} \tag{4.30}$$

We henceforth work under the assumption that M and $\mathcal{G}_3$ remain valid to all orders in ℓ. We ought to be careful in our definition of mass which is given in Einstein-AdS gravity by the subleading constant term in g_{tt}. Here, however, the higher order terms in the effective theory modify the definition by adding corrections beginning at order ℓ^2. We can account for this ambiguity internally provided we use the renormalized Newton's constant. On this, we note that we will continue to fix the renormalized quantities ℓ_3 and $\mathcal{G}_3$ which appear in the exact metric instead of the bare parameters in the effective action, G_3 and L_3. The function $F(M)$ depends on $\mathcal{G}_3 M$ only through x_1 but is otherwise independent of ℓ/ℓ_3 so as we change the strength of the backreaction for a fixed (renormalized) mass, $\mathcal{G}_3 M$, the function does not change.

Making use of the holographic dictionary, it can be shown that the metric induced on the brane indeed solves the semi-classical equation with higher order derivatives(14), though this must be done order by order and quickly becomes tedious. The stress tensor of the holographic CFT can be found in increasing orders of ℓ^2. It was shown in (14) that at order ℓ^2, the conformal symmetry of the CFT is broken on the brane due to the cutoff ℓ. Using the relationship $\frac{\ell}{1+(\ell/\ell_3)^2} = 2cG_3$, we can eliminate ℓ and give the stress energy tensor in terms of magnitudes on the brane alone. For small ℓ we find,

$$\left\langle T_b^a \right\rangle = \frac{c}{8\pi}\frac{F(M)}{r^3}\,\mathrm{diag}\{1,1,-2\}\left(1+\mathcal{O}\left(cG_3/\ell_3\right)^2\right) \tag{4.31}$$

where we observe the strength of the quantum corrections from the CFT is determined entirely by c and $F(M)$ for small ℓ. In the limit of $\ell \longrightarrow 0$, the metric (4.27) can be interpreted as a classical solution to the Einstein equations. Within this limit of small backreaction, the corrections to the classical geometry are $\mathcal{O}(cG_3)$. The CFT is therefore consistently solved simultaneously with the three-dimensional gravitational equations, yielding an exact backreaction of the CFT degrees of freedom for finite ℓ, for both light and heavy CFTs through the non-perturbative resummation of the higher-curvature corrections.

Because the classical BTZ solution is recovered when $\kappa = -1, \ell = 0$, we refer to the range of $\ell > 0$ as the QuBTZ. Lastly, we note that ℓ/ℓ_3 does not enter directly into $F(M)$ and depends only on the backreaction through the rescaling of G_3 to $\mathcal{G}_3$. The dependence of the stress tensor on M at low orders in ℓ is simple as there is no term in $\left\langle T_b^a \right\rangle \propto \ell^2$ and any subsequent $\mathcal{O}(\ell^3)$ behaviour

comes from the higher-curvature corrections.

A fascinating result of this analysis is that the range of masses on the brane are finite[26],

$$-\frac{1}{8\mathcal{G}_3} \leq M \leq \frac{1}{24\mathcal{G}_3} \tag{4.32}$$

For a fixed value of $\mathcal{G}_3 M$, we have that for $\kappa = -1$ there exist two branches covering this mass range,

$$\begin{aligned} &\textbf{Branch (1b)} \ : \ \kappa = -1, \quad 0 < x_1 < \sqrt{3} \\ &\textbf{Branch (2)} \ \ : \ \kappa = -1, \quad \sqrt{3} < x_1 < \infty \end{aligned} \tag{4.33}$$

which the authors interpreted as corresponding to Casimir dominated (1b) and thermal (Hawking radiation) dominated (2) configurations.

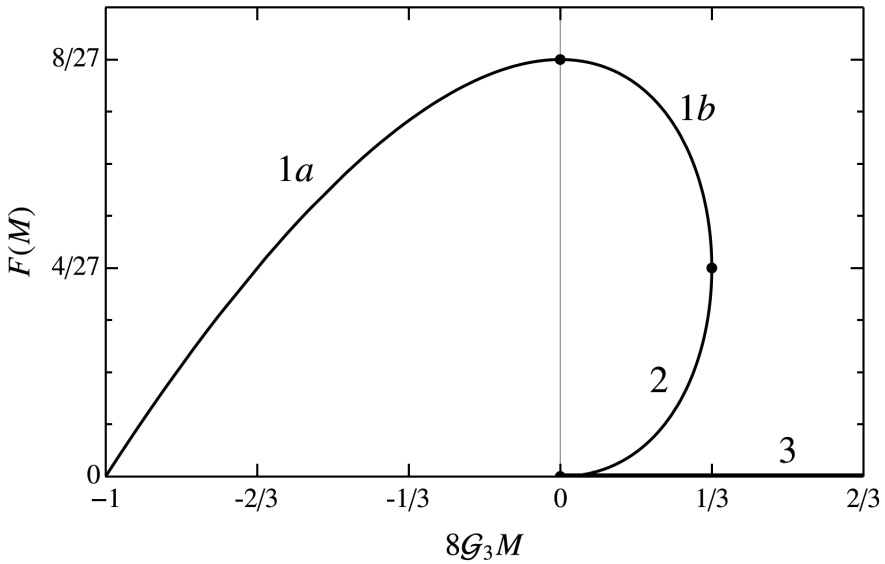

Figure 4.3: Plots of $F(M)$ as a function of $8\mathcal{G}_3 M$ taken from (14). The branch labelled (1a) corresponds to $\kappa = 1$ solutions while branch (3) gives the black string solutions which are the only other bulk solution in this setup admitting higher mass solutions. These solutions are clearly in the ground state of the CFT as $F(M) = 0$. Branches (1b) and (2) correspond to QuBTZ solutions dominated by Casimir and thermal modes respectively.

A novel feature of this solution is the finite mass range, which the authors argued is a consequence of holographically representing the CFT by a four dimensional bulk theory. This bound is likely not a general feature of the braneworld construction but rather represents a limit on

[26]We include here the range of negative masses reached by $\kappa = 1$, corresponding to a dressed conical singularity, but leave aside this for consideration in future research.

a more general class of QuBTZ-type solutions for which the CFT is captured by localized bulk black holes. In the following chapter, we see that this effect yields interesting consequences for the physics on the brane.

Chapter 5

Physics on the Brane

We have encountered many facets of the QuBTZ solutions, however, we so far lack a good picture of how physics manifests on the brane for the range of z and ν values. It will be most instructive to work in the small ℓ/ℓ_3 limit where we may apply the RT prescription on the brane. The physical horizon will be given by the real positive root of $H(r)$ as was previously noted, with the radius of the circular horizon given by $r = \Delta r_h$, meaning that r_+ ought to be considered the black hole horizon induced in the bulk.

We can assume that ℓ/ℓ_3 and μ inhabit sensible ranges where a positive root exists and find a more convenient paramaterization,

$$z = \frac{\ell_3}{r_+ x_1} \tag{5.1}$$

and

$$\nu = \frac{\ell}{\ell_3} \tag{5.2}$$

where one can interpret z as determining the uncorrected BTZ mass and ν as a dimensionless backreaction parameter[27]. One can eliminate x_1, or μ, and r_+ using

$$\begin{aligned} x_1^2 &= -\frac{1}{\kappa}\frac{1-\nu z^3}{z^2(1+\nu z)} \\ r_+^2 &= -\ell_3^2 \kappa \frac{1+\nu z}{1-\nu z^3} \\ \mu x_1 &= -\kappa \frac{1+z^2}{1-\nu z^3} \end{aligned} \tag{5.3}$$

[27] From here on we shall refer to orders in the backreaction ℓ and ν interchangeably.

with ν and z as parameters the ADM mass is

$$M = \frac{1}{2\mathcal{G}_3}\frac{z^2\left(1-\nu z^3\right)(1+\nu z)}{\left(1+3z^2+2\nu z^3\right)^2} \tag{5.4}$$

where $\mathcal{G}_3 = \frac{G_3}{\sqrt{1+\nu^2}}$ and the coefficient of the stress tensor is

$$F(M) = 8\frac{z^4\left(1+z^2\right)(1+\nu z)^2}{\left(1+3z^2+2\nu z^3\right)^3} \tag{5.5}$$

In this form it is not apparent that $F(M)$ depends only on $\mathcal{G}_3 M$ and not separately on ν, but of course it is still true since

$$\partial_\nu F(M) - \partial_z F(M)\partial_\nu\left(\mathcal{G}_3 M\right)/\partial_z\left(\mathcal{G}_3 M\right) = 0 \tag{5.6}$$

In this parametrization κ is not present in the expressions for physical quantities and is defined implicitly by,

$$\kappa = \text{sign}\left(\nu z^3 - 1\right) \tag{5.7}$$

which covers the entire range of branches (1) and (2) of bulk black holes of finite size by letting

$$0 \le \nu < \infty, \quad 0 \le z < \infty \tag{5.8}$$

The temperature of the horizon, relative to the canonical timelike Killing vector on the brane, $\partial/\partial t$, is

$$\begin{aligned} T &= \frac{\Delta H'(r_+)}{4\pi} \\ &= \frac{1}{2\pi\ell_3}\frac{z\left(2+3\nu z+\nu z^3\right)}{1+3z^2+2\nu z^3} \end{aligned} \tag{5.9}$$

where r_+ is the positive root of $H(r)$. In the limit that $\nu \longrightarrow 0$, we return the standard expression for the BTZ solution[28],

$$\begin{aligned} ds^2 &= -\left(\frac{r^2}{\ell_3^2} - 8\mathcal{G}_3 M\right)dt^2 + \frac{dr^2}{\frac{r^2}{\ell_3^2} - 8\mathcal{G}_3 M} + r^2 d\phi^2 \\ &= -\left(\frac{r^2 - r_h^2}{\ell_3^2}\right)dt^2 + \frac{\ell_3^2 dr^2}{r^2 - r_h^2} + r^2 d\phi^2 \end{aligned} \tag{5.10}$$

[28]We could also take $F(M) = 0$ as illustrated in Figure 4.3 however $F(M) = 0$ only occurs when $\mathcal{G}_3 M = 0$ which is uninteresting. There also exist black string solutions for which $F(M) = 0$ and $0 \le M < \infty$ however we shall not discuss them here.

where $r_h^2 = 8G_3 M \ell_3^2$, the standard expression for the horizon of a spherical BTZ black hole. In this limit, we find that $\mathcal{G}_3 \longrightarrow G_3$, $M \longrightarrow \frac{1}{2G_3}\frac{z^2}{(1+3z^2)^2}$ and $T \longrightarrow \frac{1}{2\pi\ell_3}\frac{2z}{1+3z^2}$ such that even in the limit of zero backreaction the range the classical masses in this theory is limited to $0 \leq G_3 M \leq \frac{1}{24}$ with corresponding radii in the limit $\frac{r_h}{\ell_3} \leq \frac{1}{\sqrt{3}}$. We see that z controls the classical mass of the black hole induced on the brane, reaching a maximum at $z = \frac{1}{\sqrt{3}}$ and going to zero monotonically on either size of this value. Naturally, the inclusion of backreaction alters this maximum but the salient point is that this model only allows for corrections to small black holes. This limitation prevents us from taking helpful limits such as that of the planar black hole, a point which we return to in Part III.

The polynomial dependence of important physical parameters in parameters r, v and z obfuscates the behaviour of observables of interest on the brane. We can, however, draw some general conclusions about the behaviour of physical parameters of interest by plotting them as a function of z and v as in Figure 5.1 and Figure 5.2 respectively.

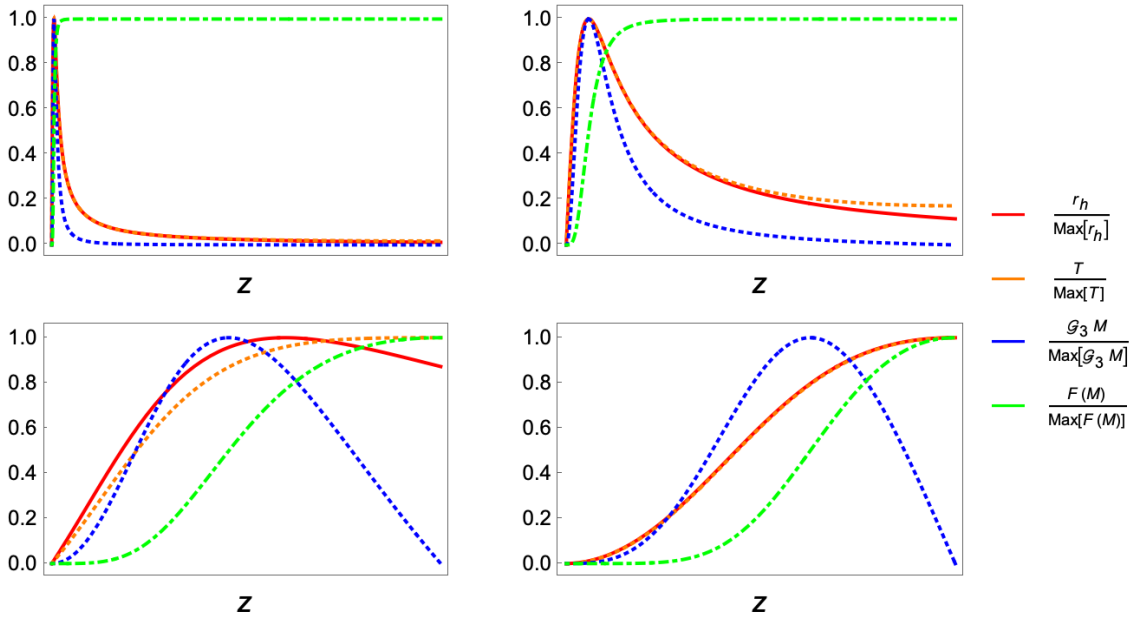

Figure 5.1: A plot of the black hole horizon on the brane r_h, its temperature T, its mass $\mathcal{G}_3 M$ and the CFT state function $F(M)$ normalised by their maximum value for $v = \{10^{-6}, 10^{-3}, 10^{0}, 10^{3}\}$ (ordered left to right, top to bottom) and $0 < z < v^{-1/3}$. We see $F(M)$ is monotonically increasing function of z.

Fixing the backreaction and varying z can be thought of as choosing a backreaction strength and then seeing how this alters the parameters as we change the mass of the classical solution. In the first plot in Figure 5.1, we see for small v, we pass very quickly from the thermal (2) to the Casimir (1b) branch and the temperature is determined almost entirely by the radius and the renormalized mass. As expected, for small backreaction the solution remains close to the classical

behaviour in which the temperature is determined entirely by the horizon radius. Furthermore, the maximum value of the mass, temperature and horizon radius is reached close to the transition point from branch (2) to (1b) at $F(M)/\,\mathrm{Max}[F(M)] = 0.5$. In the second and third plots, we see that as z is increased the behaviour becomes more complicated causing deviations from the classical behaviour, shifting the maximum values due to mixing of the mass and CFT state terms. Notably, the maximum values of the physical parameters move further to the right in their respective ranges of z[29] and in the limit of large backreaction, the behaviour of temperature and radius once again coincide and only reach their maximum value in the upper bound of z. In contrast to the small v case, the temperature and radius behaviour follows $F(M)$ more closely, indicating that the high energy conformal fields become dominant over the mass.

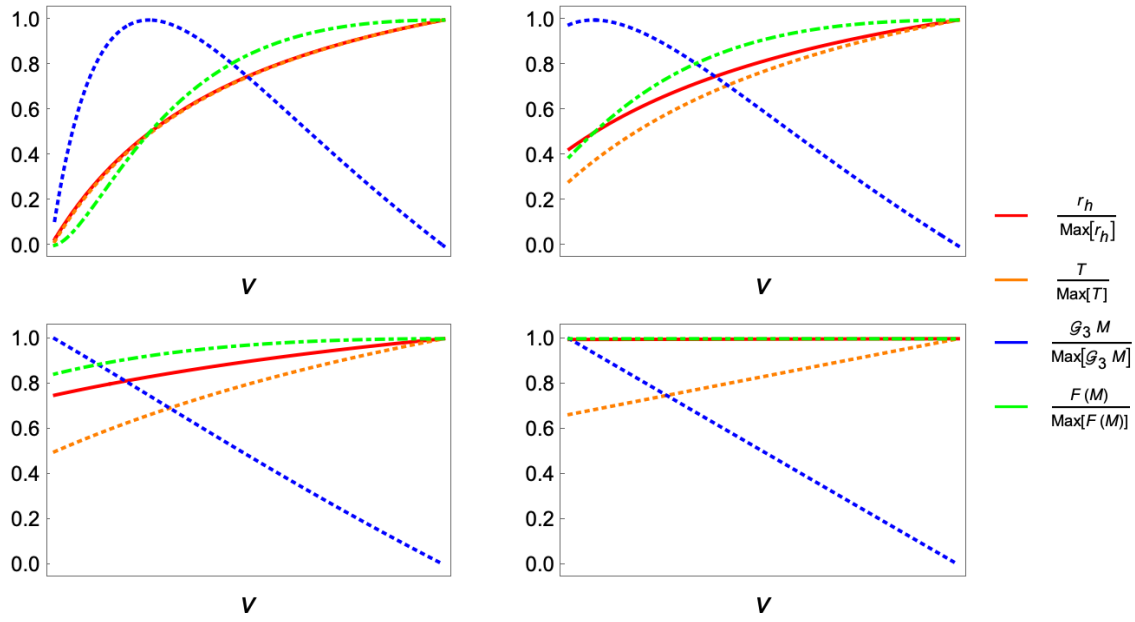

Figure 5.2: A plot of the black hole horizon on the brane r_h, its temperature T, its mass $\mathcal{G}_3 M$ and the CFT state function $F(M)$ normalised by their maximum value for $z = \{10^{-1}, 5\times10^{-1}, 10^{0}, 10^{1}\}$ (ordered left to right, top to bottom) and $0 < v < z^{-3}$. We see $F(M)$, r_h and T are all monotonically increasing functions of v.

Unlike the previous case in which varying z for fixed v covered the full range of $\mathcal{G}_3 M$ and $F(M)$, we note that fixing z and varying v generically does not cover the range of physical solutions and hence there exists some cutoff value of z beyond which only branch (1b) solutions exist. From Figure 5.2, it is clear that for a fixed z both $F(M)$ and r_h are monotonically increasing functions of v. Since $F(M)$ increases monotonically with v, one can find the critical value z_* explicitly by considering the values of z such that $F(M) > 4/27$ for all $v \geq 0$,

[29] It is important to stress that as we increase v, the range of z decreases such that the z-axes are of different scales in accordance with (5.7).

$$8\frac{z^4(1+z^2)}{(1+3z)^3} > \frac{4}{27} \implies z > \frac{1}{\sqrt{3}} \tag{5.11}$$

Hence, for $z_* > \frac{1}{\sqrt{3}}$ the only consistent QuBTZ solutions reside on branch (1b).

Conversely, for $z_* < \frac{1}{\sqrt{3}}$, there exist two values of ν which give the same mass for a fixed z,

$$0 < \nu_1 < \frac{1-9z^4}{z^3+9z^5}; \quad \nu_2 = \frac{1-z^3(\nu_1+9z(1+z\nu_1))}{z^3+9z^5+8z^6\nu_1} \tag{5.12}$$

and

$$\begin{aligned} \nu_2 > \nu_1, \quad &\text{for} \quad 0 < \nu_1 < \frac{1-3z^2}{4z^3} \\ \nu_2 < \nu_1, \quad &\text{for} \quad \frac{1-3z^2}{4z^3} < \nu_1 < \frac{1-9z^4}{z^3+9z^5} \end{aligned} \tag{5.13}$$

where additional constraints have been imposed on ν_1 in terms of z such that the full range (5.7) of ν_1 is not generally covered. Additionally, it should be apparent that the range of possible values of ν decreases monotonically to the limit $\nu_1 \longrightarrow 0$ as $z \longrightarrow \frac{1}{\sqrt{3}}$. As previously established, for fixed $8\mathcal{G}_3 M$ and z, the solution with the higher backreaction belongs to the (1b) branch whilst the lower belongs to branch (2). Furthermore, we observe that we can find the global maximum of r_h by noting that for $\nu = 0$, the global maximum is at z_* and that both r_h and $F(M)$ increase monotonically with ν such that we must choose the largest value of ν allowed by (5.7) given by $\nu \longrightarrow 3\sqrt{3}$,

$$\text{Max}[r_h/\ell_3] \leq \frac{2}{\sqrt{3}} \tag{5.14}$$

which is precisely twice the size of the $\nu = 0$ maximum. Unfortunately, this does not assuage us of the limitations of working with small black holes and we must proceed without this comforting assumption.

For small ν, the range of z covered is large and we see the full spectrum of physical results. Increasing the backreaction, the behaviour of these parameters linearises. Perhaps more interesting is that for small backreaction, the classical horizon radius-temperature relationship is well observed but as we leave the small ν limit and become confined to the (1b) branch, the horizon radius behaviour follows the behaviour of $F(M)$ more closely. This observation further supports the notion that the dominant effects on the (1b) branch are generated by the high energy Casimir modes of the CFT stress-energy tensor which scales with $F(M)$, whilst in the small coupling limit the dominant effects are thermal. The advantage of such an analysis is that one may be interested in seeing how a classical black hole, with mass determined entirely by z, is altered by increasing the backreaction of the CFT.

5.1 Stability of the Branches

So far we have not broached the subject of the worrisome ambiguity of dual mass solutions on branch (1b) and (2) in any great detail. The existence of two equal mass QuBTZ solutions with different CFT states is curious and begs the question: which will be the most physical. Naturally, one expects that thermal solutions ought to be the more physical solutions when viewed as perturbative corrections to the classical BTZ behaviour. To investigate this, we employ some reasoning from thermodynamics under the assumption that the most sensible comparison results from fixing the classical mass parameter z and ADM mass $\mathcal{G}_3 M$ and comparing the two values of v for values where both solutions exist. One may consider other comparisons in which one fixes the value of z and allows the renormalized mass and the backreaction to vary. From the brane perspective this would not be particularly physically meaningful as one would not be guided by physical observables.

It was observed in (14) that the negative mass branches have negative specific heat, $\partial M/\partial T$ and hence will not reach equilibrium with their Hawking radiation and will eventually evaporate. The hotter branch (2) always has positive specific heat whilst the story for the colder branch (1b) is more subtle. For some fixed v, the specific heat diverges at two points on branch (1b), once at $M = 0$ and another at a finite mass $M_1(v)$. Energy fluctuations in a thermal state are given by

$$\langle \delta E^2 \rangle = T^2 \frac{\partial E}{\partial T} \tag{5.15}$$

and hence it was argued that branch (1b) will be susceptible to large thermodynamic fluctuations, hinting at instability. In the range $M_1(v) < M < \frac{1}{24\mathcal{G}_3}$, the solutions have negative specific heat and hence may be able to evaporate through the transparent boundary theory. From the perspective of entanglement islands, this prospect is rather interesting as it suggests that the islands would reside in the bulk picture as proposed in (13).

To diagnose this more rigorously, we make the reasonable claim that the physical solution will be that with the smaller free energy, $\mathcal{F}$. To do so, we follow (93) in which we make use of the regularised on-shell action, $\mathcal{S}^\epsilon$

$$\beta \mathcal{F} = \mathcal{S}^\epsilon \tag{5.16}$$

where ϵ is the inverse cutoff scale of the radius. Though generally divergent, differences in free energy will be finite in the limit $\epsilon \longrightarrow 0$. In the QuBTZ theory, we make use of the bulk action which is accurate to all orders in ℓ and has a simple Einstein gravity dual such that it can be calculated using the Euclidean Einstein Hilbert action. This result takes into consideration the conformal fields residing outside of the bulk and hence we are calculating the free energy of the entire configuration on the brane rather than just that of the black hole. Firstly, we recall that the

bulk Ricci curvature is given by (4.8) and hence the bulk Ricci scalar is[30]

$$R_{(Bulk)} = -12\left(\frac{1}{\ell^2} + \frac{1}{\ell_3^2}\right) = -\frac{12}{\ell_4^2} \tag{5.17}$$

The Einstein-Hilbert action for the bulk with Euclidean metric g_E is given by

$$\begin{aligned} S^{\epsilon} =& \frac{1}{8\pi G_4}\int d^4x\,\sqrt{g_E}R_{(Bulk)} \\ =& \frac{-12}{8\pi\ell_4^2 G_4}\int_0^{\beta} dt_E \int_0^{2\pi\Delta} d\phi \int_0^{x_1} dx \int_{r_+}^{1/\epsilon} dr \frac{\ell^4 r^2}{(\ell + rx)^4} \\ =& \frac{-\ell\beta\Delta}{2\ell_4^2 G_4}\left[\frac{r_+^3(2\ell + r_+x_1)}{(\ell + r_+x_1)^2} - \frac{(2\ell\epsilon + x_1)}{\epsilon^2(\ell\epsilon + x_1)^2}\right] \end{aligned} \tag{5.18}$$

from which we may rewrite the free energy in terms of the effective theory parameters as,

$$\mathcal{F}(z, v) = \frac{(1 - v^2)^{3/2}}{2G_3 v^2(zv(z^2 - 3) - 4)}\left(\frac{(1 + 2zv)}{z^2\sqrt{(1 + zv)(1 - z^3v)}} - \frac{(z^3v - 1)(2\epsilon v + \sqrt{\frac{1-z^3v}{1+zv}})}{6\epsilon^2(\epsilon v + \sqrt{\frac{1-z^3v}{1+zv}})^2}\right) \tag{5.19}$$

One can then compare the free energy of the two possible solutions by making use of (5.12) and

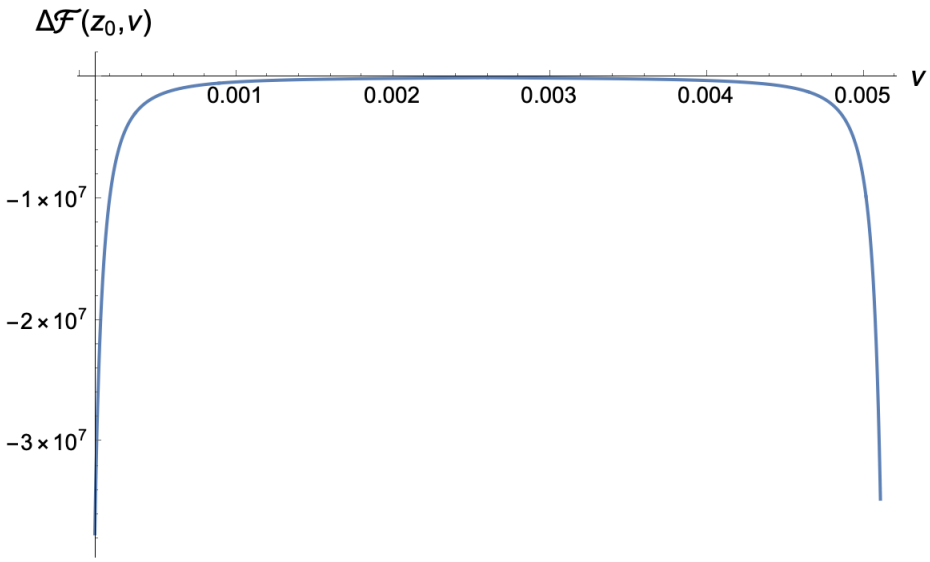

Figure 5.3: A typical plot of the difference in free energies $\Delta\mathcal{F}$ for $z_0 = 0.99\frac{1}{\sqrt{3}}$. As we lower z, the range of v increases and the difference in free energy turns more sharply.

(5.13) to find their difference, $\Delta\mathcal{F} = \mathcal{F}_{(2)} - \mathcal{F}_{(1b)}$,

[30]Naturally, one could also consider using the effective action (4.15) though this would be tedious and would limit the analysis to a subsystem of the full bulk thermodynamics.

$$\Delta\mathcal{F} = \begin{cases} \mathcal{F}(z, v_1) - \mathcal{F}(z, v_2) & \text{for } 0 < v_1 < \frac{1-3z^2}{4z^3} \\ \mathcal{F}(z, v_2) - \mathcal{F}(z, v_1) & \text{for } \frac{1-3z^2}{4z^3} < v_1 < \frac{1-9z^4}{z^3+9z^5} \end{cases} \tag{5.20}$$

the precise form of which is not particularly enlightening. As one can see from Figure 5.3, $\Delta\mathcal{F} \leq 0$ such that the thermal branch will always dominate the thermal partition function as anticipated. This analysis does not, however, give much insight into the proposed interpretation of negative heat capacity solutions on branch (1b) as evaporating through the transparent interface to the non-dynamical boundary region beyond reaffirming the relative stability of the thermal branch. Unfortunately, due to time constraints this avenue could not be explored in detail and is deferred to future study.

5.2 Geodesics in the QuBTZ

Our discussion so far has focused on global features of the bulk and its holographic correspondence. However, we would also like to gain some notions of how test particles behave on the brane, particularly infalling radial trajectories which elucidate limiting physical behaviour. Of primary interest is gaining a better understand how the presence of conformal fields and their backreaction on the geometry alter the minimal surfaces present in the bulk for subregions of the boundary CFT. These analyses will also be important in Part III of this thesis where we turn our attention to the spreading of chaos and entanglement in black holes with a holographic dual.

5.2.1 Geodesics of an Infalling Particle

In this chapter, we calculate the geodesics of infalling particles and simplify some bounds for the QuBTZ metric. We will work under the assumption that the backreaction remains small such that the higher-derivative-gravity corrections in (4.15) are suppressed and we can employ the standard techniques from Einstein gravity. We first note that there exist two familiar Killing vectors which can be read directly from the metric (4.27),

$$K = \partial_t; \quad R = \partial_\phi \tag{5.21}$$

from which we find,

$$\begin{aligned} K_\mu = -f(r)\partial_t; \quad R_\mu = r^2\partial_\phi; \\ \text{with } f(r) = \left(\frac{r^3 - 8\mathcal{G}_3 M \ell_3^2 r - \ell_3^3 v F(M)}{r\ell_3^2} \right) \end{aligned} \tag{5.22}$$

These Killing vectors generate the familiar conserved charges along geodesics corresponding to translations in ϕ and t, which are the angular momentum and energy[31] respectively.

$$E = -K_\mu \frac{dx^\mu}{d\lambda} = f(r)\dot{t}; \quad L = R_\mu \frac{dx^\mu}{d\lambda} = r^2\dot{\phi} \tag{5.23}$$

where the dot indicates a derivative with respect to the affine parameter, λ. We can then use the symmetry of the problem to recast it as,

$$\begin{aligned} \epsilon &= -f(r)\dot{t}^2 + \frac{\dot{r}^2}{f(r)} + r^2\dot{\phi}^2 \\ &= \frac{-E^2}{f(r)} + \frac{\dot{r}^2}{f(r)} + \frac{L^2}{r^2} \end{aligned} \tag{5.24}$$

where $\epsilon = \{-1, 0, 1\}$ for timelike ($\lambda = \tau$), lightlike ($ds^2 = 0$) and spacelike ($\lambda = s$) geodesics respectively. We are most interested in radially infalling trajectories where $L = 0$ and

$$\dot{r} = \pm\sqrt{\epsilon f(r) + E^2} \longrightarrow \Delta\lambda = \int \frac{dr}{\sqrt{\epsilon f(r) + E^2}} \tag{5.25}$$

Let's first consider the lightlike case first where $\epsilon = 0$,

$$\int dt = \pm \int \frac{dr}{f(r)} \tag{5.26}$$

The polynomials in $f(r)$ change sign only once, meaning that it has one positive root and we can write,

$$f(r) = \frac{1}{r\ell_3^2}(r - a)(r + b)(r + c) \tag{5.27}$$

where $a = r_h \in \mathbb{R}^+$ and b, c are the roots of the cubic $f(r)$ where one either has $\{b, c\} \in \mathbb{R}^+$ or $b = c^* \in \mathbb{C}$ depending on the sign of the determinant [32]. We can also make use of $a = b + c$ to cancel one variable, though it does not add much insight here. For more details, see Appendix E.

[31] Per unit mass

[32] We have simply used Descartes rule here. There is one sign change in f(r) and two in f(-r) implying that we have one positive real and either two negative real or two complex conjugate roots. Though the roots can be found analytically, their form is not particularly illuminating. Since our polynomial is a depressed cubic polynomial, we can easily find the determinant which gives us: $4\ell_3^6 - 27(\mu\ell\ell_3^2)^2$ in the non-canonical coordinates.

Lightlike paths

While the general equations of motion on the brane should be solved by minimizing the higher-derivative action, we note that for radially infalling lightlike paths, the solution for the constant x in the bulk coincides with that on the brane up to a conformal rescaling which factors out. The bulk theory has an Einstein dual so we need not worry about the inclusion of the higher-derivative corrections for radially infalling lightlike paths and these solutions automatically capture back-reaction to all orders in ν. These geodesics are found by solving (5.26),

$$\begin{aligned} t(r) &= \pm\, \ell_3 \frac{r_h(b-c)\ln\left(\frac{r-r_h}{r_0-r_h}\right) - b(r_h+c)\ln\left(\frac{r+b}{r_0+b}\right) + c(r_h+b)\ln\left(\frac{r+c}{r_0+c}\right)}{(r_h+b)(b-c)(r_h+c)} \\ &= \pm\, \ell_3 \frac{r_h(b-c)\ln(r-r_h) - b(r_h+c)\ln(r+b) + c(r_h+b)\ln(r+c)}{(r_h+b)(b-c)(r_h+c)} \quad \text{for } r_0 \longrightarrow \infty \end{aligned} \tag{5.28}$$

where a, b, c were defined previously. It may be instructive to consider the solution for the uncorrected case, which can be easily found to be,

$$\begin{aligned} t(r) &= \pm \left[\ell_3 \frac{\tanh^{-1}\left(\frac{r'}{r_h}\right)}{r_h} \right]_{r'=r_0}^{r'=r} \\ &= \pm\, \frac{\ell_3}{2r_h} \ln\left(\frac{(r+r_h)(r_0-r_h)}{(r-r_h)(r_0+r_h)} \right) \\ t(r) &= \pm\, \frac{\ell_3}{2r_h} \ln\left(\frac{(r+r_h)}{(r-r_h)} \right) \quad \text{for } r_0 \longrightarrow \infty \end{aligned} \tag{5.29}$$

where we choose ± for infalling and outgoing respectively. Unfortunately, this expression is not invertible, nor is it clear from this form which function is larger. We can, however, deduce from its derivative that the classical result will always be larger than the quantum corrected result. One would also like to check if there are any local changes to the near horizon behaviour according to the infalling observer. To check this, we can simply adapt our coordinates to the near horizon region. The QuBTZ and BTZ solutions are plotted against one another in Figure 5.4. Increasing the backreaction causes the infalling observer to approach the horizon faster. This can be seen more explicitly by looking at the derivatives as illustrated in Figure 5.5 where we see that the classical solution bounds the rate of approach from below, with the rate increasing monotonically with the strength of the backreaction. Further away from the black hole, the backreaction becomes negligible and the dominant effects are simply from the ADM mass. From this, we can deduce that equal ADM mass solutions with fixed z will approach the black hole faster on the Casimir branch than on the thermal branch. Notably, Figures 5.4 and 5.5 do not

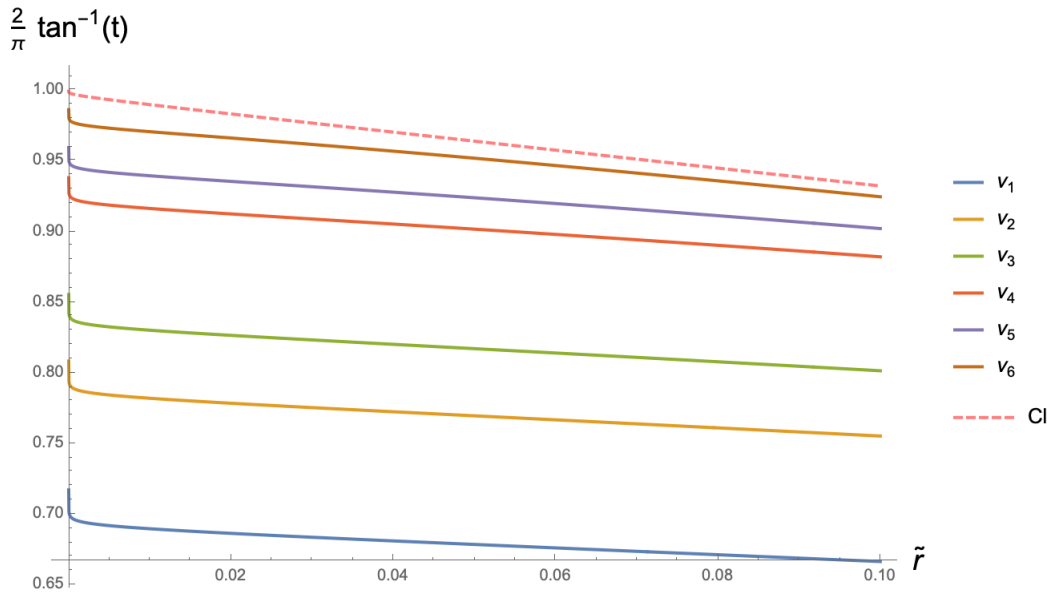

Figure 5.4: Plots of the near horizon behaviour of radial lightlike paths for $z = \frac{9}{10\sqrt{3}}$, $\nu_i = 10^{-i}$ and $\ell_3 = 1$. We have adapted the coordinates to the horizon such that $\tilde{r} = r - r_h$ and plotted against $\tan^{-1}(t)$ for ease of interpretation. The dashed line indicates the classical solution.

indicate significant changes to the near horizon behaviour for an infalling observer. One can show that for a fixed penetration depth, r_*, the lightcone of the QuBTZ will be bounded from below by the $\nu = 0$ BTZ lightcone and from above by the BTZ with r_h determined by the ADM of the QuBTZ solution.

5.3 Holographic Entanglement Entropy in the QuBTZ

We now wish to gain a better understanding of how quantum corrections alter the holographic entanglement entropy of the black hole. The authors of (14) provided analysis of how corrections alter the entropy of the black hole but did not extend this to subregions of the QuBTZ. In this subsection, we review key results of (14) and calculate the holographic entanglement entropy for subregions of the QuBTZ in the limit of small backreaction.

5.3.1 Entropy of the QuBTZ

In their original paper, Emparan et. al employed holography to identify the generalized entropy of the QuBTZ by calculating the area of the bulk black hole solution,

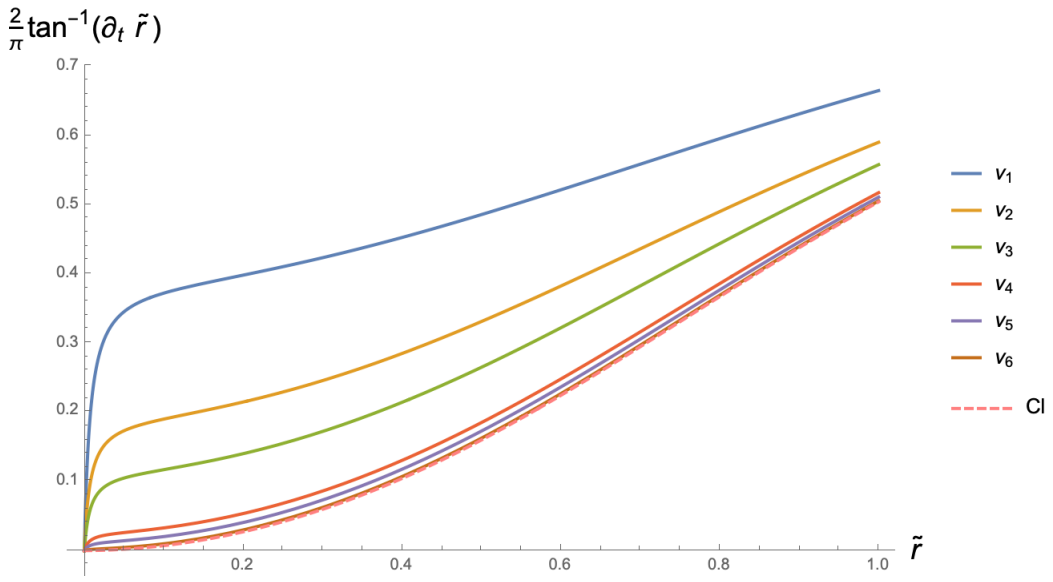

Figure 5.5: Plots of the near horizon behaviour of the lightcone for $z = \frac{9}{10\sqrt{3}}$, $v_i = 10^{-i}$ and $\ell_3 = 1$. We have adapted the coordinates to the horizon such that $\tilde{r} = r - r_h$ and plotted against $\tan^{-1}(d\tilde{r}/dt)$ for ease of interpretation. The dashed line indicates the classical solution.

$$\begin{aligned} S_{gen} =& \frac{2}{4G_4}\int_0^{2\pi\Delta} d\phi \int_0^{x_1} dx r_+^2 \frac{\ell^2}{(\ell + r_+ x)^2} \\ =& \frac{\pi \ell_3}{G_3} \frac{z\sqrt{1+v^2}}{1+3z^2+2vz^3} \\ =& \frac{\pi \ell_3}{\mathcal{G}_3} \frac{z}{1+3z^2+2vz^3} \end{aligned} \tag{5.30}$$

On the brane, we have a higher-derivative gravity theory such that the correct procedure to apply for finding the entropy of the black hole is the Wald entropy,

$$S_W = \frac{1}{4G_3}\int dx \sqrt{q}\left(1 + \ell^2\left(\frac{3}{4}R - g_\perp^{ab}R_{ab}\right) + \mathcal{O}(\ell/\ell_3)^4\right) \tag{5.31}$$

where we integrate over the horizon with induced metric q_{ab}, R and R_{ab} are the three dimensional spacetime curvatures at the horizon and $g_\perp^{ab} = g^{ab} - q^{ab}$ is the metric orthogonal to the horizon. One can expand in orders of ℓ,

$$S_{\text{gen}} = \frac{\mathrm{A}_4}{4G_4} = \frac{\mathrm{A}_3}{4G_3} + \ell\frac{\delta \mathrm{A}_3}{4G_3} + \ell^2 \mathcal{S} + S_{\text{out}}(|\phi\rangle) + \ldots \tag{5.32}$$

from which we may identify the contributions in order as: the Bekenstein-Hawking entropy

of the uncorrected BTZ black hole, corrections to its area due to leading-order quantum backreaction, the Wald entropy from higher-curvature terms in the semi-classical action and the contribution from the entanglement entropy of the conformal fields outside the horizon beginning at linear order in ℓ. Fixing M and expanding to linear order in ℓ one finds,

$$S_{\text{gen}} = \pi \ell_3 \sqrt{\frac{2M}{G_3}} \left(1 + \frac{\ell \mu}{2\ell_3}\right) - \frac{\pi \ell}{x_1} \sqrt{\frac{2M}{G_3}} + \mathcal{O}\left(\ell^2\right) \tag{5.33}$$

where the leading order term is the Bekenstein-Hawking entropy of the uncorrected black hole with a correction term $\propto \ell\mu$ coming from the quantum backreaction on the geometry and the final term coming from the entanglement entropy of the conformal fields. We justify the claim that linear order terms in ν are proportional to linear order CFT effects proportional to c by recalling that $c \approx \nu \frac{\ell_3}{2G_3}$. Neglecting higher order ν^2 terms, we find that at linear order the contribution from the entanglement entropy of CFT fields outside the horizon is given by,

$$S_{out} = S_{gen} - S_{Wald} = -\nu z S_{BTZ} + \mathcal{O}(\nu^2) \tag{5.34}$$

where we note that the entanglement entropy of the CFT need not be negative as this is simply the finite part of the entanglement entropy after reabsorbing the leading order corrections into the normalization of G_3. Generally, S_{out} is dominated by entanglement across the horizon between the black hole and the CFT with large Casimir effects. For small black holes, such as in the limits considered these effects are expected to be small and thermal effects will dominate as can be seen for small ν and z where we find,

$$S_{out} \approx -2\pi c (\pi \ell_3 T)^2 \tag{5.35}$$

where the T^2 dependence is that of a (2+1)-dimensional conformal gas. In contrast, solutions with $z \gg 1$ and $\nu \ll 1$ are located close to the global AdS_3 vacuum give a non-thermal result,

$$S_{out} \approx -2\frac{\pi}{3} c \tag{5.36}$$

For a given mass, the entropy of branch (1b) was found to be larger than that of branch (2) due to entanglement effects from the Casimir dominated CFT state. In the following subsection, we turn our attention to the more challenging problem of calculating the minimal surfaces and entanglement entropy of subregions of the QuBTZ.

5.4 Minimal Surfaces of QuBTZ Subregions

Understanding the full entanglement structure of the QuBTZ on the brane demands that we not only analyze the correspondence between global properties of the bulk and brane but also the interplay of entanglement entropy for subregions of this construction. We must consider a

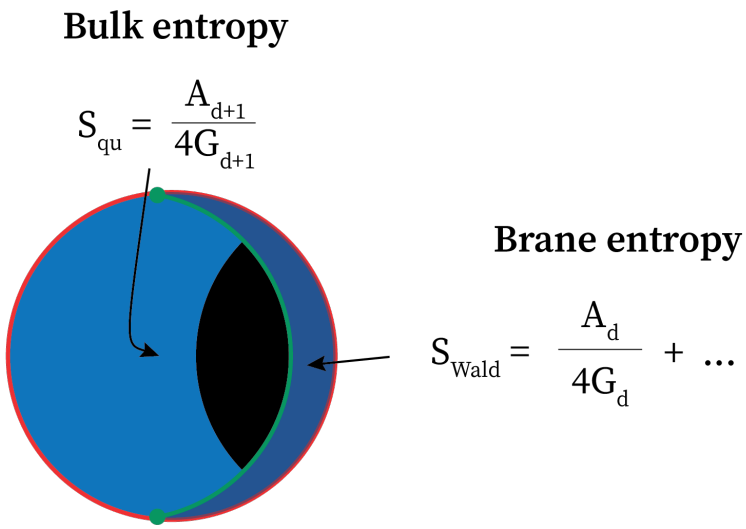

Figure 5.6: A schematic showing how the entropy is calculated in the geometric picture. The brane is indicated in green, the black region shows the bulk black hole region, red indicates the bulk conformal boundary, the dark blue region is the region integrated out and the light blue region is the bulk region outside the black hole.

number of additional complications which are not present in the global analysis.

The first such challenge emerges when we consider subregions of the bulk, where general minimal surfaces are now two-dimensional surfaces rather than simple geodesics. The second complication comes from the higher-derivative gravity theory induced on the brane which requiring the use of the Dong-Iyer-Wald formalism(9) (10) rather than the relatively simple RT formula. The third difficulty is that on both the brane and in the bulk the presence of the black hole introduces a non-trivial phase transition between the two possible minimal surfaces as in the classical case explained in Appendix D.

We focus here on the most physically relevant limit in which we consider linear corrections to the classical BTZ result from the brane perspective. In the limit of small ν the higher-derivative gravity corrections beginning at order ν^2 become irrelevant. This allows us to use the tamer RT formula for subregions in this limit. Physically, this prescription is equivalent to the FLM procedure plus contributions accounting for first order backreactions on the geometry(48).

5.4.1 Minimal Surfaces and Entanglement Entropy

Take a $t = 0$ slice of the geometry with a boundary region $\phi \in [-\phi_A, \phi_A]$ in the limit that $\nu << 1$. The metric of the constant time slice is given by,

$$ds^2|_{t=0} = \frac{dr^2}{\frac{r^2}{\ell_3^2} - 8\mathcal{G}_3 M - \frac{\ell F(M)}{r}} + r^2 d\phi^2 \tag{5.37}$$

To find the minimal surface from the RT formula, we simply need to find the geodesic connecting the point $-\phi_A$ to ϕ_A. We can choose the parameter r as our affine parameter and make use of the fact that $\phi' = \partial_r \phi$ is a Killing vector such that $\frac{\delta \mathcal{L}}{\delta \phi'} = C = r_*$.

We can then define the connected minimal surface as twice curve which minimizes the invariant length between two points defined by,

$$\begin{aligned} s &= \int_{s_i}^{s_f} ds = \int_{r=\infty}^{r=r_*} dr \mathcal{L} \\ &= \int_{r=\infty}^{r=r_*} dr \sqrt{\frac{1}{\frac{r^2}{\ell_3^2} - 8\mathcal{G}_3 M - \frac{\ell F(M)}{r}} + r^2 \phi'^2} \end{aligned} \tag{5.38}$$

Taking the variation of the invariant length with respect to ϕ' yields

$$\begin{aligned} \frac{d\phi}{dr} &= \pm \frac{r_* \ell_3}{\sqrt{r(r^2 - r_*^2)(r^3 - 8\mathcal{G}_3 M \ell_3^2 r - \ell_3^3 \nu F(M)}} \\ &= \pm \frac{r_* \ell_3}{\sqrt{r(r^2 - r_*^2)(\ell_3^2 r f(r))}} \end{aligned} \tag{5.39}$$

where r_* is the maximum radial penetration depth of the geodesic. While this particular integral does not have an exact solution, we can factorise it into,

$$\frac{d\phi}{dr} = \pm \frac{r_* \ell_3}{\sqrt{r(r^2 - r_*^2)(r - r_h)(r + b)(r + c)}} \tag{5.40}$$

where r_h, b, c are roots of $f(r)$ as before. The connected minimal surface is then given by,

$$\mathcal{E}^{(1)}(\phi_A) = \phi(r_*(\phi_A)) = \int_{r=r_*}^{r=\infty} dr \frac{r_* \ell_3}{\sqrt{r(r^2 - r_*^2)(r - r_h)(r + b)(r + c)}} \tag{5.41}$$

where we note that r_* is a function of ϕ_A alone. As in the BTZ case we must also consider that the disconnected minimal surface composed of the complement of $\mathcal{E}^{(1)}$ on the boundary as well as the contribution from the black hole horizon,

$$\mathcal{E}^{(2)}(\phi_A) = \phi(r_*(\pi - \phi_A)) \cup r_h \tag{5.42}$$

From the RT formula, the entropy is found by choosing the minimal surface which minimizes the entropy such that,

$$S = \begin{cases} \frac{1}{2G_3} \int_{r=1/\epsilon}^{r=r_*(\phi_A)} dr \sqrt{\frac{r^2}{f(r)(r^2 - r_*^2)}}, & \text{if } \phi_A < \phi_c \\ \frac{1}{2G_3} \pi r_h + \frac{1}{2G_3} \int_{r=1/\epsilon}^{r=r_*(\pi - \phi_A)} dr \sqrt{\frac{r^2}{f(r)(r^2 - r_*^2)}}, & \text{if } \phi_A \geq \phi_c \end{cases} \tag{5.43}$$

where we made use of the fact that corrections to G_3 start at $\mathcal{O}(\nu^2)$ and ϕ_c is the critical angle where the minimal surfaces change dominance. Generally, ϕ_c can be found by equating the two entropies, however, (5.43) does not have an analytical solution and we must expand to first order in ν. As stated previously, the RT prescription on the brane is only valid to first order in ν anyway.

Before we move on to calculating these quantities in the linear ν regime, it is worth commenting on some features of (5.43). Firstly, we expect that for small ν the critical angle ϕ_A^* will be close to the classical result. However, due to the fact that r_h increases monotonically with ν one expects that for fixed z,

$$|S(\phi_A) - S(\pi - \phi_A)|_{QuBTZ} \leq |S(\phi_A) - S(\pi - \phi_A)|_{BTZ} \tag{5.44}$$

implying that the Araki-Lieb inequality is saturated for smaller values of ϕ_A. We therefore anticipate that if the quantum corrected solution follows a relationship close to the classical solution $(\phi_c)_{QuBTZ} \leq (\phi_c)_{BTZ}$, though this will also depend on the shape of the minimal surface. Naturally, these expectations must be altered for the full higher-derivative theory.

5.4.2 Minimal Surface for $b = c$

There exists no general analytic solution for the minimal surface of the QuBTZ covering arbitrary values of b and c, however, it turns out that in the case when

$$8\mathcal{G}_3 M = 3\left(\frac{F(M)\nu}{2}\right)^{2/3}; \quad \Delta_3 = 0 \tag{5.45}$$

then $b = c = r_h/2$, $r_h = \sqrt{\frac{32\mathcal{G}_3 M}{3}} = (4\nu F(M))^{1/3}$ and we find the analytic solution,

$$\begin{aligned}\phi(r) &= \pm \int_\infty^{r_*} dr \frac{r_*}{\sqrt{r(r^2 - r_*^2)(r - r_h)(r + \frac{r_h}{2})^2}} \\ &= \pm \frac{4\sqrt{r_*}}{r_h}\left(\frac{1}{\sqrt{r_h + r_*}}\left(F[\kappa_1(r; r_*), \kappa_2(r_h, r_*)] - K[\kappa_2(r_h, r_*)]\right)\ldots\right. \\ &\quad \left. + \frac{2r_*}{(2r_* - r_h)}\left(\Pi[\kappa_0(r_h, r_*), \kappa_2(r_h, r_*)] - \Pi[\kappa_0(r_h, r_*), \kappa_1(r; r_*), \kappa_2(r_h, r_*)]\right)\right)\end{aligned} \tag{5.46}$$

where $\kappa_0(r_h, r_*) = \frac{2r_h}{r_h - 2r_*}$, $\kappa_1(r; r_*) = \sin^{-1}(\frac{r + r_*}{2r})$, $\kappa_2(r_h, r_*) = \frac{2r_h}{r_h + r_*}$ and F, Π and K are elliptic integrals. In terms of z and ν, these solutions occupy parameter space,

$$\nu_{b=c} = \frac{1}{3z + 4z^3} \tag{5.47}$$

such that to stay in the limit of $v_{b=c} < 1$,

$$z > z_{b=c} = \frac{(1+\sqrt{2})^{2/3}-1}{2(1+\sqrt{2})^{1/3}} \tag{5.48}$$

Clearly this function is not invertible and hence a simple expression for the critical angle eludes us. We can however, find an expression for the size of the operator on the boundary,

$$\begin{aligned}\phi_A =& \frac{4\sqrt{r_*}}{r_h}\left(\frac{1}{\sqrt{r_h+r_*}}\left(F[\pi/4,\kappa_2(r_h,r_*)]-K[\kappa_2(r_h,r_*)]\right)\ldots\right.\\ &\left.+\frac{2r_*}{(2r_*-r_h)}\left(\Pi[\kappa_0(r_h,r_*),\kappa_2(r_h,r_*)]-\Pi[\kappa_0(r_h,r_*),\pi/4,\kappa_2(r_h,r_*)]\right)\right)\end{aligned} \tag{5.49}$$

There exists an analytic solution for the entropy, however, lacking an invertible expression for the critical angle it provides little insight. The geodesic for a radially falling lightlike observer can also be shown to be

$$\begin{aligned}t(r) &= \pm\left(\frac{2}{3(2r+r_h)}-\frac{4}{9r_h}\log\left(\frac{2(r-r_h)}{2r+r_h}\right)\right)\\ &= \pm\left(\frac{2}{3(2r+r_h)}+\frac{4}{9r_h}\log\left(1+\frac{3r_h}{2(r-r_h)}\right)\right)\end{aligned} \tag{5.50}$$

We shall return to this result in Part III when we discuss the butterfly velocity in the QuBTZ.

5.4.3 Linear Backreaction Corrections

Let us then focus on the small v limit and expand (5.39) to linear order about $v = 0$,

$$\begin{aligned}\frac{d\phi}{dr} &\approx \pm\frac{r_*\ell_3}{\sqrt{r(r^2-r_*^2)}}\left(\frac{1}{\sqrt{\ell_3^2 rf(r)}}+v\partial_v\frac{1}{\sqrt{\ell_3^2 rf(r)}}\right)\Bigg|_{v=0}\\ &= \left(\frac{d\phi}{dr}\right)_{BTZ}+v\left(\frac{d\phi}{dr}\right)_{corr}\end{aligned} \tag{5.51}$$

The first term is the classical QuBTZ result with mass determined by z, whilst the second is a simple correction term. At linear order, this equation is just a first order linear ODE,

$$\begin{aligned}\left(\frac{d\phi}{dr}\right)_{corr} &= -\frac{1}{2}\frac{r_*\ell_3}{\sqrt{r(r^2-r_*^2)}}\frac{\partial_\nu(\ell_3^2 rf(r))}{(\ell_3^2 rf(r))^{3/2}}\Big|_{\nu=0} \\ &= \frac{1}{2}\frac{r_*\ell_3}{\sqrt{r(r^2-r_*^2)}}\left(\frac{\ell_3^2(h_1(z)r+h_2(z))}{(\ell_3^2 rf(r)_{cl})^{3/2}}\right)\end{aligned} \tag{5.52}$$

where we define $f(r)_{cl} = r^2 - r_h^2|_{\nu=0}$ and make use of

$$\begin{aligned}\ell_3^2 rf(r) &= r^3 - 8\mathcal{G}_3 M\ell_3^2 r - \ell_3^3 \nu F(M) \\ &\approx \ell_3^2 rf(r)_{cl} - \nu\ell_3^2 r\partial_\nu f(r)|_{\nu=0} \\ &= \ell_3^2 rf(r)_{cl} - \nu\ell_3^2\left(\ell_3^2\frac{4z^3(1+z^2)(-1+3z^2)}{(1+3z^2)^3}r - \ell_3^3\frac{8z^4(1+z^2)}{(1+3z^2)^3}\right) \\ &= \ell_3^2 rf(r)_{cl} - \nu\ell_3^2(h_1(z)r+h_2(z))\end{aligned} \tag{5.53}$$

and $h_1(z) = 8\partial_\nu\mathcal{G}_3 M|_{\nu=0}$ and $h_2(z) = \partial_\nu(\nu F(M))|_{\nu=0} = F(M)|_{\nu=0}$. Therefore, to linear order in ν with $\ell_3 = 1$, the equation (5.58) is solved as

$$\phi(r) = \pm\left(\tanh^{-1}\left(\frac{r_h\sqrt{r^2-r_*^2}}{r_*\sqrt{r^2-r_h^2}}\right) - \frac{\nu}{2}(h_1(z)\gamma_1(r;z) + h_2(z)\gamma_2(r;z))\right) + \text{Const} \tag{5.54}$$

where,

$$\gamma_1(r;z) = \int dr\frac{r_*}{r\sqrt{((r^2-r_*^2)(r^2-r_h^2)^3)}} = -\frac{r_*\sqrt{(r^2-r_*^2)}}{r_h^2(r_h^2-r_*^2)\sqrt{r^2-r_h^2}} - \frac{1}{r_h^3}\tanh^{-1}\left(\frac{r_*\sqrt{r^2-r_h^2}}{r_h\sqrt{r^2-r_*^2}}\right) \tag{5.55}$$

and,

$$\begin{aligned}\gamma_2(r;z) = &\sqrt{\frac{r^2-r_*^2}{r^2-r_h^2}}\frac{r_h^4 + 2r_*^2r^2 - r_h^2(r_*^2+r^2)}{r_h^4(r_h^2-r_*^2)r} + \frac{r_*^2}{r_h^2(r_h^2-r_*^2)}\Bigg(-(r_h^2-2r_*^2)E\left[-\sin^{-1}\left(\frac{r}{r_h}\right),\frac{r_h^2}{r_*^2}\right] + \ldots \\ &2(r_h^2-r_*^2)F\left[-\sin^{-1}\left(\frac{r}{r_h}\right),\frac{r_h^2}{r_*^2}\right]\Bigg)\end{aligned} \tag{5.56}$$

where E is the elliptic integral of the second kind and F is the elliptic integral of the first kind and the constant is found by matching $\phi(r_*) = 0$. The first term in (5.54) is precisely the same form as the classical result found in Appendix D. One notes that we can identify the $h_1(z)$ and $\gamma_1(r;z)$

and $h_2(z)$ and $\gamma_2(r;z)$ with corrections coming directly from the first order backreaction on the classical geometry and those from the CFT_3 fields below the cutoff respectively. In this sense they can be pictured as subregion generalizations of (5.33). Though we cannot simply invert this function, we can easily show that the corrections are positive such that $|\phi(r)|_{cl} \leq |\phi(r)|_{qu}$ and $S_{cl} \leq S_{qu}$.

Another alternative to the linear ν procedure is to instead take the expansion about small b,

$$\begin{aligned}\frac{d\phi}{dr} &\approx \pm \frac{r_* \ell_3}{\sqrt{r(r^2 - r_*^2)}} \left(\frac{1}{\sqrt{r^2 - r_h^2}} + b\partial_b \frac{1}{\sqrt{(r-a)(r+b)(r+a-b)}} \right)\Bigg|_{b=0} \\ &= \left(\frac{d\phi}{dr}\right)_{BTZ} + b\left(\frac{d\phi}{dr}\right)_{corr}\end{aligned} \tag{5.57}$$

where,

$$\left(\frac{d\phi}{dr}\right)_{corr} = \frac{-r_* r_h}{2r^2(r+r_h)\sqrt{(r^2 - r_*^2)(r^2 - r_h^2)}} \tag{5.58}$$

with solution

$$\begin{aligned}\phi_{corr}(r) = &\frac{1}{2r r_* r_h^2 \sqrt{r^2 - r_h^2}(r_*^2 - r_h^2)} \Bigg(r_h \sqrt{r^2 - r_*^2}(r_h^2(r + r_h) - r_*^2(3r + r_h)) - r\sqrt{r^2 - r_h^2} \ldots \\ &\Bigg((r_h + r_*)(r_h^2 - 2r_*^2) E[\alpha_1(r; r_*, r_h), \alpha_2(r_*, r_h)] + (r_* - r_h)\Bigg(r_h^2 F[\alpha_1(r; r_*, r_h), \alpha_2(r_*, r_h)] + \ldots \\ &2(r_* - r_h) r_* \Pi[\alpha_0(r_*, r_h), \alpha_1(r; r_*, r_h), \alpha_2(r_*, r_h)] \Bigg) \Bigg) \Bigg)\end{aligned} \tag{5.59}$$

where $\alpha_0(r_*, r_h) = \frac{2r_h}{r_h + r_*}$, $\alpha_1(r; r_*, r_h) = \sin^{-1}\left(\frac{(r-r_*)(r_h+r_*)}{2(r-r_h)r_*}\right)$, $\alpha_3(r_*, r_h) = \frac{4r_h r_*}{(r_h+r_*)^2}$ and E, F and Π are elliptic integrals as before. While this result is equally cumbersome it provides a better approximation particularly when the corrections to the ADM mass are dominant over those from $F(M)$.

Without an invertible expression for the linear order solution, we don't have a handy expression for the critical angle as for the BTZ case. In the following subsection we shall make some general constraints to guide our intuition.

5.5 Constraints on Minimal Surfaces

There are several ways with which we could compare the minimal surfaces enabling us to deduce some general features of the physics on the QuBTZ. An obvious complication, however, comes from the phase change from connected to disconnected minimal surfaces. We will therefore assume that this value lies close to that of a BTZ black hole with a mass determined by the horizon radius of the QuBTZ of interest and set r_* to be well away from this point and fixed for comparisons.

Before resorting to numerics, we can apply some simple intuition to place bounds on the quantum corrected solutions. Fixing z and $8\mathcal{G}_3 M$ allows for comparison between two possible backreacted corrections of a QuBTZ with mass parameter z and the same ADM mass. Assuming that we further fix r_*[33], the only change comes from the $\nu F(M)$ contribution. One can see from (5.41) that,

$$\left|\left(\frac{d\phi}{dr}\right)\right|_{cl} \leq \left|\left(\frac{d\phi}{dr}\right)\right|_{(2)} \leq \left|\left(\frac{d\phi}{dr}\right)\right|_{(1b)} \tag{5.60}$$

which from (5.43) implies that,

$$\left|\phi_{(1b)}(r; z, \nu_2, r_*)\right| \geq \left|\phi_{(2)}(r; z, \nu_1, r_*)\right| \geq \left|\phi_{cl}(r; z, \nu = 0, r_*)\right| \tag{5.61}$$

and

$$S(\mathcal{E}^{(1)})_{(1b)} \geq S(\mathcal{E}^{(1)})_{(2)} \geq S(\mathcal{E}^{(1)})_{cl} \tag{5.62}$$

where cl, (1b) and (2) indicate the BTZ, the Casimir and the thermal solutions. Note that we cannot simultaneously constrain the classical solution to have the same ADM mass and z for $M > 0$ and hence the classical comparison will generically have a different mass. This result agrees well with physical intuition from the perspective of an infalling observer. Far away from the black hole, the geometries are locally similar. Closer to the horizon the CFT effects build up in the bulk, requiring a larger entanglement wedge on the boundary. Furthermore, we note that the entropy contribution from the black hole itself is proportional to horizon of the black hole, which grows with ν. We are only interested in cases where $\nu_{(1b)}, \nu_{(2)} < 1$, which also restricts the range of allowable z to,

$$0.456 < z < \frac{1}{\sqrt{3}} \tag{5.63}$$

where the lower bound is calculated using some unenlightening roots. We can also compare the

[33]We must take care as the changing r_h and r_c as we increase ν means that we may not freely choose r_* for all values. That is, we assume that $r_* \geq r_c$ for all geometries

quantum corrected case to a classical BTZ with horizon equal to that of the QuBTZ[34],

$$\Delta\phi' = \left(\frac{d\phi}{dr}\right)_{cl} - \left(\frac{d\phi}{dr}\right)_{QuBTZ} \propto \frac{1}{\sqrt{r+r_h}} - \sqrt{\frac{r}{(r+r_h-b)(r+b)}} \tag{5.64}$$

where we used that $a = b + c$. We then find that $\Delta\phi' > 0$ provided $b < r_h$ or $-4(\mathrm{Im}[b])^2 < 0 < r_h^2$ when the determinant of the cubic is positive or negative respectively. These hold trivially for all b and r_h. Hence, this further implies

$$\left|\phi_{QuBTZ}(r; r_h, r_*)\right| \leq \left|\phi_{BTZ}(r; r_h, r_*)\right| \tag{5.65}$$

and

$$S(\mathcal{E}^{(1)})_{BTZ} \geq S(\mathcal{E}^{(1)})_{QuBTZ} \tag{5.66}$$

Making use of these two results, we find that there exists a general nesting property,

$$\begin{aligned} \left|\phi_{BTZ}(r; r_h^{(1b)}, r_*)\right| &\geq \left|\phi_{(1b)}(r; z, v_2, r_*)\right| \geq \left|\phi_{cl}(r; z, v=0, r_*)\right| \\ \left|\phi_{BTZ}(r; r_h^{(2)}, r_*)\right| &\geq \left|\phi_{(2)}(r; z, v_1, r_*)\right| \geq \left|\phi_{cl}(r; z, v=0, r_*)\right| \end{aligned} \tag{5.67}$$

so that the quantum corrected solution is always bounded from above by the classical solution with the same horizon radius and from below by the classical black hole with the same z as seen in Figure 5.7.

This nice result further suggests that the critical angle will be somewhere between that of these two results which can be determined analytically using the classical solution,

$$\phi_c^{(BTZ)}(r_h(z,0)) \leq \phi_c^{(QuBTZ)}(r_h(z,v)) \leq \phi_c^{(BTZ)}(r_h(z,v)) \tag{5.68}$$

These results give some intuition regarding the behaviour of minimal surfaces in the small v limit which does not require an analytical solution for the quantum corrected minimal surface. To confirm this analysis, one could determine the size of ϕ_A as a function of r_* numerically and find the values of $r_*(\phi_A)$ and $r_*(\pi - \phi_A)$. One could then plot the entropy of the two minimal surfaces as a function of r_* and find where the two minimal surfaces become equal. This procedure, however, is tedious and is not particularly enlightening and so we defer it to later research.

[34]This is distinct from simply fixing the ADM mass for which the results are less clear-cut. In the case at hand there is a contribution from $vF(M)$ so the classical solution will generally have a different ADM mass.

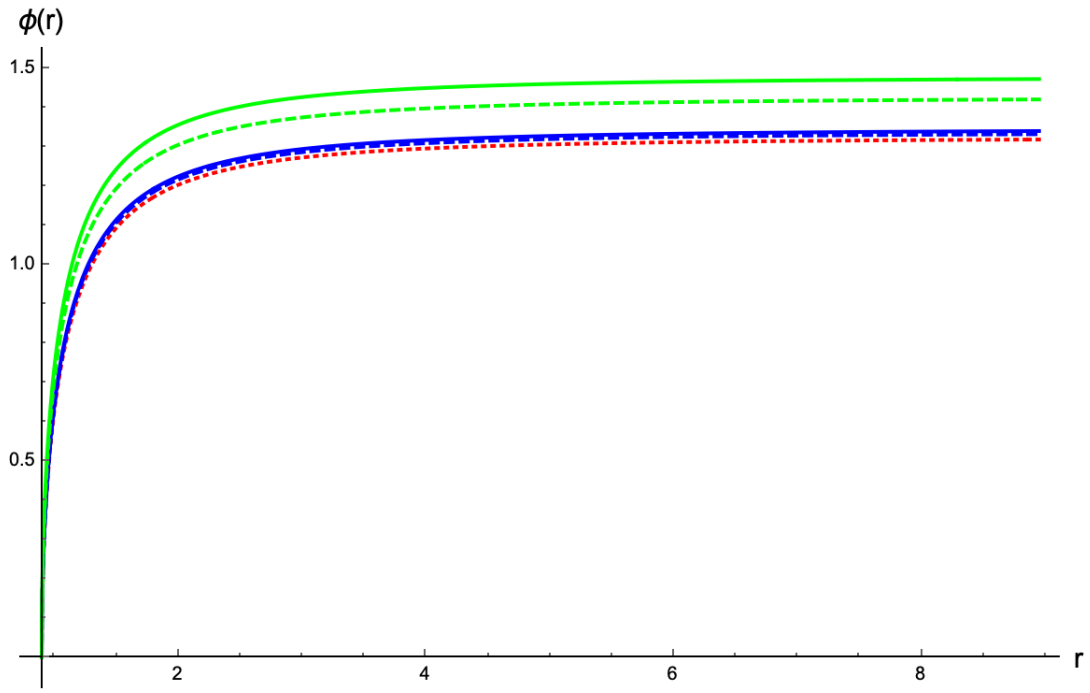

Figure 5.7: This figure shows the positive branch of the minimal surface for the unperturbed case (Red, Dotted), the thermal solution (Blue, Dashed), the Casimir solution (Green, Dashed) and the BTZ results with $r_h^{(2)}$ (Blue) and $r_h^{(2)}$ (Green) for the values $z = \frac{9}{10\sqrt{3}}$, $\nu_1 = 0.1$, $\nu_2 = 0.6$.

Part III

Holography, Chaos and Quantum Corrected Butterflies

Nature abounds with complex and inherently chaotic behaviour for which our optimistically reductionist models are often insufficient to accurately describe. Even small classical systems can exhibit chaotic dynamics, without the additional woes of the inherent indeterminism of quantum mechanics. In spite of the exact microscopic behaviour of individual particles or operators, we can treat chaotic systems stochastically allowing us to make reasonable predictions of weather patterns or thermal systems, for example. In the context of holographic systems, we can employ the tools of the AdS/CFT correspondence as a means by which we can model thermalization and scrambling in strongly coupled quantum systems. Of particular interest is modelling information scrambling in black holes with holographic duals as well as using entanglement to place bounds on information spreading and transport coefficients(94)(95).

In this chapter, we review notions of classical and quantum chaos and its realisation in holographic systems. These techniques are then applied to calculate the so-called Butterfly Velocity, v_B quantifying the rate at which information spreads in a chaotic system. When applied to the QuBTZ solution, one finds that the standard approaches proposed by (15) and (16) suggest a superluminal value for v_B when backreaction from the bulk CFT is included. This unexpected result is intriguing and, *prima facie*, runs contrary to claims that these procedures are robust under the addition of quantum and higher-derivative gravity corrections (96)(97). We discuss potential sources for this discrepancy by focusing on the small ν limit of the QuBTZ construction which one expects to give results perturbatively close to those of the classical value. When one calculates the rate of growth of the operator on the boundary numerically one indeed confirms that $v_B \geq 1$. These corrections were found to be several orders of magnitude below expected linear order when calculated at one thermal length from the horizon. Furthermore, we note that there presently exists scant mention of how to generalize this procedure to smaller (non-planar) black holes motivating a reappraisal of the assumptions employed by Mezei and Stanford. We further argue that the standard methodology of (15) and (16) should be adapted for small black holes. In this prescription, one calculates the butterfly velocity at the critical angle on the boundary or radius in the bulk where the minimal surface transitions from the connected to the disconnected phase rather than at a thermal length from the horizon.

Chapter 6

Chaos in Holographic Systems

The study of chaotic systems began as early as Poincaré's discovery of non-periodic elliptic orbits which never approach a fixed point. This behaviour is an example of deterministic chaos, illustrating that even classical systems with a small number of degrees of freedom can exhibit chaotic behaviour.

So, what is it we mean by chaos? There remains no universally accepted definition but we may fall back on an heuristic notion that states which start close to one another in phase space can exhibit trajectories which diverge exponentially from one another over time. This behaviour is most generally captured by the Lyupanov exponent, λ, characterizing the rate of separation of infinitesimally close trajectories of dynamical systems in phase space. Quantitatively, under the assumption that we can linearize this separation in the large t limit, we find

$$|\delta Z(t)| \approx e^{\lambda t}|\delta Z_0| \tag{6.1}$$

where $|\delta Z_0|$ is the separation of states in initial configuration. Technically, there exists a spectrum of Lyupanov exponents which are characterised by the possible different orientations of the initial state separation vector. Systems with a compact phase space exhibit chaotic behaviour provided the largest of these Lypanov exponents is positive. These notions were developed and formalised in the following century and a half, culminating in a rich yet still incomplete understanding of complex systems.

Naturally, one may wonder how such behaviour manifests in quantum systems which are inherently indeterministic. In particular, we are interested in the so-called scrambling of information in many-body systems. Suppose we act some local operator and we wish to see how this fine-grained local information spreads dynamically under time evolution. The original information mixes with other local degrees of freedom until the original information contained in this local operation becomes scrambled over a large number of degrees of freedom. Equivalently, we can state that for chaotic systems the growth of a local operator under standard Heisenberg

evolution effectively redistributes the local information to global information.

In the holographic context, we can study how information is scrambled in strongly coupled systems by modelling quantum quenches in which some excess energy density is added to the system. We recall that the bulk dual to a thermal CFT in the AdS/CFT correspondence is a black hole geometry, however, this represents a global state of the boundary theory in the static limit. We may instead be interested in how one can build up such a state by applying local operations until these fine grained degrees of freedom are scrambled across the full spacetime. In this limit, the information is scrambled and the density matrix of the CFTs becomes mixed and manifest as a non-local degrees of freedom characterised simply by the state of our boundary theory and a subsequent phase transition which we would expect from the change in the global topology of the space. Equally, we may be interested in what happens to local information as it falls into the black hole or how scrambling effects obervables in strongly coupled quantum systems. In the following, we provide an overview of chaos in quantum systems before delving into chaotic dynamics in holographic systems.

6.1 Chaos in Quantum Systems

A simple probe, and functional definition characterising quantum chaos, appearing in the literature comes from the commutator-squared,

$$\begin{aligned} C(\boldsymbol{x}, t; \rho) &\equiv -\operatorname{tr}(\rho[O_1(\boldsymbol{x}, t), O_2(0,0)]^\dagger[O_1(\boldsymbol{x}, t), O_2(0,0)]) \\ &= -\langle |[O_1(\boldsymbol{x}, t), O_2(0,0)]|^2 \rangle_\beta \end{aligned} \tag{6.2}$$

defined for local operators O_1, O_2 in the equilibrium state ρ with inverse temperature $1/\beta$. Beyond the locality constraint and the assumption that these operators do not drastically change the energy density[35], these operators may be entirely arbitrary and have the simple heuristic interpretation analogous to the classical state, paramaterising their state separation in Hilbert space. The commutator-squared produces a lightcone-like spread of quantum information in the system which is characterised by two state-dependent quantities: its quantum Lyupanov exponent and its butterfly velocity, v_B.

To picture why the OTOC is so useful, we can imagine that we make a small perturbation of the system at $O_2(0,0)$ and then another at $O_1(\boldsymbol{x}, t)$ and measure the correlation function. We can then calculate the time reversed correlation function where we first apply $O_1(\boldsymbol{x}, t)$ and then another at $O_2(x, 0)$. In general, we expect that the correlation functions $\langle O_2(0,0)O_2(\boldsymbol{x}, t)\rangle_\beta$ to decay exponentially with t for late times as it dissolves into the thermal soup. After some (generally) finite time, one will be unable to distinguish which order these operators were applied and their

[35] Equivalently, we assume that there is negligible backreaction on the system but non-trivial change to the entanglement structure.

commutator will approach zero. Hence, the commutator quantifies how well one can distinguish perturbations of a quantum system in a state-dependent and relativistic scheme. At small t and $\boldsymbol{x}$, one can recover the information of which operator was applied first by 'measuring' the commutator[36], thus giving a notion of the memory the system has of its microscopic details over time. Only looking at the commutator, however, may gives a sign ambiguity and may present some cancellations which we can remove by taking the norm of this value. As an easy toy example, consider that O_1 and O_2 are both unitary and Hermitian such that,

$$\begin{aligned} C(\boldsymbol{x}, t; \rho) &= \langle O_1 O_2 O_2 O_1 + O_2 O_1 O_1 O_2 - O_1 O_2 O_1 O_2 - O_2 O_1 O_2 O_1 \rangle_\beta \\ &= 2(1 - \mathrm{Re}[O_2 O_1 O_2 O_1]) \end{aligned} \tag{6.3}$$

where we suppress coordinates for simplicity define the OTOC as $O_2 O_1 O_2 O_1$[37]. In a chaotic system, the OTOC decays from its maximum at unity to zero whilst $C(\boldsymbol{x}, t; \rho)$ grows from zero to its maximum of two.

These operators are local and hence the spread of information must be causally connected, leading to an effective 'lightcone' like spreading of information referred to as the butterfly cone. The behaviour of this lightcone is characterized by the rate at which the information spreads known as the quantum Lyupanov exponent, and a characteristic velocity both of which depend upon the state of the system. Just beyond this emergent butterfly cone for $t > 0$, the OTOC behaves approximately as

$$C(x, t; \rho) \sim e^{-\lambda(|x - x_0|/v_B - t)^{1+p}/t^p} \tag{6.4}$$

where p is some system dependent real number and v_B is the butterfly velocity which can be defined as the the rate of growth of the double-commutator when $C(x, t; \rho) = 1$. When we take the limit of large local degrees of freedom, the factor p generally goes to zero and the behaviour becomes approximately exponential[38]. In (6.4) we note that the behaviour is characterised by both exponential growth and diffusion. For quantum systems, the butterfly velocity therefore gives a profound insight into transport and information spreading. The butterfly velocity gives a state dependent speed of information propagation in quantum systems which is advantageous over the Lieb-Robinson velocity[39](98). The butterfly velocity is defined analogously to the Lieb-Robinson velocity, but using the OTOC instead of the commutator-squared. This definition then depends upon the state of ρ.

[36]We are being liberal with measurement here as this set-up would necessitate a system which could be reversed in time or some exact copy which would violate no-cloning.

[37]We made use of $O_i^\dagger = O_i$ and $O(t) = U^\dagger(t) O(0) U(t)$, where $U^\dagger(t) U(t) = 1$

[38]This is not precisely true of all systems, such as spin chains, for which $p > 0$ and therefore there is a additional 'broadening' effect on the dispersion of information, however we will assume that $p = 0$ throughout the this thesis.

[39]The Lieb-Robinson velocity gives a state independent locally emergent lightcone for for systems with a finite Hilbert space.

We can also define the 'state-dependent Lyapunov exponent' using (6.4),

$$\lambda(v;\rho) \equiv \lim_{t\to\infty} \frac{1}{t} \ln C(vt, t;\rho) \tag{6.5}$$

The butterfly velocity cone can be defined as

$$v_B(\rho) \equiv \sup\{\nu \,:\, \lambda(v\hat{n};\rho) \geq 0\} \tag{6.6}$$

where $\hat{n}$ is a unit normal vector. Within this cone, all Lyupanov exponents are greater than or equal to zero and $C(x,t;\rho) \approx 1$ everywhere. We emphasize that v_B is defined as a local quantity which cannot simply be determined at an arbitrary point. Physically, it captures the rate at which quantum operators grow under chaotic Hamiltonian dynamics and hence characterizes the rate of approach to the late time thermal value of the entropy.

6.2 Quantum Quenches and Thermalization

Accurately modelling non-equilibrium dynamics is a notoriously difficult affair. A simple but analytically rich model of non-equilibrium processes in many-body quantum mechanical systems comes through quantum quenches. A quantum quench involves turning on some excitation of a system in its ground state at $t = 0$ and then allowing it to evolve. When the change in the Hamiltonian of the system is homogenous over the entire system, the quench is global whilst if we consider some subregion of the entire system it is referred to as a local quench. In particular, such a mechanism is valuable for studying thermalization in strongly interacting systems[40] and distinguishing between pure and mixed states in AdS/CFT. The AdS/CFT correspondence gives an appealing model for thermalization as the strong interactions of the boundary theory ensure that such an excitation spreads efficiently through the system.

From here on, we shall assume that we are working in the AdS/CFT picture and hence the CFT coupling and gauge group N are both large[41]. For global quenches, we impart some finite energy to a strongly coupled system such that the energy is quickly distributed throughout the system. As always, we may purify the state by going to the TFD configuration. For $t > 0$, time evolution of the state remains unitary and hence the system remains pure. Tracing out some region in the total Hilbert space leaves us with a thermal density matrix which (for sufficiently small regions) approaches the canonical distribution. The picture is clear, by tracing out the complement we have effectively thermalized this subregion so that it remains in local equilibrium with an effective bath(99)(100).

[40] By thermalization, we mean studying how systems go from pure to thermal systems under the addition of energy. Further, we are mostly interested in systems which eventually come to thermal equilibrium.

[41] For more general treatments, see Chapter 7 of (19)

This simple observation shows us that we cannot distinguish between a pure state of the quantum quench and a thermal mixed state from coarse grained quantities such as correlation functions alone. If, however, we consider the entanglement entropy, we are free to choose how much of the system we wish to trace out and hence we have additional information to distinguish the mixed and the pure quench states. Thereby, the entanglement entropy is an invaluable tool for studying quantum quenches and models of thermalization. In the context of AdS/CFT, quantum quenches are particularly interesting as the thermalization of the boundary CFT gives us information on the formation of black holes in the bulk.

Explicit models of thermalization have been studied in models of black hole formation with an infalling shell of matter(101). In such models, the infalling matter is given by the Vaidya-AdS metric and geodesics in AdS_3 are glued to the BTZ shell after the it collapses beyond the event horizon, accounting for the refraction through the infalling matter. Higher dimensional models have also been discussed in (102)(103)(104).

6.3 Purity and Thermalization

The AdS/CFT correspondence tells us that quenches of the boundary CFT correspond to black hole formation. In particular, we may wonder if the late time evolution saturates such that it thermalizes to the eternal black hole. For local correlation functions, this is precisely what happens. If this were to hold for all observables, however, we would quickly come up against a contradiction by creating a mixed state from a pure state. Fortunately, however, we can resolve this apparent paradox by making use of the homology constraint.

If we consider an evolution of the HEE for both A and $\bar{A}$ we can make sense of this. In the infinite past, before the quench, there is no black hole and hence A and $\bar{A}$ share a common entangling surface and $S(A) = S(\bar{A})$. Once the black hole forms, however, there is now a physical horizon in the bulk. However, one finds that the extremal surface $\mathcal{E}_{\bar{A}}$ wraps around the horizon and hence contains the thermal contribution. We recall that the second asymptotic region is no longer present in the case of the eternal black hole, hence we can show that the extremal surface $\mathcal{E}_A$ is homologous to $\bar{A}$ despite the presence of the horizon. To see this, one may deform $\mathcal{E}_{\bar{A}}$ continuously to $\mathcal{E}_A$ without obstruction by moving the surface far back into the past before collapse. By doing so, the surface moves outside of the horizon where this homology is manifest. Hence, the horizon acts as a physical entangling surface which traces out its complement.

From this argument, we see that the global homology constrain ensures that our total system remains in a pure state and hence from the holographic perspective, any quantum quench of a holographic state remains pure (101)(105). In particular, the fine-grained entropy of the total system vanishes. A crucial ingredient in this argument is that the homology surface is spacelike. What should we make of the physical meaning of the entropy of the horizon in such a model? The entanglement entropy for subsystems approaches the result of a treatment of a finite tem-

perature CFT with its IR contribution approaching the black hole entropy. One can simply say that the coarse grained entropy of some small subsystem is well approximated by the thermal density matrix such that the region we have traced out acts as a heat bath for a sufficiently small subsystem. Correlation functions and other local measurements, however, can not distinguish between a thermal or a quench state [42]. Because the thermal value dominates the partition function, we require exponentially precise measurements to distinguish the quench state from the thermal state. We stress that entanglement entropy, however, is not a local observable and instead encodes information about the wavefunction such that if one could access the fine-grained contribution for the geometry, they would be able to distinguish between a pure quenched state and a mixed state.

6.4 Spread of Information in Holographic Systems

One appealing feature and recurring theme in AdS/CFT is that we can keep track of notions of helpful information which we may use to diagnose otherwise complicated physical phenomena such as phase transitions or thermalization. Pioneering work in this direction was done in (106)(107) in which the authors classified distinct phases of the evolution of entanglement entropy through the poetically named 'entanglement tsunami'.

Suppose we quench the system at $t = 0$ by dumping excess energy into the system. This energy is first distributed amongst pairs of entangled quanta. The number of these quanta will be proportional to the energy density ε[43]. The phases of the entanglement tsunami can be split into approximately three phases under the assumption that the system thermalizes to T_{eq} at late times. The thermalization value also sets an equilibrium length scale through its inverse $\beta_{eq} = T_{eq}^{-1}$, allowing for useful approximations provided that our system is reasonably large and the energy density remains approximately constant. We also assume that the region of interest is macroscopic such that we are not limited to UV features of the entanglement entropy and define the length scale of the system, A, to be ℓ_A. We can then characterise the following distinct phases by their statistical distributions. At early times, the system will not be in local equilibrium, at intermediate times local equilibrium emerges and at late times the system reaches some global equilibrium value.

1. $t \leq \beta_{eq}$: During this phase, local equilibrium has not been reached and we expect the rate of change in entropy to be largest. Due to causality and the locality of the quantum dynamics, the entanglement entropy only receives contributions from near the entangling surface.

[42] That is, without being able to make precise measurements of high point correlators.

[43] These should not be thought of as quasi-particle excitations as this would not be a good model within a strongly coupled (holographic) QFT. We assume in this picture that the energy density should be approximately constant here.

Therefore, only modes in the vicinity of the entangling surface will contribute. One may then introduce some dimensional analysis to show that the entanglement entropy should grow quadratically following the quench,

$$\Delta S_A = \frac{\pi}{d-1} \varepsilon \mathrm{A}(\partial A) t^2 + \ldots \tag{6.7}$$

Heuristically, we ought to expect this to be the case as pre-thermalization behaviour will take on the characteristic entanglement entropy area-law behaviour. Furthermore, it was proposed in (16) that

$$\frac{d}{dt} S[A(t)] \leq v_E s_{th} \mathrm{A}(\partial A) \tag{6.8}$$

implying that the rate of entanglement growth never grows faster than right after a quench.

2. $\beta_{eq} \ll t \ll \ell_A$: Parts of the system have now reached local equilibrium but we still remain far away from a global equilibrium phase such that only patches are equilibrated [44]. In this regime, we anticipate a transition from the area-law to the thermal (IR) volume-law entropy behaviour in a small ribbon about the entangling surface. Dimensional analysis can again be employed to show that the leading order behaviour is linear with time. The volume-law behaviour only emerges in a small region about the entangling surface such that we have: $\Delta S_A \propto T_{eq}^{d-1} \mathrm{A}(\partial A)$. We can normalise the result by some local equilibrium thermal entropy density, s_{eq},

$$\Delta S_A = v_E s_{eq} \mathrm{A}(\partial A) t + \ldots \tag{6.9}$$

where v_E is defined as the entanglement velocity(108)(107)(106). One can in fact take (6.9) to define the entanglement velocity as the speed of information propagation when the change in entropy becomes linear. A more instructive intuition can be formed by considering that the entanglement surface at intermediate times is surrounded by an approximately homogenous 'ribbon' within A. This ribbon broadens out along a wavefront formed by the quanta produced at early times. The entanglement velocity then represents the spread of the vanguard quanta linearly with time, or more simply the speed of propagation of entangled quanta. From the definition, we note that v_E can also be considered to be independent of the shape of A. In (16), it was argued that v_E can be linked to the probability that operators do not grow under a quench.

3. $t \gg \ell_A$: The wave eventually engulfs A and the entanglement entropy no longer increases, plateauing to some thermal equilibrium value. The subsystem A is now thermalised and the

[44] Precisely what these patches are will be dependent on a large number of factors such as unperturbed geometry, types of allowed interactions etc.

reduced density matrix ρ_A becomes practically indistinguishable from the thermal density matrix such that $\rho_A \approxeq \rho_A^{eq}$. In this regime, the system reaches saturation,

$$S_A = s_{eq} \mathrm{V}(\partial A) \tag{6.10}$$

The authors of (106)(107) also noted that there exists a universal upper bound of the rate of growth of entanglement in holographic systems which can be easily found by differentiating (6.9). From causality, one may naively expect that such a bound is given by the speed of light $v_E \leq 1$, however, a stronger upper bound can be found by considering a collapsing shell of matter forming an AdS_{d+1} black hole dual to the thermal Gibbs ensemble in the boundary theory(109)(110). In this model, it was proposed that the upper bound on the rate of entanglement growth is

$$R(t) \leq v_E^* = \frac{(\eta-1)^{(\eta-1)/2}}{\eta^{\eta/2}}; \quad \eta = \frac{2(d-1)}{d} \tag{6.11}$$

For conformal systems with $d > 2$, this bound on the entanglement velocity lies between $v_s = \frac{1}{\sqrt{d-1}} \leq v_E^* \leq 1$ where v_s is the speed of sound in the system. This suggests that the quanta which equilibrate the system and the entanglement quanta are distinct. For free-streaming particles, we have the stronger bound

$$v_E^{free} = \frac{\Gamma(\frac{d-1}{2})}{\sqrt{\pi}\Gamma(d/2)} \tag{6.12}$$

and it can be easily seen that for $d > 2$, $v_s < v_E^{free} < v_E^*$.

Yet another interesting bound in this context is the speed of the emergent lightcone, v_{LC}. This lightcone can be defined as the region outside of which the OTOC has exponentially small support such that operators will approximately commute when $x > v_{LC} t$. Naturally, $v_B \leq v_{LC} \leq 1$.

Just before the saturation regime, the system has lost any fine-grained knowledge of its original state. This is expected from ergodcity, as a thermal density matrix may have emerged from an infinite number of initial configurations. Such a system then exhibits the key features of a chaos as it goes from some specific initial configuration towards a typical state in a thermal distribution[45]. Indeed, we can examine the rate of approach to the late time asymptote using the butterfly velocity. It has been suggested that such a value can be interpreted as a continuum extension of the Lieb-Robinson bound (98). For holographic systems, the butterfly velocity is given by,

$$v_B = \sqrt{\frac{2d}{d-1}} \tag{6.13}$$

In the context of thermalization, the butterfly velocity can be defined as the upper bound on

[45]Naturally, this is true of any thermal system but it never hurts to labour an important point.

the saturation rate for holographic systems[46]. You can therefore not thermalize a system faster than the butterfly velocity. This definition can also be linked to our previous definition of the v_B as the speed at which chaos spreads through the system.

We remark, however, that in (111) the authors found that following a global quench the evolution of small subsystems occurs on timescales below the local equilibrium scale. One consequence of this is that this entanglement tsunami picture we have sketched no longer applies. In particular, the instantaneous rate of entanglement growth is not constrained by causal dynamics but rather its time average.

6.5 Butterflies and Shockwaves

To study the sensitive dependence of holographic systems on initial conditions, we can return to our earlier set-up where we discussed how small perturbations at the boundary in the distant past give an impulsive shockwave solution at $t = 0$ corresponding to a spherically symmetric infalling null-shell. In this picture, we make no assumptions about the topology of the horizon itself it remains general to planar and global black hole solutions.

We now consider a stress-energy tensor which is localised in the angular directions such that the perturbation acts as a infalling null trajectory from the distant past, residing entirely on the right horizon of the TFD. Without loss of generality, we take the the source to be at the north pole of a $(d-1)$-sphere for a $(d+1)$-dimensional black hole. We make the ansatz that $\tilde{v} = v + h(\Omega)$, where Ω is the solid angle of the $(d-1)$-sphere. One can then substitute this ansatz solution into the Einstein equations by evaluating the Ricci tensor of the patched metric[47] and solving Einstein's equations for a stress tensor with a matter source,

$$T_{uu} \propto \delta(u)\delta^{d-1}(\Omega) \tag{6.14}$$

such that we find that the equation,

$$\left(\nabla^2_{S^{d-1}} - \frac{(d-1)}{2} r_h f'(r_h)\right) h(\Omega) \propto \delta^{d-1}(\Omega) \tag{6.15}$$

revealing that $h(\Omega)$ is simply a Green's function for a large mass particle on the sphere. For large $(d+1)$-dimensional Schwarzschild black holes, one finds $f'(r_h) = \frac{dr_h}{\ell^2}$ such that it decays with angular distance ϕ from the north pole as

$$h(\Omega) \propto e^{-\sqrt{\frac{d(d-1)}{2}} r_h \Omega/\ell_{d+1}} \tag{6.16}$$

[46] For uncharged black holes

[47] See Appendix A of (112). This calculation is rather involved and so we omit it here.

We then have a notion of how the perturbation spreads on the boundary which we can compare to our knowledge of how the perturbation along $\tilde{u}_W$ grows with t_W which is given by $\tilde{u}_W(t_W) \propto e^{f'(r_h)t_W/2}$. One can then find the butterfly velocity, v_B by setting their exponents equal such that level sets of increasing t_W propagate outwardly with a maximum velocity,

$$v_B = \frac{\ell_{d+1}\Omega}{t_W} = \sqrt{\frac{d}{2(d-1)}} \tag{6.17}$$

One may also wonder what happens if we use global coordinates. In this case, we have,

$$f'(r_h) = \frac{1}{\ell_{d+1}}\left(d\frac{r_h}{\ell_{d+1}} + (d-2)\frac{\ell_{d+1}}{r_h}\right) \tag{6.18}$$

and

$$\begin{aligned} v_B =& \ell_{d+1}\frac{f'(r_h)}{2}\sqrt{\frac{2}{(d-1)f'(r_h)r_h}} \\ =& \ell_{d+1}\sqrt{\frac{f'(r_h)}{2r_h(d-1)}} \\ =& \sqrt{\frac{d}{2(d-1)} - \frac{(d-2)}{2(d-1)}\frac{\ell_{d+1}^2}{r_h^2}} \end{aligned} \tag{6.19}$$

which remains valid above the Hawking-Page transition. For $d > 2$, one sees that butterfly velocity for a global black hole is bounded from above by the planar solution. In $d = 2$, this constraint does not apply and one instead finds that the global and planar solutions are mathematically equivalent. In the following section, we explore a simpler but equivalent method for calculating the butterfly velocity in holographic systems.

6.6 Determining the Butterfly Velocity in Holographic Systems

We shall refer to this new technique as the Mezei-Stanford prescription(16). This method is appealingly simple, making use of the the subregion duality of the boundary theory to bound the spread of the chaos in the bulk. Under certain circumstances, this procedure can be considered to be equivalent to finding the saturation time for the entropy of a ball-shaped region after a global quench much like the shockwave method.

We again act with some light local operator W_x on a thermal state initially at equilibrium. Suppose that initially one may recover information regarding which operator was applied by taking a local measurement in the vicinity of the point x. As time passes, the information is

scrambled as it is delocalised over a growing region in the bulk. At time $(-t)$ we are able to recover a maximal amount of information about the perturbation, or equally, there is a local quench of the system at time $(-t)$ such that the 'size' of the operator is simply the smallest region containing a significant amount of the information about the original state. The size of an operator has no universal definition but roughly corresponds to a measure of the influence that a local operator has on other local degrees of freedom. For theories admitting a dual gravitational description, one can determine this size explicitly by making use of the subregion duality. This duality, which we recall for simplicity, states that subregions of the boundary theory give complete descriptions of the bulk subregion. For static bulk duals, we recall that this region is be found using the RT formula whilst more general cases require the QES or HRT prescriptions.

We suppose that we act with a local operator on the boundary of the bulk picture, letting it fall radially towards the horizon. After some time t, the smallest subregion required to reconstruct significant information about the operator is the entanglement wedge, which corresponds to the maximal region over which information about the initial perturbation may be contained.

For simplicity, consider the general planar black hole in radial coordinates

$$ds^2 = -f(r)dt^2 + \frac{dr^2}{f(r)} + V(r)dx^2 \tag{6.20}$$

In the near horizon limit, we can take the first order expansion of $f(r)$ about $r = r_h$,

$$f(r) = f'(r_h)(r - r_h) + \mathcal{O}((r - r_h)^2) \tag{6.21}$$

which gives us,

$$ds^2 \approxeq -f'(r_h)(r - r_h)dt^2 + \frac{dr^2}{f'(r_h)(r - r_h)} + V(r)dx^2 \tag{6.22}$$

We then shift our coordinates such that $\sigma = \sqrt{r - r_h}$ and $dr = 2\sigma d\sigma$.

If $V(r) = r^2$, the original metric is of a familiar spherical region of the black hole. In this case, the near horizon geometry is of a spatial cone and we can identify the inverse temperature from the time coordinate as,

$$\left(\frac{2\pi}{\beta}\right)^2 = \left(\frac{f'(r_h)}{2}\right)^2 \implies f'(r_h) = \frac{4\pi}{\beta} \tag{6.23}$$

and the near horizon metric is given by,

$$ds^2 = -\left(\rho^2 + \mathcal{O}(\rho^4)\right)\left(\frac{2\pi}{\beta}\right)^2 dt^2 + d\rho^2 + \left(r_h^2 + \frac{2\pi r_h \rho^2}{\beta} + \mathcal{O}(\rho^4)\right)\frac{dx_i dx_i}{\ell_3^2} \tag{6.24}$$

This calculation therefore holds for any spherical region of the boundary. Though we the x_i are Poincaré coordinates, in $(d+1) = 3$ this method holds in global coordinates under the rescaling

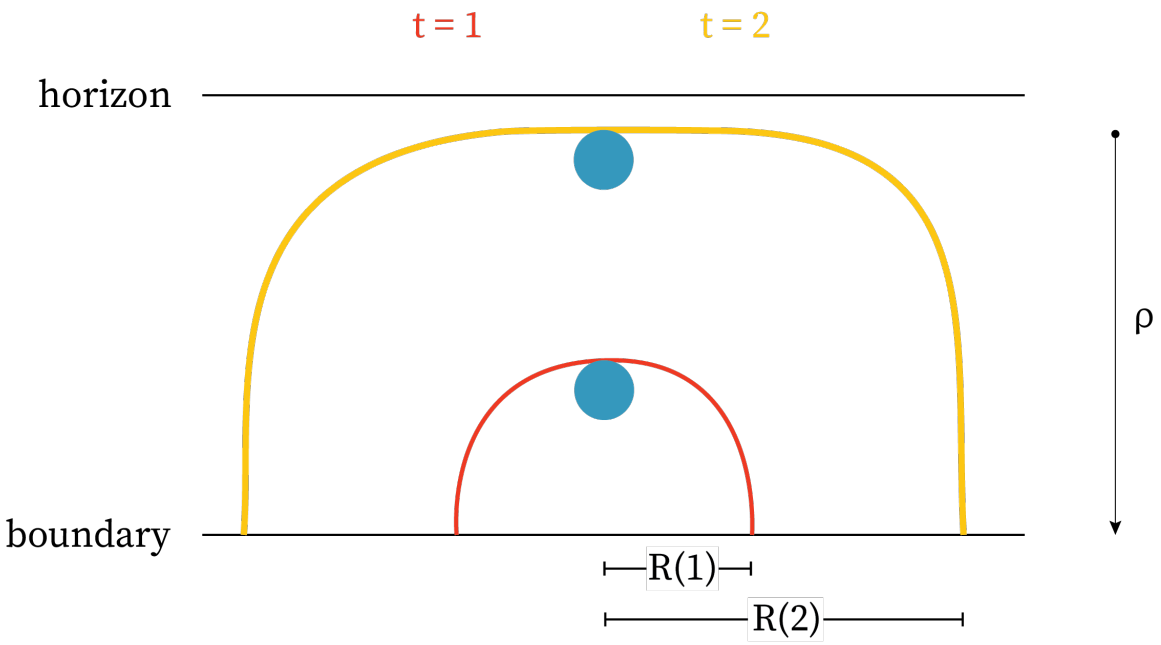

Figure 6.1: A schematic of the growth of the entanglement wedge for a light infalling particle (blue) for $t_1 < t_2$. For holographic systems the growth of the entanglement wedge places an upper bound on the spread of fine-grained information on the boundary. The upper bound of growth on the boundary is given by a ball shaped region of radius $R(t)$ about $x_i = 0$ where $R(0) = 0$.

$x_i/\ell_3 \longrightarrow \phi$.

From this simple calculation, we can proceed to a consideration of the near-horizon behaviour of light rays,

$$ds^2 = 0 \implies \rho(t) = \rho_0 e^{-\frac{2\pi}{\beta}t} \tag{6.25}$$

To estimate the size of the light operator $W_x(t)$, we can consider the smallest boundary region such that the RT surface extends to the radius $\rho(t)$ on a constant t-slice of the boundary theory. Here, we simply take some spherical region of the boundary of radius R and take make use of the symmetry of the space to paramaterize ρ as $\rho(x_i)$ so that it only depends on the radius at the boundary. In general, this requires computing the minimal surface area by minimizing the area functional,

$$
\begin{aligned}
A =& \int d^{d-1}\xi \sqrt{\det[h]}; \quad h_{ij} = \left(\frac{d\rho}{d\xi_i}\frac{d\rho}{d\xi_j} + \left(g_{x_i x_i} \frac{dx_i}{d\xi_i}\frac{dx_i}{d\xi_j} \right) \right) d\xi_i d\xi_j \\
=& \frac{r_h^{d-1}}{\ell_{d+1}^{d-1}} \int d^{d-1}x \sqrt{\det\left\{ \partial_i\rho\partial_j\rho + \left(1 + \frac{2\pi}{\beta r_h}\rho^2 \right)\delta_{i,j} \right\}}
\end{aligned}
\tag{6.26}
$$

We are interested in the near horizon limit, where RT surface begins to wrap the black hole and hence most of the RT surface remains very close to the horizon. Around the horizon, $\partial_i\rho$ is also very small. We can then expand this area functional to order ρ^2 using $\det\{1+X\} \approx 1 + \mathrm{Tr}\{X\}$ for small X to give,

$$
\begin{aligned}
A =& \frac{r_h^{d-1}}{\ell_{d+1}^{d-1}} \int d^{d-1}x \left(1 + \frac{1}{2}\frac{\ell_{d+1}^2}{r_h^2}(\partial_i\rho)^2 + \frac{1}{2}\frac{2\pi(d-1)}{\beta r_h}\rho^2 + \mathcal{O}(\rho^4, (\partial_i\rho)^4) \right) \\
\approx& \frac{r_h^{d-3}}{\ell_{d+1}^{d-3}} \int d^{d-1}x \left(\frac{r_h^2}{\ell_{d+1}^2} + \frac{1}{2}(\partial_i\rho)^2 + \frac{1}{2}\mu^2\rho^2 \right)
\end{aligned}
\tag{6.27}
$$

where $\mu^2 = \frac{2\pi(d-1)}{\beta r_h}$. We can then minimize this by solving the equation of motion $\partial_i^2\rho = \mu^2\rho$. These solutions will vary approximately exponentially as a function of x^i as in the $d = 2$ case,

$$
\begin{aligned}
\rho(x) &= A\sinh(\mu|x|) + B\cosh(\mu|x|) \\
&\implies \rho(x) = \rho_* \cosh(\mu x)
\end{aligned}
\tag{6.28}
$$

where $\partial_x\rho|_{x=0} = 0$ and $\rho|_{x=0} = \rho_*$. A more general solution in the near-horizon limit was derived in (113),

$$
\rho(x_i) = \rho_* \frac{\Gamma(a+1)}{2^{-a}\mu^a} \frac{I_a(\mu|x|)}{|x|^a}
\tag{6.29}
$$

Where $a = \frac{d-3}{2}$ and I_a is the modified Bessel function,

$$
I_a(\mu|x|) = \sum_{m=0}^{\infty} \frac{1}{m!\Gamma(m+a+1)} \left(\frac{\mu|x|}{2} \right)^{2m+a}
\tag{6.30}
$$

When $\rho > \beta$, the minimal surface exits the near horizon limit and, due to the steep derivative, the minimal surface reaches the boundary within an order one distance in x. We can then approximate the size of the operator R as corresponding to the CFT region over which the initial perturbation has spread. This can be given in terms of ρ_* to within an order one error by solving the equation,

$$\beta = \rho_* \frac{\Gamma(a+1) I_a(\mu R)}{2^{-a}\mu^a R^a} = \rho_* \sum_{m=0}^{\infty} \frac{1}{m! a^m} \left(\frac{\mu R}{2}\right)^{2m} \approx \rho_* e^{\mu R} \tag{6.31}$$

In the last step we have neglect prefactors and subleading terms and make the approximation that $\rho_* \approx e^{-\mu R}$. The infalling particle must be contained within the entanglement wedge, $\rho_* \leq \rho(t)$, which in turn implies that $R \geq \tilde{v}_B t$ and,

$$\tilde{v}_B = \frac{2\pi}{\beta\mu} = \sqrt{\frac{2\pi \ell_{d+1}^2}{(d-1)\beta r_h}} \tag{6.32}$$

For an SAdS black hole in Einstein gravity, $T = \frac{1}{\beta} = \frac{1}{4\pi \ell_{d+1}} \left(d \frac{r_h}{\ell_{d+1}} \right)$ and the butterfly velocity is equal to that using the shockwave method, $\tilde{v}_B = v_B = \sqrt{\frac{d}{2(d-1)}}$.

We started with a local perturbation W_x and time evolved it. To measure this operator on the boundary CFT at some later time, relativistic causality tells us that the largest ball we need will be of radius t in the field theory. However, this bound is too strong as the emergent light cone $v_B = v_{LC}$ constrains the spread of information about this operator such that we need only measure the smaller subregion of radius $v_B t$ related to the entanglement wedge. The boundary domain of the smaller region does not contain $W_x(-t)$ as a local operator but instead contains it approximately as a non-local operator over it domain of dependence. That is to say, this operator is approximately smeared over the entanglement wedge and the corresponding boundary subregion.

Naturally, we could use a non-spherical region, a massive operator, or consider some non-radial trajectory but such considerations would not change the upper bound. To see why, note that non-radial paths introduce an additional contribution to the potential such that it no longer monotonically decreases as it moves towards the horizon. For significantly large angular momenta, the operator will in general have to tunnel through this potential. It should be apparent that this will lead to a butterfly velocity smaller than the global upper bound. Furthermore, massive operators will likewise include an additional potential which will only act to slow the spread of information. It was speculated in (16) that deforming the region will also fail to change the global upper bound for obvious reasons.

In the following section we discover that a naive application of the Mezei-Stanford approach presents problematic results, motivating additional discussion and alterations to the methodology.

6.7 Butterfly Velocity for the QuBTZ for Small Backreaction

Recently, it has been argued in (96) that corrections to all orders in both backreaction and quantum corrections leave the butterfly velocity calculation invariant. To directly verify this for the case at hand, however, one must solve the equations of motion for the higher-derivative theory and then apply the generalised Iyer-Wald construction (114). We once again limit ourselves to the small ν limit where the RT prescription is sufficient to calculate the size of the boundary operator.

Naively applying Mezei-Stanford prescription, we see that the butterfly velocity is distinct from the pure BTZ case, $v_B = 1$, due to changes in the temperature-horizon radius relationship,

$$\beta_{qu} = \frac{4\pi}{f'(r_h)} = \frac{4\pi\ell_3^2 r_h}{(r_h+b)(r_h+c)} = \frac{4\pi\ell_3^2 r_h^2}{2r_h^3+\ell_3^3\nu F(M)} \tag{6.33}$$

and the Butterfly Velocity reads,

$$\tilde{v}_B^{(qu)} = \sqrt{\frac{2\pi\ell_3^2}{\beta_{qu} r_h}} = \sqrt{\frac{(r_h+b)(r_h+c)}{2r_h^2}} = \sqrt{\frac{2r_h^3+\ell_3^3\nu F(M)}{2r_h^3}} \tag{6.34}$$

For small ℓ we may also expand (6.34) to linear order in ν,

$$\begin{aligned}\tilde{v}_B^{(qu)} =& v_B^{(cl)} + \nu\partial_\nu v_B^{(qu)}\|_{\nu=0} + \mathcal{O}(\nu^2)\\ \approx& v_B^{(cl)} + \nu\frac{\pi}{v_B^{(cl)}}\partial_\nu\left(\frac{T^{(qu)}}{r_h^{(qu)}}\right)\Big|_{\nu=0}\end{aligned} \tag{6.35}$$

Recalling that $v_B^{(cl)} = 1$,

$$\begin{aligned}\Delta v_B \approx& \tilde{v}_B^{(qu)} - v_B^{(cl)}\\ =&\pi\nu\left(\frac{r_h\partial_\nu T^{(qu)}|_{\nu=0} - \partial_\nu r^{(qu)_h}|_{\nu=0} T}{r_h^2}\right)\\ =&\pi\nu\frac{T}{r_h^2}\left(r_h\frac{(1+3z^2)(3z+z^3)-4z^3}{2(1+3z^2)} - \frac{2(z^2+z^4)}{(1+3z^2)^2}\right)\\ =&\pi\nu\frac{T}{r_h}\left(\frac{(1+3z^2)(3z+z^3)-4z^3-2(z+z^3)}{2(1+3z^2)}\right)\\ =&\frac{\nu}{2}\left(\frac{(1+3z^2)(3z+z^3)-4z^3-2(z+z^3)}{2(1+3z^2)}\right)\\ =&\frac{\nu(z+z^3)}{4} \geq 0\end{aligned} \tag{6.36}$$

For small v and z, we remain on the thermal branch and therefore close to the classical behaviour as seen in Figure 6.2.

In the limit of zero backreaction, $b, c \longrightarrow 0$ and $\tilde{v}_B^{(qu)} = v_B = 1$ as expected. For non-zero values, however, $b, c > 0$ and hence this method yields $v_B^{(qu)} > 1$, implying that the butterfly velocity in such a system is superluminal. In lieu of an analytic solution for general cases, we can compare the growth of the boundary operator over time in the QuBTZ to that in the BTZ by taking the differences between $\dot{\phi}(r) = d\phi/dt$,

$$\Delta\dot{\phi}(r) = \dot{\phi}_{qu}(r) - \dot{\phi}_{cl}(r) \propto \sqrt{(r + r_h - b)(r_h + b)/r)} - \sqrt{r + r_h} \tag{6.37}$$

such that $\Delta\dot{\phi}(r) > 0$ when

$$r_h > b \tag{6.38}$$

which is satisfied trivially for all $v > 0$. Naturally, this result is interesting as it implies that information is spread acausally in the system.

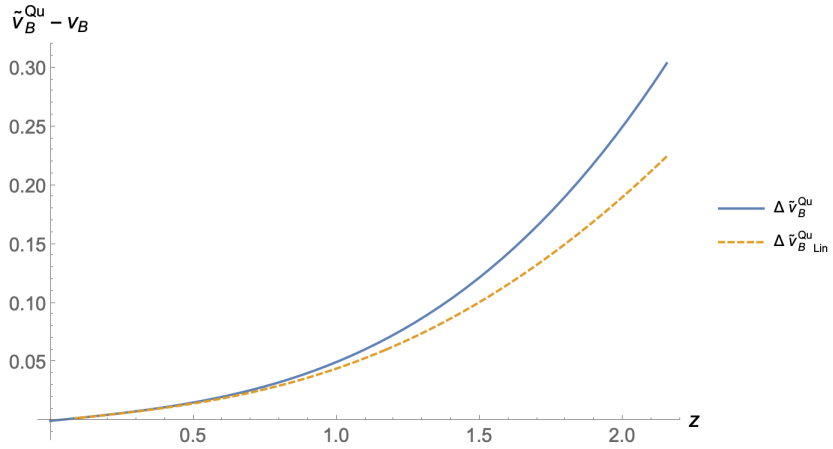

Figure 6.2: A plot of the difference between the butterfly velocity calculated using the Mezei-Stanford approach and the classical result, $\Delta\tilde{v}_B^{(qu)}$, and the expansion of this result to linear order in v, $(\Delta\tilde{v}_B^{(qu)})_{Lin}$, for $v = 0.1$.

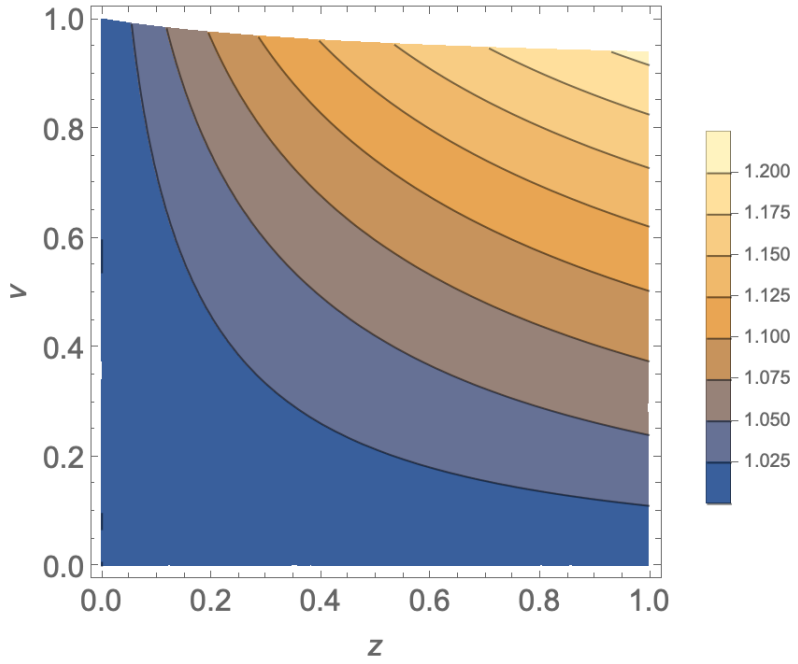

Figure 6.3: A contour plot of the value of the $\tilde{v}_B^{(qu)}$ calculated using the entanglement wedge method developed in (16) as values of v and z in the limit of $\ell \ll 1$ and restricted to $vz^3 \leq 1$. We see that as quantum corrections are incorporated, the butterfly velocity grows monotonically, exceeding the causal limit $v_B = v_{LC} = 1$.

Chapter 7

Dissecting the Butterfly

At this juncture, we ought to revisit some assumptions regarding the Mezei-Stanford procedure. The obvious culprit for the discrepancies emerges from assumptions about the size of the black hole and the energy density. Presently, this procedure has not been extended to account for small black holes in global coordinates let alone those with quantum corrections. We explore these assumptions and discover that when the butterfly velocity is calculated numerically, one finds that it indeed confirms that in the small backreaction limit $v_B \geq 1$. Independent of this result, we argue that the prescription of calculating the butterfly velocity one thermal length from the horizon fails to capture the physical content of the butterfly velocity for the QuBTZ and small black holes more generally. Instead, we propose that the physically relevant distance from the horizon should instead be set by the critical radius and angle where the connected and disconnected phases of the minimal surface exchange dominance. We propose an alteration to the existing Mezei-Stanford approach which we argue holds for small black holes with quantum corrections such as the QuBTZ.

7.1 Numerical Calculation of Butterfly Velocity

Changes to the near horizon behaviour will generically emerge when quantum corrections are included. In the context of the QuBTZ, the presence of the $vF(M)/r$ term in the metric indicates that there will be non-trivial deviation from the normal Rindler dynamics close to the horizon for small black holes. One would then expect that we must be careful in discarding sub-leading order contributions to the near horizon behaviour as in (6.25) and (6.25).

Using numerical integration, we calculated the explicit value of the butterfly velocity without discarding any subleading terms but retaining the prescription that it be determined one thermal length r_β from the horizon,

$$v_B = \frac{\phi(r_\beta)}{t(r_\beta)} \tag{7.1}$$

where $r_\beta = r(\rho = \beta) = r_h + \pi\beta$. In Figure 7.1, one can see the $v_B > 1$ for $0 < \nu < 1$. The corrections to the butterfly velocity increase rapidly for small values of ν and z before asymptoting as $\nu = 1$ is approached. One explanation is that as one increases the backreaction, the horizon radius grows and r_β grows non-linearly. Corrections to the classical solution in $f(r)$ scale as $1/r$ meaning that, although we are increasing the backreaction strength, we must also consider that there will also be an additional balancing effect from the fact that our limits keep us further away from the black hole such that as r_β increases the contribution of conformal fields near the horizon begins to asymptote to a fixed value. Naturally, as we increase ν the higher-derivative corrections become relevant and our RT calculations break down so one must also consider that these effects may also be altered by the inclusion of higher-derivative gravity contributions close to $\nu = 1$. These corrections will be explored further in follow-up work.

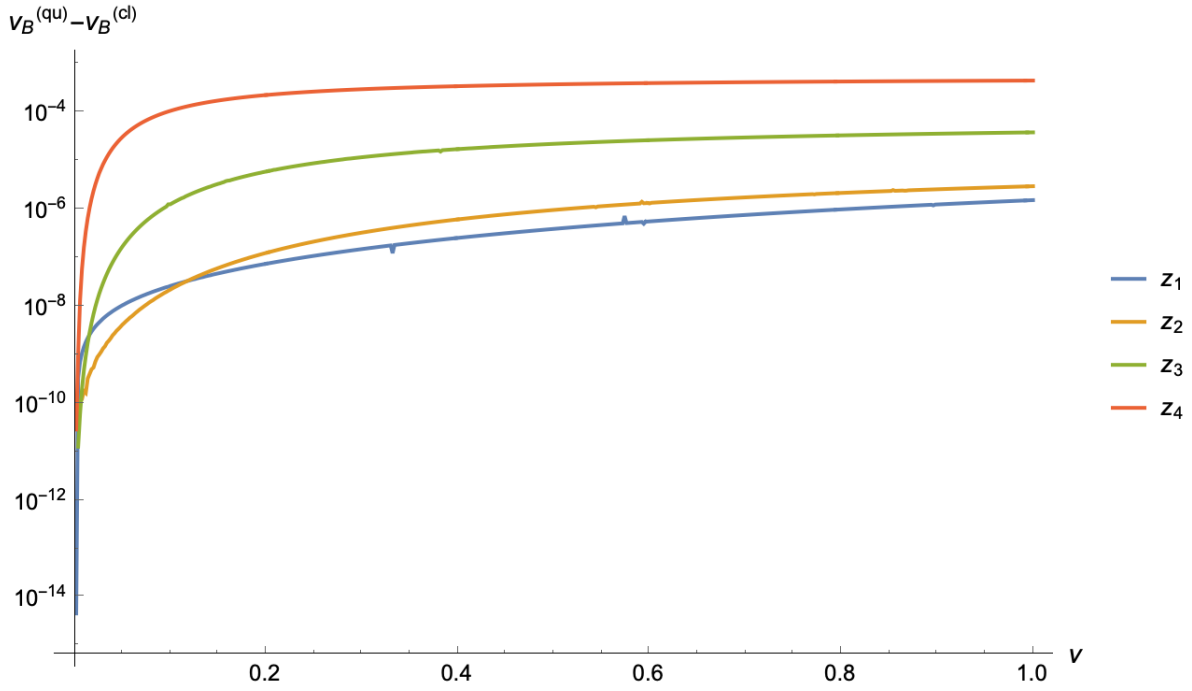

Figure 7.1: A plot of the correction to the butterfly velocity as a function of r_* for $z_i = 10^{i/2}$. Similar results hold for $z < \frac{1}{\sqrt{3}}$, however, these corrections are relatively small and sensitive to rounding errors. Small variations are apparent on z_1 which are likely due to sensitivity to rounding errors in Mathematica.

Though we do not have a general analytic result, we can check that these numerical results are no anomalous or solely due to rounding errors by considering the analytic results obtained in subsection 5.4.2. These results are depicted in Figure 7.2 which exhibits similar behaviour to the numerical results. Whilst this result is troubling under causal considerations, the fact that $v_B^{(qu)} > v_B^{(cl)}$ is not entirely surprising if one considers that v_B is essentially a rate of diffusion for quantum information. With this physical intuition in hand, one imagines that the information

about the operator is not only scrambled by the black hole itself but also by quantum fields outside its horizon.

At this stage it remains unclear where the problem emerges from. Our results indicate that either the QuBTZ construction is unphysical, that the Mezei-Stanford prescription is inapplicable or that higher-derivative gravity and quantum corrections within the bulk may come to the rescue of causality. The first suggestion, at least in the planar approximation, seems to be an unlikely explanation in light of the model obeying the first law of black hole thermodynamics. However, there may be some subtlety to this which is obscured on the brane but may manifest in the bulk picture. Furthermore, we note that due to the cancellation of the conformal factor for radially infalling lightlike paths, bulk and brane calculations are equivalent and valid to all orders in ν in contrast to the boundary calculation which only remains valid to linear order in ν. To account for corrections to all orders, one could instead calculate minimal surfaces in the bulk picture, however, these minimal surfaces are solutions to non-trivial differential equations which could not be explored in the confines of this thesis. The second proposal is more likely on account of the number of significant assumptions about the system, some of which we discuss in the following section. Mezei and Stanford argued that their prescription remains valid for higher-derivative gravity theories, though this may also be altered when considering a non-constant energy density and a non-planar solution. One could further calculate the butterfly velocity by making use of the OTOC directly or checking whether higher-derivative corrections indeed change the QuBTZ result however time restrictions limit such lines of inquiry and so we defer this to later work. Another interesting consideration comes from applying the results of (59) who found that the rate of entanglement spreading for small subregions is not limited by causality. Since the thermal scale is pushed further away as the black hole horizon decreases, the boundary subregion defining it also decreases. In such a picture, we are forced to consider that we must use small subregions and hence these results may be explained and analysed in a perturbative expansion. In the remainder of this thesis, we shall assume that this is not the case and return to this point in future research.

Though our results are discouraging for the plight of causality in the QuBTZ, one may also have expected that corrections to the butterfly velocity at linear order in ν would scale closely with the backreaction strength. In the following subsection, we discuss whether the prescription of calculated v_B at $r = r_\beta$ consistently provides a sensible place to probe the desired physics in small black holes and propose that the relevant point migrates from its thermal value in general cases.

7.2 Migration of the Butterfly

Although the question of whether the butterfly velocity in the QuBTZ or more general double holographic braneworld constructions is superluminal remains an outstanding problem, our investigations noted an absence of the Mezei-Stanford prescription for global solutions and small

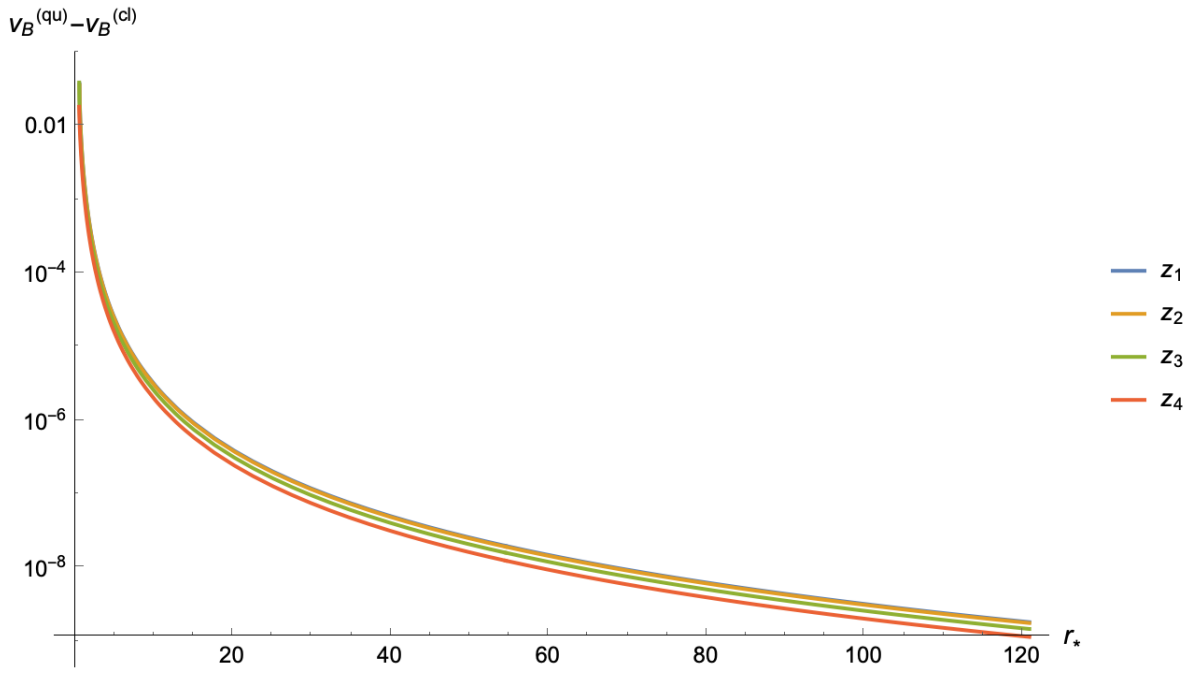

Figure 7.2: A plot of the correction to the butterfly velocity as a function of r_* for $\{z_1, z_2, z_3, z_4\} = \{1.5z_{b=c}, 2z_{b=c}, 2.5z_{b=c}, 3z_{b=c}\}$, where $z_{b=c}$ was defined in (5.48) and v is determined by (5.47). It is worth noting that above $z_{b=c}$, the backreaction strength for such solutions is a monotonically decreasing function of z such that larger z values lead to smaller backreactions. Small deviations in z_1 are again likely due to sensitivity to rounding errors in Mathematica.

black holes away from the planar limit. Throughout our discussion of the Mezei-Stanford approach we were certain to highlight assumptions made in arriving at their result. We must confront two crucial assumptions: (a) the energy density is approximately uniform (b) the black hole is large[48]. In general, one cannot make such assumptions and hence it would be ideal to derive a more general prescription. Unfortunately, our research yielded no such attempts, motivating us to propose a revision of the existing methodology.

The first assumption allows us to assign an effective length scale to the system corresponding to the inverse temperature, β. From (4.31) it is clear that at linear order, the energy density near the horizon of small QuBTZ black holes will not satisfy this assumption, especially as the size of the black hole approaches zero and CFT modes build up. The second assumption is more profound. In our previous discussion of the QuBTZ, we found that the inclusion of backreaction bounds the horizon from above such that $0 \leq r_h \leq \frac{2}{\sqrt{3}} \approx \mathcal{O}(\ell_3)$ and we can no longer assume that we can go to planar coordinates nor ignore the transition between the connected and disconnected phases of the minimal surface. There is no Hawking-Page transition in $d + 1 = 3$ dimensional systems

[48]Whilst the planar limit is often used for simplicity it is not required so 'largeness' of the black hole should be taken to mean that it is above the Hawking-Page transition.

and hence no lower bound on stable global solutions (115) forcing us to consider infinitesimally small black holes as physically permissible solutions. Crucially, the butterfly velocity is defined in terms of local quantities such that we must define a physically reasonable and consistent scheme telling us where the butterfly velocity should be measured. In light of these considerations, we must open our minds to the possibility that the butterfly migrates as the size of the black hole decreases. Where should one then calculate the butterfly velocity?

Let us return to a more organic notion of what the butterfly velocity means physically: it is the upper bound on how quickly one can thermalize the system. In the bulk picture of the infalling perturbation, we consider that the infalling perturbation is not just being scrambled by the black hole but also by the CFT_3 fields outside its horizon. One then imagines that a full picture would require some notion of local entropy densities as well as the thermal equilibrium density calculated purely from the black hole. Rather than doing this, we can stick to considering how the global properties such as entanglement entropy change as the perturbation becomes scrambled. One expects that a) the minimal surface will begin to wrap the black hole b) the entanglement entropy between the region and its complement will be close to the thermal entropy. Both of these indicate that near such a point it would be difficult to determine within which entanglement wedge this perturbation was located: that connected to the bulk or the disconnected wedge. At this point, information about the perturbation is spread over either of these topologically distinct regions, giving a sensible notion of scrambling. Analogous to the BTZ in Appendix D, the minimal surface begins to wrap the black hole close to the critical angle. Here, the entanglement entropy approaches the entanglement plateau and saturates the Araki-Lieb inequality at S_{BH}.

Naturally, one may ask why the Mezei-Stanford prescription works for large SAdS black holes. Firstly, for a large black hole the energy density will be approximately constant and hence it is reasonable that once the perturbation is within a thermal length of the black hole the initial perturbation is quickly scrambled. Furthermore, as horizon radius of the SAdS solution increases the thermal scale and critical point overlap, as one can see from Figure 7.4. Therefore, the distinction between the thermal and critical scales is moot for large black holes. For small black holes, however, the thermal length scale is orders of magnitude larger than r_h and r_c such that the minimal surface does not yet begin to wrap the horizon. Additionally, considering the cubic radial dependence of the energy density of the QuBTZ solution, it is clear that the butterfly velocity calculated at r_β will fail to completely pick up the near-horizon quantum effects. This explanation gives a plausible reason for the corrections to the butterfly velocity being many orders of magnitude smaller than linear order in v. To labour the point, at linear order we have an intuitive picture of the CFTs living on the brane between the horizon and the conformal boundary which build up the closer we get to the horizon much like in a physical black hole. If for example, we set the penetration depth r_* to be far away from the black hole then we will fail to capture the quantum corrections at all and we will only see classical effects.

This observation leads us to the proposal that one must instead calculate the butterfly velocity

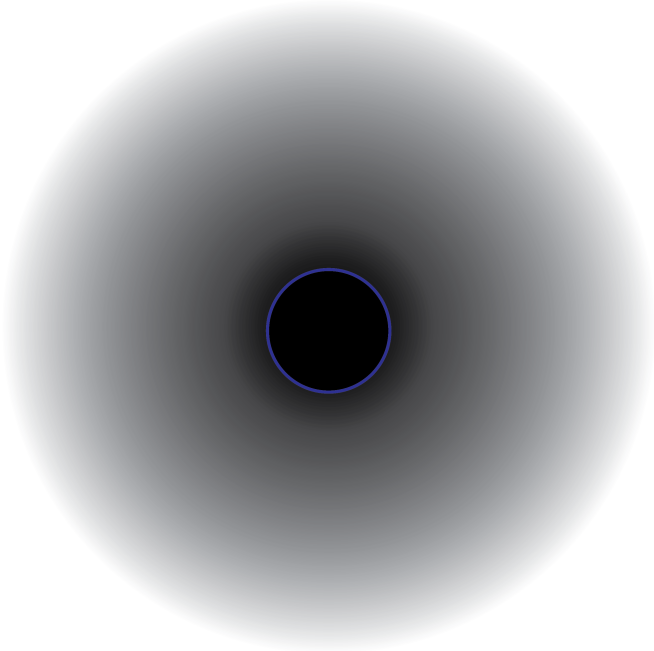

Figure 7.3: A simple illustration showing the build up of CFT_3 fields (grey) as one approaches the horizon (blue).

at the critical point where the minimal surfaces change dominance. For the BTZ black hole one can show explicitly that,

$$\frac{r_c}{r_\beta} = \frac{2\coth(\pi r_h) - 1}{1 + \frac{2\pi^2}{r_h^2}} \tag{7.2}$$

such that small black holes will have r_β far from the critical point r_c. One can further calculate the butterfly velocity at r_c analytically for the BTZ using (5.28) and (D.13). Unfortunately, this result returns the trivial result $v_B = v_{LC} = 1$ for all values of r_* as expected and hence fails to provide insight into our conjecture. Due to time restrictions, we were unable to provide a more rigorous argument in favour of this prescription for classical black holes. Regardless, we can consider that the canonical point where one should calculate the butterfly velocity is indeed at r_c for the QuBTZ as in Figure 7.5 where we take the maximum penetration depth to be,

$$r_* = r_c + \alpha r_\beta \tag{7.3}$$

where r_c is the critical radius of the classical solution.

As predicted, as we approach r_c we find that the butterfly velocity of the quantum corrected solution becomes of order $v \times 10^{-1}$. This result agrees more closely with our expectations of near linear behaviour close to the critical radius. This result, though encouraging, relied upon the approximation that $r_c^{(QuBTZ)} \approx r_c^{(BTZ)}$ for small v. In our future investigations, we hope to derive a

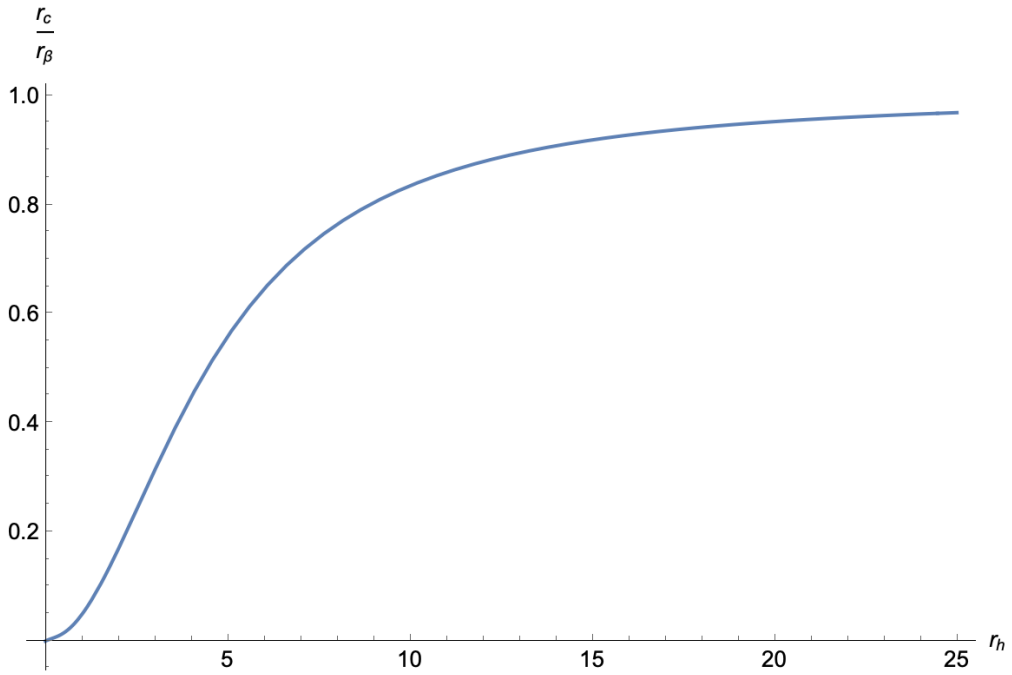

Figure 7.4: A plot of the ratio of the critical radius r_c to the thermal radius r_β as a function of r_h for the classical BTZ. For small r_h, we note that r_c is orders of magnitude smaller than r_β, whilst for small black holes, they become approximately equivalent.

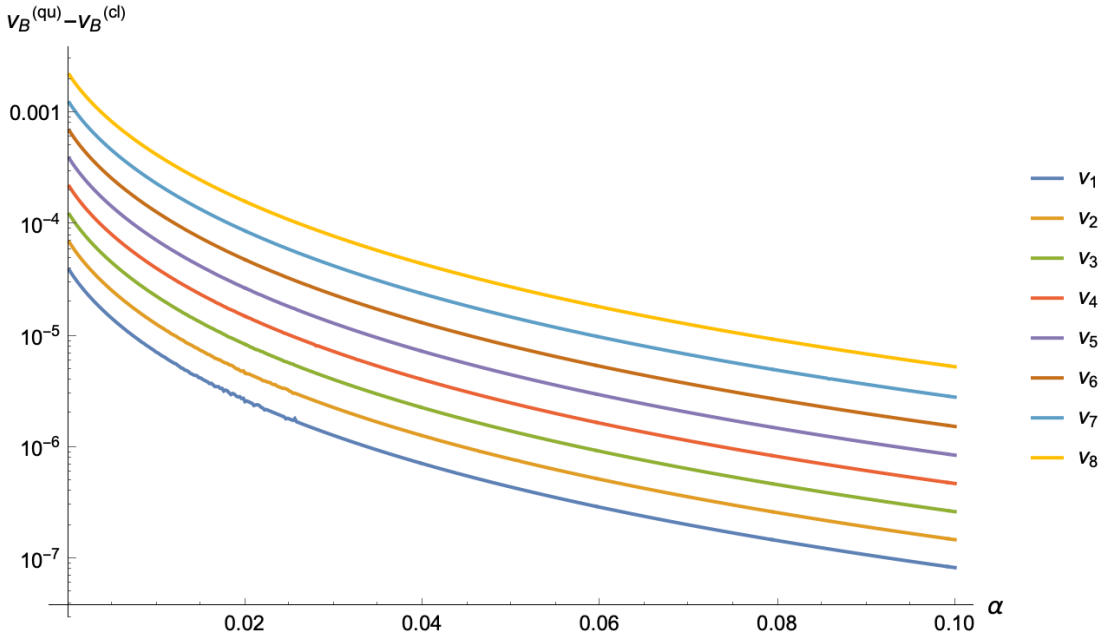

Figure 7.5: A plot of showing the difference between the classical and quantum corrected results against α for $v_j = 0.1 \times 10^{-j/4}$ and $z = \frac{9}{10\sqrt{3}}$. Taking $\alpha \longrightarrow \infty$, we find that $v_B \longrightarrow 1$ as expected.

better bound on the location of the critical radius allowing for more accurate approximations of the precise value of the butterfly velocity in this scheme.

Part IV

Outlook and Concluding Remarks

This thesis set out to illuminate kinematic and dynamic aspects of the QuBTZ model, applying them as a non-trivial way to calculate the butterfly velocity of a BTZ black hole to linear order in quantum corrections. Through these investigations we provided insight into the unusual two-branch mass solutions and were able to illuminate overlooked features of the QuBTZ solution with particular emphasis on the dynamics of subregions on the brane. We show that a naive calculation following (16) produces superluminal values at linear order in v. This result was confirmed analytically in the case where the negative roots of $f(r)$, are equal ($b = c$) and numerically for more general values where $b \neq c$. In remains unclear at this juncture whether higher-derivative gravity corrections will resolve this. We address a gap in the literature regarding the calculation of v_B using subregion duality for smaller black holes in global coordinates. This led us to reevaluate the assumptions of this methodology and propose an alteration to the Mezei-Stanford approach.

In Part I of the thesis, we provided a detailed overview of holography and its relation to quantum information. This part was included to give the novice holographer a broad and pedagogically minded review of key concepts and techniques in holography. We derived a number of key results and gave examples of how the AdS/CFT duality posits an intrinsic link between semi-classical gravity and quantum entanglement.

We devoted Part II to demystifying many of the complicated and unorthodox features of the QuBTZ, providing original calculations of global features as well as geodesics and holographic entanglement entropy calculations for subregions of the brane to linear order in the backreaction. We investigated the nature of the two branches of the QuBTZ and illustrated that there only existed consistent solutions with equal z mass parameter and ADM mass $\mathcal{G}_3 M$ within a finite range of z values. The maximum radius of the QuBTZ was shown to be twice the maximum radius of the uncorrected solution and of order ℓ_3. The free energy of these two solutions was calculated illustrating that the thermal branch is thermodynamically preferable over the Casimir branch. The classical equations of motion were used to derive analytic expressions for infalling radial timelike (to linear order in v) and lightlike geodesics (to all orders in v). Numerical methods were employed to calculate the spacelike minimal surfaces for the QuBTZ and analytical results were derived for the special class of solutions where the negative roots of $f(r)$ are equal ($b = c$). As one would expect from the monotinicity of relative entropy, the QuBTZ minimal surface resulted in larger minimal surfaces than the classical solutions and hence larger entanglement entropies. Making use of the equations of motion for the minimal surfaces, we showed that for a fixed penetration depth, the quantum corrected solutions were bounded from above by the minimal surfaces of classical BTZ black holes with a mass determined by the horizon radius of the quantum corrected solution and from below by those of the classical BTZ solution with fixed z and $v = 0$. Armed with this result, we argued that the critical radius of the QuBTZ should then be somewhere between that of the two solutions. Analytic results for the minimal surface to first order in v were also calculated.

Making use of our results in Part II, Part III explored how chaos spreads in the QuBTZ model. Applying the methods of Mezei and Stanford, we found that their simple formula for the butterfly velocity produced a superluminal butterfly velocity. Both numerical for general values of b and c and the analytic results for the special case $b = c$ support this finding. We assert that this approximation is insufficient in describing black holes with near horizon corrections and non-uniform energy density. Following the more fundamental claim that the butterfly velocity could be calculated using the subregion duality, we performed numerical calculations showing that $v_B > 1$ when backreaction effects were included. These corrections were orders of magnitude smaller than those expected, leading us to further question whether the thermal length r_β provides an appropriate coordinate at which one should calculate the butterfly velocity for small quantum corrected black holes. Though this calculation did not resolve causal concerns, it did reveal a gap in the literature regarding an equivalent subregion duality approach for smaller global black holes well below the planar limit. We conjectured a reasonable generalisation of this method in which we propose that the butterfly velocity should be calculated near the critical radius where the connected and disconnected minimal surfaces exchange dominance. Whilst this conjecture was heuristic and less rigorous than we would like, it was able to capture the anticipated near linear order v effects in the corrections to the classical butterfly velocity.

Unfortunately, time constraints prevent us from a more rigorous treatment of the myriad of fascinating possibilities one might pursue in both the QuBTZ model or the proposed extension to the Mezei-Stanford methodology. Being generous to our own efforts, one may remark that the mark of promising science is that it generates as many new insightful questions as it sought to answer. In the following, we provide an outlook and a number of promising extensions to this thesis which we endeavour to explore in upcoming work.

Outlook and New Horizons

Before discussing some more general proposals, we shall touch upon some facets of the QuBTZ model and our proposal which we were unable to investigate fully,

1. *Higher-Derivative Gravity Corrections*: Integrating out the CFT modes above the cutoff induces a higher-derivative gravity theory on the brane. Due to the general difficulty of their inclusion and scope of this thesis we limited ourselves to the linear order backreaction effects, allowing us to apply the RT prescription. Inclusion of the higher-derivative terms would provide a more general and reliable analysis of the interesting features of the QuBTZ. In particular, (16) argued that their butterfly velocity calculation remained consistent to all orders in higher curvature couplings for four-derivative gravity which has been further supported in (96). This result may require modification when considering non-planar solutions and non-constant energy densities. In Appendix B of (16), it was noted that due to the butterfly velocity describing a high energy scattering problem, it may require stringy

Regge corrections. It was shown in (116), however, that at the order calculated in α', these corrections did not alter the butterfly velocity. They further noted that these higher order corrections generally require a massive gravity theory for stability, which is a natural feature of the Randall-Sundrum-like braneworld models employed. More recently, the authors of (97) also considered stringy corrections to the butterfly velocity and were able to show that the rank of the gauge group and the string couplings did, in fact, lead to corrections in the butterfly velocity but not in the upper bound of the Lyupanov exponent. These results, however, do not take into consideration the additional presence of fields outside the horizon or their backreaction on the geometry. In the QuBTZ, the low energy CFT modes ($\propto c$) and the higher-derivative gravity effects begin to mix at order v^2 and would therefore provide an interesting candidate for further exploration. Additionally, the small corrections to v_B calculated in this thesis could well be cancelled by these higher-derivative corrections. At this order, the conformal symmetry is also broken on the brane, a result which has not yet been explored in detail.

2. *Dressed Singularities and Rotating QuBTZ Solutions*: The QuBTZ contains an additional branch (1a) of negative mass solutions interpreted in (14) as dressed conical singularities. It was further claimed that these solutions implied a manifest form of the cosmic censorship conjecture. Classical conical singularities are described by taking $r_h \longrightarrow i\ell_{d+1}\sqrt{1-\mu}$ with $\mu \in [0, 1)$ in the classical BTZ solution. Furthermore, one may be interested in calculating v_B for the dressed conical singularities for which closed timelike curves can exist. Therefore, a comparison between the two may provide some fascinating insights. Furthermore, the authors of (14) extended the QuBTZ to a range of rotating solutions which one may explore.

3. *Bulk Minimal Surface Calculations*: On the brane, we are restricted to perturbation theory and effective higher-derivative gravity. In contrast, calculating minimal surfaces on the boundary gives non-perturbative results for the generalized entropy to all orders in both v and c. Furthermore, one can calculate entanglement entropies using the relatively simple RT formula. The RT formula, however, demands that we minimize the full four-dimensional (three-dimensional time slice) bulk area functional. This is unlikely to yield analytical results and so need numerical toolkits must be developed. Following this procedure, however, we would be able to isolate contributions order-by-order in v and c to determine the entanglement entropy between the brane and the CFTs outside of the horizon in the bulk picture as in (5.32) but for subregions rather than the full QuBTZ.

4. *Proof of Small Black Hole Proposal*: The proposed modification to the Mezei-Stanford procedure was only considered in the twilight of this thesis. In future, we would like to formulate a more robust argument in its favour through consideration of Wilson loops as explicit

probes of operator behaviour and QIT arguments. As discussed, the result $v_B = v_{LC} = 1$ remains exact for BTZ and hence trivial for all r_* in the classical case. It would be interesting to see if this prescription produces new results when applied to higher dimensional models with known phase transitions for the minimal surfaces.

5. *Higher Dimensional QuBTZ*: Another interesting extension to the QuBTZ, or more general braneworld constructions, would be to consider higher dimensional constructions. One proposal would be to introduce additional axes of rotation to a QuBTZ-like model. It would be particularly interesting to see if the bound on the ADM mass and radius are also present or is perhaps relaxed in higher dimensions. It was argued in (14) that this feature was a consequence of holographically representing the CFT by four-dimensional gravity rather than a property of braneworld constructions.

6. *Finding Critical Points*: Using heuristic approaches we argued that the critical angle of the QuBTZ was bounded from above and below. Without analytic results, finding a precise solution will require tedious numerical calculations. Finding exact values for the critical points would allow us to more accurately calculate the butterfly velocity in our proposal. Additionally, such critical points may be found if there does exist an exact solution for the bulk minimal surface or through considering the boundary dual of a CFT_3 coupled to a conformal defect.

Beyond these extensions which build directly from concepts discussed explicitly, we may also consider entirely new directions,

1. *Islands*: Another fascinating feature of braneworld constructions comes through the simplicity with which one can describe quantum extremal islands(13). In the QuBTZ, it was suggested by (14) that the unstable solutions on branch (1b) may evaporate into the CFT_3 via the transparent boundary. This phenomena deserves further scrutiny, but may provide an interesting model of black hole evaporation in which the islands are interpreted as living on the bulk theory outside of the brane.

2. *Quantum Bit Threads*: The RT formula can be reformulated in terms of divergenceless, norm-bounded vector fields called bit threads (117). These bit threads allow for a more information theoretically friendly notion of minimal surfaces which are redefined as constant surfaces along which the norm bound is saturated. Due to the divergenceless condition, these bit thread are constrained to start and end on conformal boundaries or horizons. More recently, a number of quantum bit thread proposals have been suggested (17)(118). These proposals generally seek to include quantum corrections by altering this divergenceless condition, allowing the bit threads to effectively tunnel through the bulk. In (17), Rolph

proposes a model inspired by a double holographic picture similar to the QuBTZ construction where islands are likewise interpreted as living in the higher dimensional bulk or, equivalently, along the CFT_{d+1}. The QuBTZ model would therefore be a non-trivial check of this prescription. Using the techniques of (119), one could further construct explicit quantum bit thread configurations in the higher dimensional picture and project them onto to the brane.

Appendix A

Causal Domains in QFT

To extend our lattice quantum mechanics intuitions, we assume that our Hilbert space is non-compact and replace the wavefunction with a wavefunctional $\Psi(\Phi(x))$, where $\Phi(x)$ is a label for some collection of fields defined at point, $x \in \Sigma$ and Σ is some spatial slice of our Lorentzian and globally hyperbolic spacetime, $\mathcal{M}$ at fixed time[49]. The previous procedure of tracing out $\bar{A}$ is now replaced by one in which we integrate over all fields in the domain $x \in \bar{A}$. We now have a technical challenge in that we must take the logarithm of a continuum operator in order to define our entropy measures.

We define a bipartite system $A \cup \bar{A} = \Sigma$. The entanglement surface, ∂A, which is defined as the boundary between the two regions is now a co-dimension 2 hypersurface in our spacetime. As one may intuit, the continuum limit will force us to introduce an explicit UV regulator ϵ in order to tame any divergences. This is equivalent to a tubular neighbourhood of ∂A of width ϵ which regulates the short distance entanglement between the degrees of freedom in A and $\bar{A}$. As before, the reduced density matrix captures the entanglement information between the two parts of our bipartite system and once calculated one can straightforwardly calculate the entanglement entropy[50].

For local relativistic QFTs, the past and future evolution of information on a Cauchy slice allow us to reconstruct the state of the QFT on the entirety of the Lorentzian manifold $\mathcal{M}$. That is to say that the unitarity of evolution allows us to assert that the past and future domains of dependence $D^{\pm}[\Sigma]$ create the background spacetime on which the QFT lives. Similarly, this applies to any subset of Σ such that the domain of dependence of A, $D[A] = D[A^{+}] \cup D[A^{-}]$ is the region where the reduced density matrix ρ_A can be uniquely evolved given the Hamiltonian acting on the system.

Generally, domains of dependence of our bipartite system do not cover the full spacetime

[49] We note that x now represents some coordinate chart on the manifold.

[50] To fix gauge ambiguity of which subset ∂A is in, we simply assume that it belongs to either A or $\bar{A}$ in a consistent way

and we must also account for any regions which can be influenced by the entanglement surface ∂A. This subtlety is paramount to understanding the later notion of the entanglement wedge. We can now denote a general point $p \in \mathcal{M}$ and its causal structure by $J^{\pm}[p]$ such that we can further define the causal future (past) of the entanglement surface by $J^{\pm}[\partial A]$. Consequently, we can construct the full manifold $\mathcal{M}$ by taking

$$\mathcal{M} = D[A] \cup D[\bar{A}] \cup J^{+}[\partial A] \cup J^{-}[\partial A] \tag{A.1}$$

The codimension-2 spacelike surfaces ∂A have a two-dimensional normal bundle with a Lorentzian metric signature such that we can always visualise them as a point in 2D space(120).

This formulation in terms of causal domains allows us to formulate constraints on the entanglement entropy which follow naturally from our notions of causality in relativity. Evolving states in the Hilbert space by unitary transformations supported only in regions A or $\bar{A}$ (ie. $\mathcal{H}_{\mathcal{A}}$ or $\mathcal{H}_{\bar{\mathcal{A}}}$) then the leaves the von Neumann and Rényi entropies for the total system Σ invariant but changes the entanglement structure between subregions of Σ. We could also consider some perturbation or deformation of the spatial slice such that $\rho_{\Sigma} \longrightarrow \rho_{\Sigma'}$. This deformation is related to the original slice by unitary operations constructed from localised A and $\bar{A}$ operators.

Consider a general construction by fixing a state in the infinite past ($t \longrightarrow -\infty$) and with some perturbation of the Hamiltonian supported by some region $\sigma_{\delta H}$. By virtue of causality, only points in the causal future of this region can be affected. Ergo, any region of the spacetime which does not intersect $J^{+}[\Sigma_{\delta H}]$ remains unaffected. This class of perturbations can only affect the entanglement spectrum (eigenvalues of our reduced density matrices) in the region $J^{+}[\Sigma_{\delta H}] \cap J^{-}[\partial A]$. In this case, these perturbations influence both regions in our bipartite system and can therefore modify the entanglement entropy. We can then reverse the time ordering and fix our state as $t \longrightarrow \infty$ then the region which can be affected by this perturbation is $J^{-}[\Sigma_{\delta H}] \cap J^{+}[\partial A]$. One can then consider a case in which we fix the state in the infinite past and infinite future. In this case one may heuristically imagine a causal wedge being defined between these two events.

We can summarise the causal properties as:

1. The entanglement spectrum ρ_A depends only on the causal domain of the region A and not on any specific choice of Cauchy slice. The entanglement spectrum (entanglement entropy) is referred to as a 'wedge observable' [51]

2. If we fix the state in the infinite past or infinite future then the entanglement spectrum of ρ_A is unaffected by local deformations in regions $D[A]$ or $D[\bar{A}]$.

3. The entanglement can be altered in the case that we fix the state in the infinite past (future)

[51] One must however be careful to note that it is not an observable in the usual quantum mechanical sense as the operator $S_A = \rho_A \log \rho_A$ is clearly non-linear.

in which case the entanglement spectrum will be altered provided that $J^+[\Sigma_{\delta H}] \cap J^-[\partial A]$ ($J^-[\Sigma_{\delta H}] \cap J^+[\partial A]$).

The entanglement wedge plays an essential role in understanding information spreading in quantum systems and, by extension, holographic gravity theories. In Part III we employ this duality to connect information spreading in the bulk to its boundary dynamics.

Appendix B

The Gravitational Replica Trick

The replica trick applies not only to standard effective QFTs but also to gravitational fields epresented by the metric of the theory. Naturally, gravitons are non-renormalisable in such theories however the semi-classical limit can still give instructive results. We can construct an n-cover manifold made of glued n copies of the original, $\mathcal{M}_n$ then write out a path integral for all fields on the manifold(52)[52],

$$Z_n = \int_{\mathcal{M}_n} \mathcal{D}\phi e^{-S[\phi]} \tag{B.1}$$

where we identify $\tau_E = \tau_E + n\beta$. In the most general case, the contribution to the entropy should not only be from matter fields but also from gauge fields. This gives a first order correction to the original result by Hawking and Bekenstein. We shall to restrict ourselves to the first order of the semiclassical case here in which we will find that we recover the Hawking Bekenstein result for the Schwarzchild black hole.

Let's now ignore the matter fields and make the semi-classical approximation that the metric is fixed at the saddle point, or the classical solution to the action,

$$\begin{aligned} Z_n &= \int_{\mathcal{M}_n} \mathcal{D}g e^{-S_{grav}[g]} \longrightarrow Z_n^{(\text{s. cl.})} \\ &= e^{-S_{grav}[g]}\big|_{\text{g fixed}} \longrightarrow \log Z_n = -S_{grav}(g_n) \end{aligned} \tag{B.2}$$

where the Euclidean time integral goes over $\tau_E : 0 \longrightarrow n\beta$

We recall that the metric for a Schwarzschild Black hole in maximally symmetric spacetimes is

[52] For simplicity, we assume that the original manifold is static

$$ds^2 = -f(r)dt^2 + \frac{dr^2}{f(r)} + r^2 d\Omega_{d-2}^2 \tag{B.3}$$

where $f(r) = 1 - k\frac{r^2}{L^2} - \frac{16\pi GM}{(d-2)\Omega_{d-2}r_h^{d-3}}$ in which k is some constant curvature and L is some length scale. By going to Euclidean time and then rearranging our metric near the boundary, we get:

$$\beta = \frac{1}{T} = \frac{4\pi}{f'(r_h)} \tag{B.4}$$

We can plot this as a cigar, with the horizon at the tip as given by Figure 2.1. In the single sheet case, there is no conical deficit at the horizon and this is what determines the appropriate period of the Euclidean time.

In the n-fold case, our gluing changes the periodicity of Euclidean time to n-times its original but this also changes the position on the horizon and the value of the mass as:

$$f(r_n, M_n) = 0; \quad \frac{f'(r_n, M_n)}{4\pi} = \frac{1}{n\beta} \tag{B.5}$$

The resulting geometry then gives a new saddle point that we need to calculate the Renyi entropy. In the semiclassical approximation, details about the full manifold become irrelevant and all we need is its behaviour at the horizon and at infinity.

We can now insert the saddle point values into the expression for the Von Neumann entropy.

$$S_{vN} = \partial_n (S_{grav}[g_n] - nS_{grav}[g_1])|_{n=1} \tag{B.6}$$

The basic approach we take is to consider that the geometry g_n is an n fold cover of the original but smoothed out at the horizon. We also have a replica symmetry $\mathbb{Z}_n$ which shifts the euclidean time by β and iterates over the replicas.

We can now consider the quotient manifold, $\mathcal{M}_n/\mathbb{Z}_n$ such that we now have an orbifold. We can imagine that at all point on the manifold it is taking into account the degeneracy of the original manifold and reducing the angle 2π to $2\pi/n$. This is fine for all points on the manifold except for those which are fixed points of the $\mathbb{Z}_n$ action. In this case, those points are all on the surface of the horizon as they are simply mapped to the same points when we go from $\mathcal{M}_n \longrightarrow \mathcal{M}/\mathbb{Z}_n$ and so we have a conical singularity for all points on the horizon with an angular decefit

$$\Delta\phi_n = 2\pi\left(1 - \frac{1}{n}\right) \tag{B.7}$$

To reiterate, the geometry of the orbifold is locally the same as the $1/n$-th part of the original replica manifold except at the tip of the cone. Therefore, we expect that the full action integral over the original manifold is just equal to $n$times the copy of the orbifold except at the tip of the cone. This makes clear that:

$$S_{grav}[g_n] = \frac{n}{16\pi G}\int_{\mathcal{M}_n/\mathbb{Z}_n}\sqrt{g_n}\big(R[g_n] + (d-2)\Lambda\big)|_{reg} \tag{B.8}$$

Here, reg means that we should remove the conical singularity at the horizon.

We may change the geometry slightly near the horizon by smoothing out the cone. We denote this regularised geometry by $\tilde{g}_n$. Now that it is regular, the action is well defined on the orbifold. This is no longer a true saddle point of the original action, and doesn't satisfy the Einstein Equations. We can assume that the new geometry is close to the original and only differs in first order by $n-1$. Since the metric g_n extremizes the action, there is no change to the action to first order in the approximation,

$$S_{grav}[g_n] \approx \frac{n}{16\pi G}\int_{\tilde{\mathcal{M}}_n/\mathbb{Z}_n}\sqrt{g_n}(R[\tilde{g}_n] + (d-2)\Lambda) + \mathcal{O}((n-1)^2) \tag{B.9}$$

The only contribution in our final result from this geometry will therefore come from near-horizon region,

$$\begin{aligned} S_{vN} &= \frac{d}{dn}(S_{grav}[g_n] - nS_{grav}[g_1])|_{n=1} \\ &= \frac{d}{dn}(nS_{grav}[\tilde{g}_n]|_{\tilde{\mathcal{M}}_n/\mathbb{Z}_n} - nS_{grav}[g_1])|_{n=1} \\ &= n\frac{d}{dn}(S_{grav}[\tilde{g}_n]|_{\tilde{\mathcal{M}}_n/\mathbb{Z}_n})|_{n=1} + (S_{grav}[\tilde{g}_n]|_{\tilde{\mathcal{M}}_n/\mathbb{Z}_n} - S_{grav}[g_1])|_{n=1} \\ &= n\frac{d}{dn}(S_{grav}[\tilde{g}_n]|_{\tilde{\mathcal{M}}_n/\mathbb{Z}_n})|_{n=1} \end{aligned} \tag{B.10}$$

Since $g_1 = \tilde{g}_1$ the terms cancel. Furthermore, outside of the smoothed region, the geometry is equal to the saddle point geometry g_n so when we take the derivative and so it obeys the Einstein equations. Hence, we only need the result at the horizon.

We can then split the smoothed cone region into two parts, the (r, τ_E) and the $(d-2)$ dimensions along the horizon. The action is translationally invariant in these horizon directions so the integration just produces the area A of the horizon.

We then only have the two dimensional integral over the smoothed cone region, which can be solved easily by using that the Ricci scalar in two dimensions,

$$R = \tilde{g}^{\mu\nu}_{(n,2)}R_{\mu\nu} = K\tilde{g}^{\mu\nu}_{(n,2)}\tilde{g}^{(n,2)}_{\mu\nu} = 2K \tag{B.11}$$

where K is the Gauss curvature. We point out that $\tilde{g}^{\mu\nu}_{(n,2)}$ is the (r, τ_E) component of the smoothed metric.

We now use the Gauss Bonnet theorem which relates the Gaussian curvature to the angular defecit by

$$\int_{\text{sm cone}} K = \Delta\phi \implies \int_{\text{sm cone}} \sqrt{\tilde{g}_{(n,2)}} R^{(2)} = 4\pi(1 - \frac{1}{n}) \tag{B.12}$$

giving,

$$S_{grav}[g_n] - nS_{grav}[g_1] \approx \frac{4\pi n}{16\pi G}\left(1 - \frac{1}{n}\right)\text{Area}_H + \mathcal{O}((n-1)^2) \tag{B.13}$$

from which we take the derivative with respect to n to get

$$S = \frac{d}{dn}\left(\frac{4\pi n}{16\pi G}\left(1 - \frac{1}{n}\right)\text{Area}_H\right)\Big|_{n=1} = \frac{\text{Area}_H}{4G} \tag{B.14}$$

As we can see, there we have indeed obtained the Hawking-Bekenstein result for the entropy. There exists a more general procedure created by Wald for the case where we have higher order derivatives and functions of the curvature in the action which relies upon a detailed treatment of conserved currents on the horizon.

Appendix C

The Covariant RT Conjecture (HRT)

The RT conjecture is an extremely useful tool for calculating holographic entanglement entropy of static spacetimes, however, we would like to extend this to the case in which the spacetime itself is dynamic. Not long after the RT conjecture was first put forward, Hubeny, Ranganami and Takayanagi published (8) in which they provided a completely covariant extension to the RT formula commonly referred to as the HRT proposal.

To see where the ambiguity lies, we consider some time dependent von Neumann entropy for boundary region A,

$$S_{vN}[\rho_A(t)] = -\operatorname{Tr}[\rho_A(t)\ln\rho_A(t)] \tag{C.1}$$

For the static case, we can simply go to Euclidean time and find an unambiguous definition of the area which does not evolve in time. When we consider the time dependent case, the area of such a surface is no longer well defined as the Lorentzian signature permits us to apply deformations in the time direction which could make this area arbitrarily small. If we are permitted to simply minimize over this co-dimension two area, we could always reduce the entropy to zero and hence the RT formula loses all meaning.

To move towards a solution, we note that in Euclidean signature the proper length of a spacelike geodesic is given by a local minimum of the area functional while in Lorentzian spacetimes we must find a saddle point which is a local extremum of the area functional. This gives us some intuition that we ought to expect the Lorentzian analogue of the RT surface to represent an extremal rather than minimal surface.

The HRT proposal was inspired by Bousso's lightcone construction which allows for the construction of a covariant entropy bound (48). Bousso's entropy bound states that the entropy flux[53] integrated over a light sheet $L_{m(A(t))}$ is bounded from above by the Bekenstein Hawking entropy of the surface[54]:

[53] This is defined as entropy per unit area, where the area is simply a co-dimension two spacelike region

[54] For the sake of simplicity, we shall continue to use $m(A)$ here despite the fact that the surface is no longer

$$S(L_{m(A(t))}) \leq \frac{\mathrm{A}[m(A(t))]}{4G_N} \tag{C.2}$$

The lightsheet $L_{m(A(t))}$ of a co-dimension two bulk spacelike surface, $m(A(t))$, can be constructed using four congruences[55] which extend from the region $m(A(t))$. These congruences represent in-going and out-going and past and future domains of dependence of the region. This means that the geodesics converge to point and form a caustic.

To motivate the HRT conjecture, consider the subregion $A(t)$ on the boundary CFT which has boundary $\partial A(t)$ and density matrix $\rho_A(t)$. We now construct future/past directed lightsheets $L^{\pm}_{\partial A(t)}$ defined by the region stretching from $\partial A(t)$ into the bulk. In the bulk, our co-dimension two bulk surface $m(A(t))$ is then defined by the intersection of these two lightsheets, $m(A(t)) = L^{+}_{\partial A(t)} \cap L^{-}_{\partial A(t)}$.

The proposal can be defined in the bulk as:

$$S_{vN}[\rho_A(t)] = \min_{m(A(t))} \left(\frac{\mathrm{A}[m(A(t))]}{4G_N} \right) = \frac{\mathrm{A}[m_{min}(A(t))]}{4G_N} \tag{C.3}$$

where $m_{min}(A(t))$ is a minimum of all surfaces $m(A(t))$ which can be produced with this light sheet construction. The null geodesic $\theta_{\pm}$ expansion on the light sheets is always non-positive ($\theta_{\pm} \leq 0$) such that we can continuously deform some generic surface in the set $m(A(t))$ into the boundary which is defined as the surface which saturated the bound so we have vanishing null geodesic expansion, $\theta_{\pm} = 0$. This means that the minimal surface we find from the light sheet construction is equivalent to an extremal surface, $m_{ext}(A(t))$ provided that this extremum obeys:

1. The boundary of the CFT subregion A is the same as the boundary of the extremal surface $m_{ext}(A(t))$: $\partial A(t) = \partial m_{ext}(A(t))$.

2. The extremal surface is homologous to $A(t)$ such that $A(t) \cup m_{ext}(A(t))$ form the boundary of some d-dimensional spacelike surface in $\mathcal{M}$.

3. The extremal surface has a vanishing null-geodesic expansion. This means that along $m_{ext}(A(t))$, the trace of the null extrinsic curvatures $(\xi_{\pm})^{\mu}_{\mu}$ is vanishing:

$$\theta_{\pm} = (\xi_{\pm})^{\mu}_{\mu} = h^{\rho}_{\mu} h^{\sigma\mu} \nabla_{\rho} (N_{\pm})_{\sigma} = 0 \tag{C.4}$$

   where $h_{\mu\nu}$ is the induced metric along the extremal surface $m_{ext}(A(t))$, $N^{\mu}_{\pm}$ are the two null vectors orthogonal to $m_{ext}(A(t))$ normalised such that $g_{\mu\nu} N^{\mu}_{+} N^{\nu}_{-} = -1$. This condition demands that $m_{ext}(A(t))$ lies within the set of all surfaces which obey our first two conditions

minimal and that we need not make specific reference to a boundary region A to define this bound.

[55] We recall that a congruence is a set of integral curves of a nowhere vanishing vector field in a Lorentzian manifold which can be interpreted as a model of spacetime. In this case, we foliate the spacetime by a set of null geodesics.

(ie. are within our causal domain). Extremizing over this set,

$$S_{vN}[\rho_A(t)] = \text{ext}_{m(A(t))}\left(\frac{\text{A}[m(A(t))]}{4G_N}\right) = \frac{\text{A}[m_{ext}(A(t))]}{4G_N} \tag{C.5}$$

4. If the surface which meets the first three criteria is non-unique then one chooses that with the minimal area.

It has been shown that the HRT formulation obeys the desired properties of entanglement entropy as defined in Chapter 1 for dynamical spacetimes. An additional approach was introduced by Wall in (121) known as the maxi-min prescription. In this formulation, the extremal surface can be found by foliating the spacetime with a set of spacelike Cauchy slices Σ_A where $\Sigma_A \subset \partial A$. We then pick a single Cauchy slice at time t, $\Sigma_{A(t)}$ and find the minimal surface on this slice which is anchored to the boundary region $\partial A(t)$ and homologous to A. Once this is done, we must find the minimal surface over time which is equivalent to finding its minimum over all possible choices of Cauchy slices,

$$S_{vN}[\rho_A(t)] = \max_{\Sigma_{A(t)}} \min_{m(A(t))}\left(\frac{\text{Area}[m(A(t))]}{4G_N}\right) = \frac{\text{Area}[m_{ext}(A(t))]}{4G_N} \tag{C.6}$$

What this prescription makes apparent is that we are looking for a saddle point of the area functional located at a local minimum with respect to the spatial coordinates and at a local maximum with respect to time.

Appendix D

RT Surfaces for Spherically Symmetric Geometries in $(d+1) = 3$

Below we calculate the RT surfaces of two simple spherically symmetric geometries in AdS_3 in global coordinates: the AdS_3 solution and the BTZ black hole.

D.1 AdS_3 in Global Coordinates

We shall assume that $t = 0$ and that we are considering a region such that $\phi \in [-\phi_A, \phi_A]$. The metric of the constant time slice with AdS length, ℓ_3, is given by:

$$ds^2 = \frac{\ell_3^2}{r^2 + \ell_3^2} dr^2 + r^2 d\phi^2 \tag{D.1}$$

To find the minimal surface, we simply need to find the geodesic connecting the points $(-\phi_A)$ and ϕ_A. The minimal surface is then found by solving the equation:

$$\frac{d\phi}{dr} = \pm \frac{C\ell_3}{r\sqrt{(r^2 + \ell_3^2)(r^2 - C^2)}} \tag{D.2}$$

where C is a constant. For a general geodesic starting at (r_0, ϕ_0) with slope $\frac{d\phi}{dr}|_{(r_0,\phi_0)} = \dot{\phi}_0$,

$$C = \frac{r_0^2\sqrt{(r_0^2 + \ell_3^2)}}{\sqrt{\ell_3^2/\dot{\phi}_0^2 + r_0^2(r_0^2 + \ell_3^2)}} \tag{D.3}$$

It is simple to check that if we parameterize this path by the deepest point r_* such that at $\phi_0 = 0$, $r_0 = r_*$ and $\dot{\phi}_0^{-1}$ we find that $C = r_0$. For the minimal surface, this equation is solved by:

$$r(\phi) = \ell_3 \cos\phi_A \sqrt{\frac{1}{\cos^2\phi - \cos^2\phi_A}} \tag{D.4}$$

Where we have used that the deepest point can be parameterised by $r_* = R\cot(\phi_A)$ [56].

D.2 BTZ in Global Coordinates

We again assume that $t = 0$ and that we are considering a region such that $\phi \in [-\phi_A, \phi_A]$. The metric of the constant time slice is given by:

$$ds^2 = \frac{\ell_3^2}{r^2 - r_h^2} dr^2 + r^2 d\phi^2 \tag{D.5}$$

Of course, we see that we return the global AdS with the identification $R = ir_h$ such that the period of ϕ has been altered. To find the minimal surface, we simply need to find the geodesic connecting the points $(-\phi_A)$ and ϕ_A.

$$\frac{d\phi}{dr} = \pm \frac{C\ell_3}{r\sqrt{(r^2 - r_h^2)(r^2 - C^2)}} \tag{D.6}$$

where C is a constant. For a general geodesic starting at (r_0, ϕ_0) with slope $\frac{d\phi}{dr}|_{(r_0,\phi_0)} = \dot{\phi}_0$, we can write,

$$C = \frac{r_0^2\sqrt{(r_0^2 - r_h^2)}}{\sqrt{\ell_3^2/\dot{\phi}_0^2 + r_0^2(r_0^2 - r_h^2)}} \tag{D.7}$$

It is simple to check that if we parameterize this path by the deepest point r_* such that at $\phi_0 = 0$, $r_0 = r_*$ and $\dot{\phi}_0^{-1} = s_0$ we find that $C = r_*$. In this case, there exist two minimal surfaces,

$$\mathcal{E}^{(1)} = r(\phi, \phi_A, r_h) = r_h\sqrt{\frac{\cosh^2(\frac{r_h\phi_A}{\ell_3})}{\cosh^2(\frac{r_h\phi_A}{\ell_3}) - \cosh^2(\frac{r_h\phi}{\ell_3})}} \tag{D.8}$$

and

$$\mathcal{E}^{(2)} = r(\phi, \pi - \phi_A, r_h) \cup r_h \tag{D.9}$$

where we used that the deepest point can be parameterised by[57].

$$r_* = r_h \coth\left(\frac{r_h\phi_A}{\ell_3}\right) \tag{D.10}$$

To find the entanglement entropy, one must calculate the area of each surface. In three di-

[56] This follows from solving the equation using that $C = r_*$ and then similarly solving the equation for general C and then matching the conditions at ϕ_A as desired.

[57] This follows from solving the equation using that $C = r_*$ and then similarly solving the equation for general C and then matching the conditions at ϕ_A as desired by demanding that at $\phi \longrightarrow \phi_A$ as $r \longrightarrow \infty$.

mensions, this can be done by calculating the proper length of the minimal surfaces divided by $4G_3$,

$$\begin{aligned} S_A(\mathcal{E}^{(1)}) =& \frac{\ell_3}{4G_3} 2 \int_{r_*}^{r_f} dr \sqrt{\frac{1}{r^2 - r_h^2} + r^2 \left(\frac{d\phi}{dr}\right)^2} \\ =& \frac{c}{3} \int_{r_*}^{r_f} dr \sqrt{\frac{r^2}{(r^2 - r_h^2)(r^2 - r_*^2)}} \\ =& \frac{c}{3} \left[\sinh^{-1} \left(\sqrt{\frac{r^2 - r_h^2}{r_h^2 - r_*^2}} \right) \right]_{r_*}^{r_f} \\ =& \frac{c}{3} \log \left(\frac{\sqrt{r_f^2 - r_*^2} + \sqrt{r_f^2 - r_h^2}}{r_h \sqrt{\coth^2(\frac{r_h \phi_A}{\ell_3}) - 1}} \right) \\ =& \frac{c}{3} \log \left(\frac{2}{\epsilon r_h} \sinh \left(\frac{r_h \phi_A}{\ell_3} \right) \right) \\ =& \frac{c}{3} \log \left(\frac{\beta}{\pi \epsilon} \sinh \left(\frac{r_h \phi_A}{\ell_3} \right) \right) \end{aligned} \tag{D.11}$$

where in the first line we used the symmetry about $\phi = 0$, in the second last line we made use of the fact that $r_f = \frac{1}{\epsilon}$ is much larger than r_h, r_* in the limit that $\epsilon \longrightarrow 0$ and finally we made the identification $r_h = 2\pi\ell_3^2/\beta$ and $R = 2\pi\ell_3$ is the size of a spatial circle. The two possible minimal surfaces are thus given by:

$$S_A = \begin{cases} \frac{c}{3} \log \left(\frac{\beta}{\pi\epsilon} \sinh \left(\frac{R}{\beta} \phi_A \right) \right), & \text{if } \phi_A < \phi_A^* \\ \frac{c}{3} \pi r_h + \frac{c}{3} \log \left(\frac{\beta}{\pi\epsilon} \sinh \left(\frac{R}{\beta} (\pi - \phi_A) \right) \right), & \text{if } \phi_A \geq \phi_A^* \end{cases} \tag{D.12}$$

Which is minimal depends upon the critical angle ϕ_A^* which can be found by finding the point where the HEE associated to the two possible minimal surfaces is equal, $S_A(\mathcal{E}^{(1)}) = S_A(\mathcal{E}^{(2)})$ giving,

$$\phi_A^*(r_h) = \frac{\ell_3}{r_h} \coth^{-1} \left(2 \coth \left(\frac{\pi r_h}{\ell_3} \right) - 1 \right) \tag{D.13}$$

Note that in the large r_h limit we find, $\lim_{r_h \to \infty} \phi_A^* = \pi$ as we would expect.

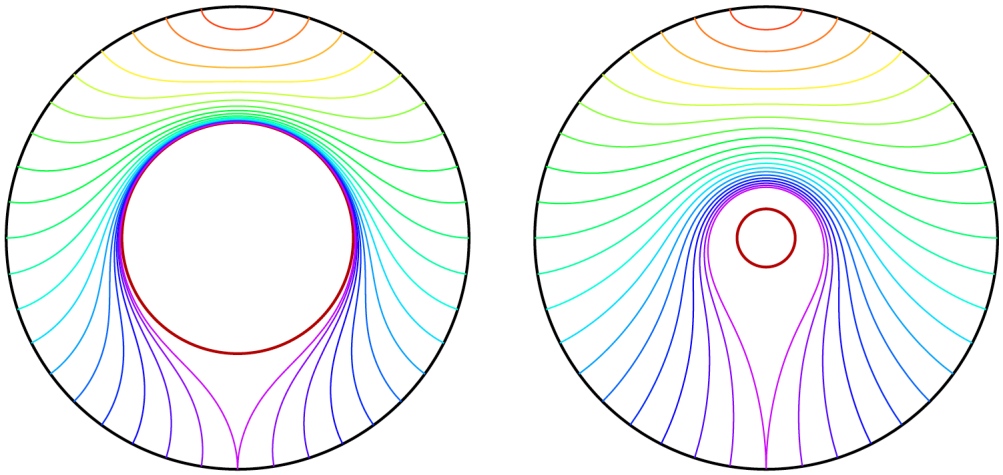

Figure D.1: A plot showing minimal surfaces in the BTZ with black holes of radius $r_h = 1$ and $r_h = 0.2$ on the left and right respectively. The central circle is the black hole horizon and the minimal surfaces corresponding to $0 \leq \phi_A \leq \pi$ colour coded from red to purple respectively. The radial coordinate has been compactified such that $\rho = \tan^{-1}(r)$(122).

D.3 Cosmic Strings in $(d+1) = 3$

To move towards the cosmic string (or conical singularity) results, one simply makes the identification $r_h = i\ell_3\sqrt{1-\mu} = i\ell_3 r_{c.h.}$ where $\mu \in [0,1)$ to find the $t = 0$ slice metric in $\ell_3 = 1$ coordinates,

$$ds^2 = \frac{1}{r^2 + r_{c.h.}^2} dr^2 + r^2 d\phi^2 \tag{D.14}$$

and the minimal surface equation,

$$\frac{d\phi}{dr} = \pm \frac{C\ell_3}{r\sqrt{(r^2 + r_{c.h.}^2)(r^2 - r_*^2)}} \tag{D.15}$$

where r_* parameterizes the deepest point in the bulk. The connected minimal surface is given by,

$$\mathcal{E}^{(1)} = \phi(r, r_*, r_h) = \pm \frac{1}{r_{c.h.}} \left(\frac{\pi}{2} - \tan^{-1} \left(\frac{r_* \sqrt{(r^2 + r_{c.h.}^2)}}{r_{c.h.} \sqrt{(r^2 - r_*^2)}} \right) \right) \tag{D.16}$$

or

$$\mathcal{E}^{(1)} = r(\phi, r_*, r_h) = \frac{r_{c.h.} r_*}{\sqrt{r_{c.h.}^2 \sin^2(\pi/2 - r_{c.h.}\phi) - r_*^2 \cos^2(\pi/2 - r_{c.h.}\phi)}} \tag{D.17}$$

We can also find that

$$r_* = \pm r_{c.h.} \tan(\pi/2 - r_{c.h.}\phi_A) \tag{D.18}$$

Where we use the positive solution for $0 \leq \phi_A \leq \frac{\pi}{2r_{c.h.}}$ and the negative for $\frac{\pi}{2r_{c.h.}} \leq \phi_A \leq \frac{\pi}{r_{c.h.}}$. Unlike the QuBTZ, there is no horizon and hence there exists only a connected phase for the minimal surface. We can also find the entanglement entropy for a region,

$$\begin{aligned} S_A(\mathcal{E}^{(1)}) =& \frac{\ell_3}{4G_3} 2 \int_{r_*}^{r_f} dr \sqrt{\frac{1}{r^2 + r_{c.h}^2} + r^2 \left(\frac{d\phi}{dr}\right)^2} \\ =& \frac{c}{3} \int_{r_*}^{r_f} dr \sqrt{\frac{r^2}{(r^2 + r_{c.h.}^2)(r^2 - r_*^2)}} \\ =& \frac{c}{3} \left[i \sin^{-1} \left(\sqrt{\frac{r^2 + r_{c.h.}^2}{r_*^2 + r_{c.h.}^2}} \right) \right]_{r_*}^{r_f} \\ =& \frac{c}{3} \log \left(\frac{1}{\epsilon} \frac{1 - i}{\sqrt{r_*^2 + r_{c.h.}^2}} \right) \end{aligned} \tag{D.19}$$

where in the first line we used the symmetry about $\phi = 0$, in the second last line we made use of the fact that $r_f = \frac{1}{\epsilon}$ is much larger than r_h, r_* in the limit that $\epsilon \longrightarrow 0$. This result certainly looks to be problematic in light of its imaginary component. However, if we take a difference of the entropy in regions A and B with penetration depths r_* and r_{**} respectively we find that,

$$\Delta S = S_A - S_B = \frac{c}{3} \log \left(\sqrt{\frac{r_{**}^2 + r_{c.h.}^2}{r_*^2 + r_{c.h.}^2}} \right) \tag{D.20}$$

Regardless, these results are certainly unusual and warrant further investigation, particularly when considering in light of the possibility of the Branch (1a) solutions to the QuBTZ.

Appendix E

Roots and Timelike Paths

In this subsection, we provide supplementary information regarding the roots of $f(r)$ and extend our small ℓ analysis to radial timelike paths in the bulk. Neither of these results are central to this thesis but are included for the sake of completeness.

E.1 Lightlike Paths

For radially infalling lightlike paths, the reality of the roots of $f(r)$ are determined by the determinant of the polynomial,

$$\Delta_3 = 4\ell_3^6(8\mathcal{G}_3 M)^3 - 27(vF(M)\ell_3^3)^2 \tag{E.1}$$

where positive, zero and negative values correspond to the cases in which the roots are all real, real with two repeated roots and one real root and two complex conjugate roots respectively. This gives the non-canonical conditions:

$$\begin{aligned} \ell_3 &> \frac{3\sqrt{3}}{2}\mu\ell; \quad \Delta_3 > 0 \\ \ell_3 &= \frac{3\sqrt{3}}{2}\mu\ell; \quad \Delta_3 = 0 \\ \ell_3 &< \frac{3\sqrt{3}}{2}\mu\ell; \quad \Delta_3 < 0 \end{aligned} \tag{E.2}$$

or in the canonical coordinates:

$$\begin{aligned} 8\mathcal{G}_3 M &> 3\left(\frac{F(M)\nu}{2}\right)^{2/3}; \quad \Delta_3 > 0 \\ 8\mathcal{G}_3 M &= 3\left(\frac{F(M)\nu}{2}\right)^{2/3}; \quad \Delta_3 = 0 \\ 8\mathcal{G}_3 M &< 3\left(\frac{F(M)\nu}{2}\right)^{2/3}; \quad \Delta_3 < 0 \end{aligned} \tag{E.3}$$

The nature of these roots do not seem to provide any deeper physical insight but we include them to complete the discussion.

Timelike Trajectories

In the small ℓ limit, we can then also consider the timelike trajectories of massive observers,

$$\begin{aligned} \int d\tau &= \pm\, \ell_3 \int \frac{dr}{\sqrt{E^2 - f(r)}} \\ &= \pm \ell_3 \int \frac{dr\sqrt{r}}{\sqrt{(-r^3 + \ell_3^2(E^2 + 8\mathcal{G}_3 M)r + \nu\ell_3^3 F(M))}} \end{aligned} \tag{E.4}$$

By the same logic as before, we can state that there now exists three separate conditions depending on the parameter values. The discriminant is given by:

$$\tilde{\Delta}_3 = 4\ell_3^6(8\mathcal{G}_3 M + E^2)^3 - 27\ell_3^6(\nu F(M))^2 \tag{E.5}$$

We note that unlike the previous case, the positive root to this equation is not the value of the horizon. The case in which $E = 1$ corresponds to the case in which our test particle is at rest at $r = \infty$ but we shall keep E general such that:

$$\begin{aligned} 8\mathcal{G}_3 M &> 3\left(\frac{F(M)\nu}{2}\right)^{2/3} - E^2; \quad \Delta_3 > 0 \\ 8\mathcal{G}_3 M &= 3\left(\frac{F(M)\nu}{2}\right)^{2/3} - E^2; \quad \Delta_3 = 0 \\ 8\mathcal{G}_3 M &< 3\left(\frac{F(M)\nu}{2}\right)^{2/3} - E^2; \quad \Delta_3 < 0 \end{aligned} \tag{E.6}$$

Once again, we simply write this expression as:

$$\int d\tau = \pm\ell_3 \int \frac{dr\sqrt{r}}{\sqrt{((r-A)(r+B)((r+C)))}} \tag{E.7}$$

Where A, B, C are the roots of $f(r) - E^2$. This results in the rather unwieldy expression

$$\begin{aligned}
\tau(r) =& \ell_3 \int \sqrt{\frac{-r}{((r-A)(r+B)(r+C)))}}\, dr \\
=& 2\ell_3 \sqrt{\frac{A(r-A)^2(r+C)}{r(A+C)}} \sqrt{\frac{A(r+B)}{B(r-A)}} \sqrt{\frac{r}{(r-A)(r+B)(r+C)}} \ldots \\
& \left(F\left(g_1(r;A,C) | g_2(A,B,C) \right) - \Pi\left(\frac{C}{A+C}; g_1(r;A,C) | g_2(A,B,C) \right) \right) \\
=& 2\ell_3 \sqrt{\frac{A^2}{B(A+C)}} \left(F\left(g_1(r;A,C) | g_2(A,B,C) \right) - \ldots \right. \\
& \left. \Pi\left(\frac{C}{A+C}; g_1(r;A,C) | g_2(A,B,C) \right) \right) + \text{Const}
\end{aligned} \tag{E.8}$$

where $F(x|m)$ and $\Pi(n; x, m)$ are the elliptical integral of the first and third kind respectively with parameter $m = k^2$ and the constant is found by setting $\tau(\infty) = 0$. Though it is not obvious from these solutions, there is a duality under the switching of B and C. We also define the functions

$$g_1(r;A,C) = \sin^{-1}\left(\sqrt{\frac{(A+C)r}{C(r-A)}} \right); \quad g_2 = \frac{(A+B)C}{(A+C)B} \tag{E.9}$$

In the limit that $\tilde{\Delta}_3 \longrightarrow 0$, we have $B = C$ and $g_2 \longrightarrow 1$.
We may once again compare this to the classical BTZ solution,

$$\int d\tau = \pm\ell_3 \int \frac{dr}{\sqrt{r_h^2 + E^2 - r^2}} \tag{E.10}$$

yielding

$$\tau = \pm\left[\tan^{-1}\left(\frac{r}{\sqrt{r_h^2 + E^2 - r^2}} \right) \right]_{r=\infty}^{r=r} \tag{E.11}$$

We can also look at how massive particles move in time for the classical case by using

$$E = f(r)\frac{dt}{dr}\frac{dr}{d\tau} = f(r)\sqrt{E^2 - f(r)}\frac{dt}{dr} \tag{E.12}$$

which is solved by

$$t - t_0 = \pm \int \frac{E}{f(r)\sqrt{E^2 - f(r)}} = \mp \frac{1}{r_h} \tanh^{-1}\left(\frac{Er}{r_h\sqrt{r_h^2 + E^2 - r^2}}\right) \tag{E.13}$$

which can be inverted to give

$$r = \pm\left(\frac{r_h\sqrt{(r_h^2 + E^2)}\tanh(r_h(t - t_0))}{\sqrt{E^2 + r_h^2\tanh(r_h(t - t_0))^2}}\right) \tag{E.14}$$

Rather surprisingly, there does exist an analytic solution for timelike paths in terms of $t(r)$,

$$\begin{aligned} t(r) &= \pm \int dr \frac{Er^{3/2}}{(r-a)(r-b)(r-c)\sqrt{(r-A)(r-B)(r-C)}} \\ &= \pm 2AE\sqrt{B(A-C)}\left(-\frac{AF\left(\sin^{-1}\left(\sqrt{\frac{(C-A)r}{C(r-A)}}\right) \mid \frac{(A-B)C}{B(A-C)}\right)}{(a-A)(A-b)(A-c)} + \frac{a\Pi\left(\frac{(A-a)C}{a(A-C)}; \sin^{-1}\left(\sqrt{\frac{(C-A)r}{C(r-A)}}\right) \mid \frac{(A-B)C}{B(A-C)}\right)}{(a-A)(a-b)(a-c)} \cdots \right. \\ &\quad \left. + \frac{b\Pi\left(\frac{(A-b)C}{b(A-C)}; \sin^{-1}\left(\sqrt{\frac{(C-A)r}{C(r-A)}}\right) \mid \frac{(A-B)C}{B(A-C)}\right)}{(a-b)(b-A)(b-c)} + \frac{c\Pi\left(\frac{(A-c)C}{c(A-C)}; \sin^{-1}\left(\sqrt{\frac{(C-A)r}{C(r-A)}}\right) \mid \frac{(A-B)C}{B(A-C)}\right)}{(a-c)(c-A)(c-b)}\right) + \text{Const} \end{aligned} \tag{E.15}$$

where A, B, C and a, b, c are defined as before and the constant is found by setting $t(\infty) = 0$.

Bibliography

[1] J. D. Bekenstein, "Generalized second law of thermodynamics in black-hole physics," *Physical Review D*, vol. 9, no. 12, p. 3292, 1974.

[2] C. B. . H. S. Bardeen, J.M., "The four laws of black hole mechanics," *Commun.Math. Phys.*, vol. 31, p. 161–170, 1973.

[3] C. W. Misner, K. S. Thorne, and J. A. Wheeler, *Gravitation.* Macmillan, 1973.

[4] C. R. Stephens, G. Hooft, and B. F. Whiting, "Black hole evaporation without information loss," *Classical and Quantum Gravity*, vol. 11, no. 3, p. 621, 1994.

[5] L. Susskind, "The world as a hologram," *Journal of Mathematical Physics*, vol. 36, no. 11, pp. 6377–6396, 1995.

[6] J. Maldacena, "The large-n limit of superconformal field theories and supergravity," *International journal of theoretical physics*, vol. 38, no. 4, pp. 1113–1133, 1999.

[7] S. Ryu and T. Takayanagi, "Holographic derivation of entanglement entropy from ads," *arXiv preprint arXiv:603001*, 2016.

[8] V. E. Hubeny, M. Rangamani, and T. Takayanagi, "A covariant holographic entanglement entropy proposal," *Journal of High Energy Physics*, vol. 2007, p. 062–062, Jul 2007.

[9] X. Dong, "Holographic entanglement entropy for general higher derivative gravity," *Journal of High Energy Physics*, vol. 2014, no. 1, pp. 1–32, 2014.

[10] J. Camps, "Generalized entropy and higher derivative gravity," *Journal of High Energy Physics*, vol. 2014, no. 3, pp. 1–18, 2014.

[11] N. Engelhardt and A. C. Wall, "Quantum extremal surfaces: holographic entanglement entropy beyond the classical regime," *Journal of High Energy Physics*, vol. 2015, no. 1, pp. 1–27, 2015.

[12] A. Karch and L. Randall, "Locally localized gravity," *Journal of High Energy Physics*, vol. 2001, pp. 008–008, may 2001.

[13] H. Z. Chen, R. C. Myers, D. Neuenfeld, I. A. Reyes, and J. Sandor, "Quantum extremal islands made easy, part i: Entanglement on the brane,"

[14] R. Emparan, A. M. Frassino, and B. Way, "Quantum btz black hole," *Journal of High Energy Physics*, vol. 2020, Nov 2020.

[15] S. H. Shenker and D. Stanford, "Black holes and the butterfly effect," *Journal of High Energy Physics*, vol. 2014, mar 2014.

[16] M. Mezei and D. Stanford, "On entanglement spreading in chaotic systems," *Journal of High Energy Physics*, vol. 2017, may 2017.

[17] A. Rolph, "Quantum bit threads," *arXiv preprint arXiv:2105.08072*, 2021.

[18] E. Witten, "A mini-introduction to information theory," *La Rivista del Nuovo Cimento*, vol. 43, no. 4, pp. 187–227, 2020.

[19] M. Rangamani and T. Takayanagi, *Holographic entanglement entropy*. Springer, 2017.

[20] M. Bailyn, "A survey of thermodynamics," *New York: AIP Press.*, 1994.

[21] J. Preskill, "Quantum information and physics: some future directions," *Journal of Modern Optics*, vol. 47, no. 2-3, pp. 127–137, 2000.

[22] J. Preskill, "Quantum shannon theory," *arXiv preprint arXiv:1604.07450*, 2016.

[23] E. H. Lieb and M. B. Ruskai, "Proof of the strong subadditivity of quantum-mechanical entropy," *Les rencontres physiciens-mathématiciens de Strasbourg-RCP25*, vol. 19, pp. 36–55, 1973.

[24] M. Headrick and T. Takayanagi, "Holographic proof of the strong subadditivity of entanglement entropy," *Physical Review D*, vol. 76, Nov 2007.

[25] H. Araki and E. H. Lieb, "Entropy inequalities," in *Inequalities*, pp. 47–57, Springer, 2002.

[26] J. D. Bekenstein, "Black holes and entropy," in *Jakob Bekenstein: The Conservative Revolutionary*, pp. 307–320, World Scientific, 2020.

[27] M. Natsuume, *AdS/CFT duality user guide*, vol. 903. Springer, 2015.

[28] S. W. Hawking, "Black hole explosions?," *Nature*, vol. 248, no. 5443, pp. 30–31, 1974.

[29] S. W. Hawking, "Particle creation by black holes," in *Euclidean quantum gravity*, pp. 167–188, World Scientific, 1975.

[30] K. S. Thorne, C. W. Misner, and J. A. Wheeler, *Gravitation*. Freeman, 2000.

[31] D. N. Page, "Information in black hole radiation," *Physical review letters*, vol. 71, no. 23, p. 3743, 1993.

[32] A. Almheiri, T. Hartman, J. Maldacena, E. Shaghoulian, and A. Tajdini, "The entropy of hawking radiation," *Reviews of Modern Physics*, vol. 93, no. 3, p. 035002, 2021.

[33] S. D. Mathur, "What exactly is the information paradox?," in *Physics of Black Holes*, pp. 3–48, Springer, 2009.

[34] D. N. Page, "Black hole information," in *Proceedings of the 5th Canadian conference on general relativity and relativistic astrophysics*, vol. 1, pp. 1–41, World Scientific, 1993.

[35] S. B. Giddings, "Comments on information loss and remnants," *Physical Review D*, vol. 49, no. 8, p. 4078, 1994.

[36] M. J. Chen Y. and W. E., "On the black hole/string transition," *arXiv preprint arXiv:2109.08563*, 2021.

[37] J. A. Wheeler, "Relativity, groups and topology," *edited by C. De-Witt and B. DeWitt, Gordon and Breach, New York*, p. 316, 1964.

[38] S. B. Giddings, "Black holes and massive remnants," *Physical Review D*, vol. 46, no. 4, p. 1347, 1992.

[39] J. D. Bekenstein, "How does the entropy/information bound work?," *Foundations of Physics*, vol. 35, pp. 1805–1823, nov 2005.

[40] S. B. Giddings and A. Strominger, "Loss of incoherence and determination of coupling constants in quantum gravity," *Nuclear Physics B*, vol. 307, no. 4, pp. 854–866, 1988.

[41] S. Coleman, "Black holes as red herrings: topological fluctuations and the loss of quantum coherence," *Nuclear Physics B*, vol. 307, no. 4, pp. 867–882, 1988.

[42] J. B. Hartle, "Generalized quantum theory and black hole evaporation," *arXiv preprint gr-qc/9808070*, 1998.

[43] S. B. Giddings, "Black hole information, unitarity, and nonlocality," *Physical Review D*, vol. 74, no. 10, p. 106005, 2006.

[44] J. Preskill, "Do black holes destroy information," in *Proceedings of the International Symposium on Black Holes, Membranes, Wormholes and Superstrings, S. Kalara and DV Nanopoulos, eds.(World Scientific, Singapore, 1993) pp*, pp. 22–39, World Scientific, 1992.

[45] P. Hayden and J. Preskill, "Black holes as mirrors: quantum information in random subsystems," *Journal of high energy physics*, vol. 2007, no. 09, p. 120, 2007.

[46] G. t'Hooft, "Dimensional reduction in quantum gravity," *arXiv preprint gr-qc/9310026*, 1993.

[47] R. Bousso, "The holographic principle," *Reviews of Modern Physics*, vol. 74, no. 3, p. 825, 2002.

[48] R. Bousso, "A covariant entropy conjecture," *Journal of High Energy Physics*, vol. 1999, no. 07, p. 004, 1999.

[49] E. Witten, "Anti de sitter space and holography," *arXiv preprint hep-th/9802150*, 1998.

[50] D. Harlow, "Tasi lectures on the emergence of the bulk in ads/cft," *arXiv preprint arXiv:1802.01040*, 2018.

[51] D. Harlow, "Jerusalem lectures on black holes and quantum information," *Reviews of Modern Physics*, vol. 88, no. 1, p. 015002, 2016.

[52] M. Van Raamsdonk, "Lectures on gravity and entanglement," in *New Frontiers in Fields and Strings: TASI 2015 Proceedings of the 2015 Theoretical Advanced Study Institute in Elementary Particle Physics*, pp. 297–351, World Scientific, 2017.

[53] J. Kaplan, "Lectures on ads/cft from the bottom up," 2016.

[54] J. Zaanen, Y. Sun, Y. Liu, and K. Schalm, "The ads/cmt manual for plumbers and electricians," *Universiteit Leiden, Leiden The Netherlands*, vol. 15, 2012.

[55] R. Blumenhagen and E. Plauschinn, *Introduction to conformal field theory: with applications to string theory*, vol. 779. Springer Science & Business Media, 2009.

[56] R. Blumenhagen, D. Lüst, and S. Theisen, *Introduction to conformal field theory*. Springer, 2012.

[57] I. Heemskerk, J. Penedones, J. Polchinski, and J. Sully, "Holography from conformal field theory," *Journal of High Energy Physics*, vol. 2009, no. 10, p. 079, 2009.

[58] S. S. Gubser, I. R. Klebanov, and A. M. Polyakov, "Gauge theory correlators from non-critical string theory," *Physics Letters B*, vol. 428, no. 1-2, pp. 105–114, 1998.

[59] M. Selle, "The cosmological information paradox and islands in de sitter," 2021. Preprint at https://scripties.uba.uva.nl/search?id=723677.

[60] S. W. Hawking and D. N. Page, "Thermodynamics of black holes in anti-de sitter space," *Communications in Mathematical Physics*, vol. 87, no. 4, pp. 577–588, 1983.

[61] M. Bañados, C. Teitelboim, and J. Zanelli, "Black hole in three-dimensional spacetime," *Physical Review Letters*, vol. 69, p. 1849–1851, Sep 1992.

[62] S. M. Carroll, *Spacetime and geometry*. Cambridge University Press, 2019.

[63] R. M. Wald, *General relativity*. University of Chicago press, 2010.

[64] J. Maldacena, "Eternal black holes in anti-de sitter," *Journal of High Energy Physics*, vol. 2003, no. 04, p. 021, 2003.

[65] Y. Sekino and L. Susskind, "Fast scramblers," *Journal of High Energy Physics*, vol. 2008, pp. 065–065, oct 2008.

[66] M. Van Raamsdonk, "Building up spacetime with quantum entanglement," *General Relativity and Gravitation*, vol. 42, no. 10, pp. 2323–2329, 2010.

[67] A. Almheiri, T. Hartman, J. Maldacena, E. Shaghoulian, and A. Tajdini, "Replica wormholes and the entropy of hawking radiation," *Journal of High Energy Physics*, vol. 2020, no. 5, pp. 1–42, 2020.

[68] A. Almheiri, R. Mahajan, J. Maldacena, and Y. Zhao, "The page curve of hawking radiation from semiclassical geometry," *Journal of High Energy Physics*, vol. 2020, no. 3, pp. 1–24, 2020.

[69] G. Penington, S. H. Shenker, D. Stanford, and Z. Yang, "Replica wormholes and the black hole interior," *arXiv preprint arXiv:1911.11977*, 2019.

[70] L. V. Keldysh *et al.*, "Diagram technique for nonequilibrium processes," *Sov. Phys. JETP*, vol. 20, no. 4, pp. 1018–1026, 1965.

[71] S. Ryu and T. Takayanagi, "Holographic derivation of entanglement entropy from the anti–de sitter space/conformal field theory correspondence," *Physical review letters*, vol. 96, no. 18, p. 181602, 2006.

[72] S. Ryu and T. Takayanagi, "Aspects of holographic entanglement entropy," *Journal of High Energy Physics*, vol. 2006, no. 08, p. 045, 2006.

[73] M. Headrick, A. Lawrence, and M. Roberts, "Bose–fermi duality and entanglement entropies," *Journal of Statistical Mechanics: Theory and Experiment*, vol. 2013, p. P02022, feb 2013.

[74] T. Faulkner, A. Lewkowycz, and J. Maldacena, "Quantum corrections to holographic entanglement entropy," *Journal of High Energy Physics*, vol. 2013, no. 11, pp. 1–18, 2013.

[75] C. Akers, N. Engelhardt, G. Penington, and M. Usatyuk, "Quantum maximin surfaces," *Journal of High Energy Physics*, vol. 2020, no. 8, pp. 1–43, 2020.

[76] G. Penington, "Entanglement wedge reconstruction and the information paradox," *Journal of High Energy Physics*, vol. 2020, no. 9, pp. 1–84, 2020.

[77] A. Almheiri, N. Engelhardt, D. Marolf, and H. Maxfield, "The entropy of bulk quantum fields and the entanglement wedge of an evaporating black hole," *Journal of High Energy Physics*, vol. 2019, no. 12, pp. 1–47, 2019.

[78] K. Hashimoto, N. Iizuka, and Y. Matsuo, "Islands in schwarzschild black holes," *Journal of High Energy Physics*, vol. 2020, no. 6, pp. 1–21, 2020.

[79] L. Randall and R. Sundrum, "Large mass hierarchy from a small extra dimension," *Physical Review Letters*, vol. 83, pp. 3370–3373, oct 1999.

[80] R. Emparan, A. M. Frassino, M. Sasieta, and M. Tomašević, "Holographic complexity of quantum black holes," 2021.

[81] A. Fabbri and J. Navarro-Salas, *Modeling black hole evaporation*. World Scientific, 2005.

[82] C. G. Callan, S. B. Giddings, J. A. Harvey, and A. Strominger, "Evanescent black holes," *Physical Review D*, vol. 45, pp. R1005–R1009, feb 1992.

[83] H. Verlinde, "Holography and compactification," *Nuclear Physics B*, vol. 580, pp. 264–274, jul 2000.

[84] S. S. Gubser, "AdS/CFT and gravity," *Physical Review D*, vol. 63, mar 2001.

[85] R. M. Wald, "Black hole entropy is the noether charge," *Physical Review D*, vol. 48, pp. R3427–R3431, oct 1993.

[86] R. Emparan, "Black hole entropy as entanglement entropy: a holographic derivation," *Journal of High Energy Physics*, vol. 2006, pp. 012–012, jun 2006.

[87] R. Emparan, A. Fabbri, and N. Kaloper, "Quantum black holes as holograms in AdS braneworlds," *Journal of High Energy Physics*, vol. 2002, pp. 043–043, aug 2002.

[88] J. Garriga and T. Tanaka, "Gravity in the randall-sundrum brane world," *Physical Review Letters*, vol. 84, pp. 2778–2781, mar 2000.

[89] R. Emparan, G. T. Horowitz, and R. C. Myers, "Exact description of black holes on branes," *Journal of High Energy Physics*, vol. 2000, pp. 007–007, jan 2000.

[90] J. F. Plebanski and M. Demianski, "Rotating, charged, and uniformly accelerating mass in general relativity," *Annals of Physics*, vol. 98, no. 1, pp. 98–127, 1976.

[91] R. A. Battye and B. Carter, "Generic junction conditions in brane-world scenarios," *Physics Letters B*, vol. 509, no. 3-4, pp. 331–336, 2001.

[92] S. de Haro, K. Skenderis, and S. N. Solodukhin, "Gravity in warped compactifications and the holographic stress tensor," *Classical and Quantum Gravity*, vol. 18, pp. 3171–3180, aug 2001.

[93] U. Gürsoy, E. Kiritsis, L. Mazzanti, and F. Nitti, "Holography and thermodynamics of 5d dilaton-gravity," *Journal of High Energy Physics*, vol. 2009, pp. 033–033, may 2009.

[94] A. A. Patel, D. Chowdhury, S. Sachdev, and B. Swingle, "Quantum butterfly effect in weakly interacting diffusive metals," *Physical Review X*, vol. 7, sep 2017.

[95] M. Blake, "Universal charge diffusion and the butterfly effect in holographic theories," *Physical Review Letters*, vol. 117, aug 2016.

[96] X. Dong, D. Wang, W. W. Weng, and C.-H. Wu, "A tale of two butterflies: An exact equivalence in higher-derivative gravity," 2022.

[97] S. Grozdanov, "On the connection between hydrodynamics and quantum chaos in holographic theories with stringy corrections," *Journal of High Energy Physics*, vol. 2019, jan 2019.

[98] E. H. Lieb and D. W. Robinson, "The finite group velocity of quantum spin systems," in *Statistical mechanics*, pp. 425–431, Springer, 1972.

[99] M. Srednicki, "Chaos and quantum thermalization," *Physical Review E*, vol. 50, pp. 888–901, aug 1994.

[100] J. M. Deutsch, "Quantum statistical mechanics in a closed system," *Physical review a*, vol. 43, no. 4, p. 2046, 1991.

[101] J. Abajo-Arrastia, J. Aparício, and E. López, "Holographic evolution of entanglement entropy," *Journal of High Energy Physics*, vol. 2010, nov 2010.

[102] V. Balasubramanian, A. Bernamonti, J. de Boer, N. Copland, B. Craps, E. Keski-Vakkuri, B. Müller, A. Schäfer, M. Shigemori, and W. Staessens, "Thermalization of strongly coupled field theories," *Physical Review Letters*, vol. 106, may 2011.

[103] V. E. Hubeny and H. Maxfield, "Holographic probes of collapsing black holes," *Journal of High Energy Physics*, vol. 2014, mar 2014.

[104] V. Balasubramanian, A. Bernamonti, J. de Boer, N. Copland, B. Craps, E. Keski-Vakkuri, B. Müller, A. Schäfer, M. Shigemori, and W. Staessens, "Holographic thermalization," *Physical Review D*, vol. 84, jul 2011.

[105] T. Takayanagi and T. Ugajin, "Measuring black hole formations by entanglement entropy via coarse-graining," *Journal of High Energy Physics*, vol. 2010, nov 2010.

[106] H. Liu and S. J. Suh, "Entanglement growth during thermalization in holographic systems," *Physical Review D*, vol. 89, mar 2014.

[107] H. Liu and S. J. Suh, "Entanglement tsunami: Universal scaling in holographic thermalization," *Physical Review Letters*, vol. 112, jan 2014.

[108] T. Hartman and J. Maldacena, "Time evolution of entanglement entropy from black hole interiors," *Journal of High Energy Physics*, vol. 2013, may 2013.

[109] T. Hartman and N. Afkhami-Jeddi, "Speed limits for entanglement," 2015.

[110] H. Casini, H. Liu, and M. Mezei, "Spread of entanglement and causality," *Journal of High Energy Physics*, vol. 2016, jul 2016.

[111] S. Kundu and J. F. Pedraza, "Spread of entanglement for small subsystems in holographic CFTs," *Physical Review D*, vol. 95, apr 2017.

[112] K. Sfetsos, "On gravitational shock waves in curved spacetimes," *Nuclear Physics B*, vol. 436, pp. 721–745, feb 1995.

[113] H. Liu and M. Mezei, "Probing renormalization group flows using entanglement entropy," *Journal of High Energy Physics*, vol. 2014, jan 2014.

[114] V. Iyer and R. M. Wald, "Some properties of the noether charge and a proposal for dynamical black hole entropy," *Physical Review D*, vol. 50, pp. 846–864, jul 1994.

[115] Y. Myung, "No hawking–page phase transition in three dimensions," *Physics Letters B*, vol. 624, pp. 297–303, sep 2005.

[116] S. H. Shenker and D. Stanford, "Stringy effects in scrambling," 2014.

[117] M. Freedman and M. Headrick, "Bit threads and holographic entanglement," *Communications in Mathematical Physics*, vol. 352, no. 1, pp. 407–438, 2017.

[118] C. A. Agón and J. F. Pedraza, "Quantum bit threads and holographic entanglement," *Journal of High Energy Physics*, vol. 2022, no. 2, pp. 1–55, 2022.

[119] C. A. Agón, J. de Boer, and J. F. Pedraza, "Geometric aspects of holographic bit threads," *Journal of High Energy Physics*, vol. 2019, May 2019.

[120] M. Headrick, V. E. Hubeny, A. Lawrence, and M. Rangamani, "Causality holographic entanglement entropy," *Journal of High Energy Physics*, vol. 2014, Dec 2014.

[121] A. C. Wall, "Maximin surfaces, and the strong subadditivity of the covariant holographic entanglement entropy," *Classical and Quantum Gravity*, vol. 31, no. 22, p. 225007, 2014.

[122] V. E. Hubeny, H. Maxfield, M. Rangamani, and E. Tonni, "Holographic entanglement plateaux," *Journal of High Energy Physics*, vol. 2013, aug 2013.